Progress in Polymer Science 37 (2012) 406–444

Contents lists available at ScienceDirect

Progress in Polymer Science

journal homepage: www.elsevier.com/locate/ppolysci

Self-assembly behavior of polymer-assisted clays

Chih-Wei Chiu, Jiang-Jen Lin*

Institute of Polymer Science and Engineering, National Taiwan University, Taipei 10617, Taiwan

ARTICLE INFO

Article history:
Available online 29 July 2011

Keywords:
Self-assembly
Self-organization
Intercalation
Clay film
Silicate platelet
Non-covalent

ABSTRACT

Layered silicate clays are natural crystallites that are well recognized for their practical uses, but little is known about their self-assembly behavior. In this review, we summarize the recent literature on clay interactions with organic polymers as well as clay self-assembly with organic involvement. We place emphasis on two aspects of these non-covalent interactions: first, plate-like clays can have a considerable impact on polymer properties such as hydrogels and clay films, and also on the encapsulation of bio-molecules. Second, through ionic intercalation with polymeric amine-salts, the clay layered structure units can be modified and enabled to self-assemble into ordered arrays such as rod-, dendrite-, and fiber-like microstructures. The silicate self-assembled morphologies such as worm-like and hollow microspheres were obtained in epoxy matrices and during spray drying, respectively. A mechanism was proposed for the clay self-assembly in two orientations, platelet face-to-face (ionic attraction) and edge-to-edge (organic hydrophobic effect). Further, the layered clays after the exfoliation into random platelets (1 nm in thickness) had strong propensity toward self-piling without any organic influence. Formation of lengthy rods or fibrils up to 5 μm in length and their hierarchical transformation under transmission electron microscope (TEM) electron beam bombardment and ultrasonication were observed. The clay thin-platelet geometric shape and surface ionic charge are two important parameters for the self-assembling tendency. The high surface of clay platelet has a significant impact on polymer interactions and drives the self-organization of inorganic–organic structures.

© 2011 Elsevier Ltd. All rights reserved.

Contents

Abbreviations: AFM, atomic force microscope; ATRP, atomic transfer radical polymerization; BSA, bovine serum albumin; CEC, cationic exchange capacity; CMC, critical micelle concentration; CTE, thermal expansion coefficient; LbL, layer-by-layer; LCST, lower critical solution temperature; LDH, layered double hydroxides; Mica, synthetic fluorinated mica; MMT, montmorillonite; OR gels, organic hydrogels; Organoclay, organically intercalated clays; OTR, oxygen transmission rate; PAA, poly(acrylic acid); PDADMAC, poly(diallyldimethyl-ammonium chloride); PEG, poly(ethyleneglycol); PEI, polyethylenimine; PEO, polyethylene oxide; PNIPA, poly(*N*-isopropylacrylamide); POE-amine, poly(oxyethylene)-polyamine; POP-amine, poly(oxypropylene)-polyamine; PP-g-MA, poly(propylene-maleic anhydride); PVA, polyvinyl alcohol; PVP, polyvinyl pyrrolidone; NC gels, clay–polymer nanocomposite hydrogels; NCs, nanocrystals; NMP, nanoscale mica platelets; NSP, nanoscale silicate platelets; SAXS, small-angle X-ray scattering; SCE, sodium carboxymethyl cellulose; SEBS, poly(styrene-ethylene/butadiene-styrene); SEM, scanning electron microscope; SMA, poly(styrene-maleic anhydride); SPA, sodium polyacrylate; TEM, transmission electron microscope; XRD, X-ray diffraction.

* Corresponding author. Tel.: +886 2 33665312; fax: +886 2 83691384.
E-mail address: jianglin@ntu.edu.tw (J.-J. Lin).

0079-6700/$ – see front matter © 2011 Elsevier Ltd. All rights reserved.
doi:10.1016/j.progpolymsci.2011.07.007

1. Introduction

1.1. Self-assembly of copolymers and nanomaterials

Self-assembly is an important step in bottom-up nanotechnology and often involves the use of surfactants or block copolymers as soft templates for shaping ordered structures [1–10]. Copolymers with chemically distinct blocks may undergo non-equilibrium transformation from random coils into globules or may self-organize into ordered structures. Di- and tri-block copolymers are recognized for their ability to use non-covalent bonding interactions to form various geometric shapes of nanometer dimensions [11–16]. A wide range of applications such as in patterning inorganic nanoparticles, interacting with biomaterials, and fabricating electronic devices have been reported [17–20]. The monolayer self-assembly technique can afford thin films with tailored surface properties [21–23]. The morphology can be controlled by varying the copolymer structure and process parameters such as concentration [23], temperature [24,25], pH [26], and choice of medium [27].

In addition to the above, inorganic nanomaterials are considered basic building blocks in nanotechnology. Inorganic nanomaterials may be classified according to their geometric shape and have at least one dimension in the range of 1–100 nm: spherical (e.g., metal and metal oxide nanoparticles), fibril-shape (e.g., carbon nanotube and metal wires), and platelet-like (e.g., natural smectite clays, graphite and graphene sheets), as illustrated in Fig. 1. These nanometer-scale units have inherent van der Waal's interactions that facilitate self-aggregation and, under certain controlled environments, can also lead to self-assembly and thus the formation of ordered secondary and tertiary structures with different morphologies. For example, spherical nanoparticles [28] and quantum dots [29] undergo controllable self-aggregation into ordered arrays for applications such as optics [30,31], electrical sensors [32–34], and magnetic devices [35,36]. This approach of building up the dimensional scale from nanosized units, called *bottom-up* synthesis, has been an important research topic in recent years because of its wide range of applications. Self-assembly of tiny particles such as inorganic quantum dots for optoelectronic devices [37] and the synthesis of silver nanoparticles of various shapes [38] are examples of applications that employ the aforementioned bottom-up approach. Other geometric shapes and morphologies that have been reported include inorganic nanoboxes [39], nanowires [40,41], nanospheres [42,43], nanotubes [40,44], nanocubes [45,46], and nanorods [47,48].

1.2. Natural occurrences of biomaterials and clay minerals

Non-covalent bonds, including electrostatic charge attraction, hydrogen bonds, van der Waal's forces, metal coordination, aromatic π–π stacking interactions, and hydrophobic effects, are the fundamental driving forces for the self-assembly of copolymers and nanomaterials [1–10,18–20,49–54]. Cooperative interaction among these non-covalent bonds in a particular system controls biological reactions and kinetic transformations. A simple self-assembly process may lead to selective recognition for guest materials or hierarchical transformation into higher-order structures from primary to quaternary microstructures in a sequence. In nature, self-organized structures such as double-helix DNA [55–57]; folded protein globules [58,59]; and bio-mineralization such as seashells, bones, and nacres are commonplace [60–64]. Biomaterials and biomimetic complexes [65,66]

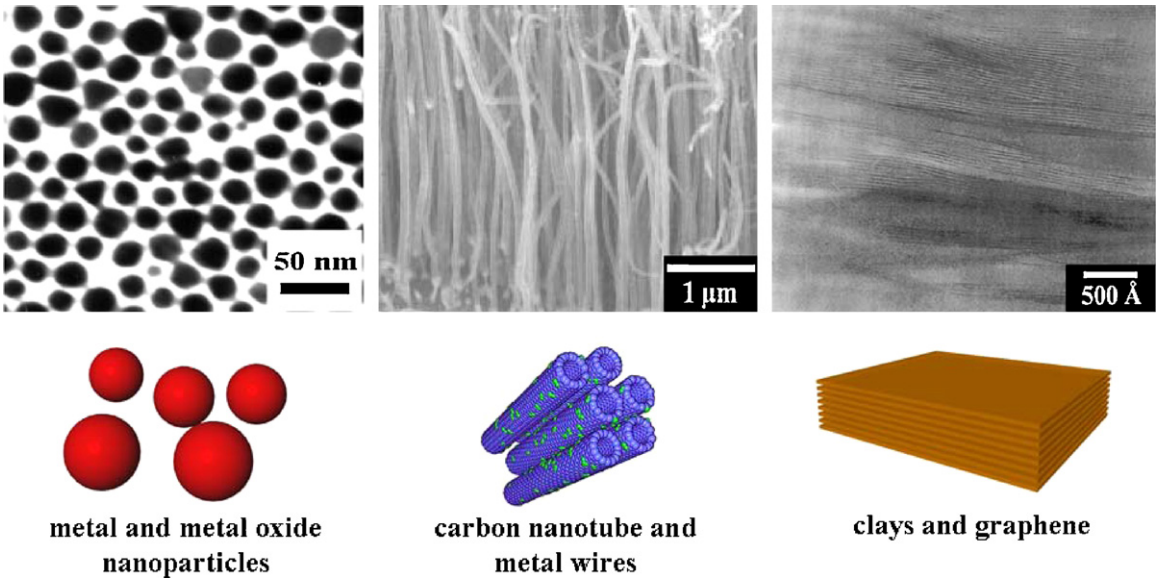

Fig. 1. Nanomaterial classification, together with examples, according to which physical dimension is in the 1–100 nm range.

self-assemble from basic organic and inorganic building blocks through non-covalent interactions in aqueous media. The hierarchy of molecular self-assembly from polymeric surfactants with a random coil structure to molecular bundles with highly ordered morphologies [67–69] and the unique phase separation of chiral copolymers resembling biomaterials [70] are examples of synthetic structures mimicking the diversity of nature.

Among the naturally occurring inorganic minerals, phyllosilicate and smectite clays with layered structures are among the most abundant and have found many industrial applications. Their generic aluminosilicate structure is composed of multiple silicate plates stacked in layers and crystalline defects with divalent metal species (counter ions) in the interlayer galleries. For the commonly utilized smectites, the fundamental units are comprised of two tetrahedral sheets sandwiched with edge-shared octahedral sheet at 2:1 structure. Smectites have been well characterized with regards to chemical composition, lamellar structure with high aspect ratio, geometric shape, surface area, and counter-ion exchange capacity. Perhaps owing to their polydispersed dimensions and contamination with amorphous impurities, the natural clays are less known for their ability to self-assemble into ordered patterns. There are only few reports regarding superstructures of mesoscopic orientation [71] and the properties of sol–gel and isotropic–nematic phase transition [72].

In this review, we summarize the recent developments in the study of the intensive interactions between silicate clay and organic polymers as well as clay self-assembly behaviors. Since the use of layered silicate clays in nanocomposites has been extensively documented, this review instead places emphasis on their chemical interactions with polymers and on clay self-assembly with organic involvement. The intercalation and the exfoliation of layered silicates are discussed with respect to modification of the structures through interlayer spacing enlargement and randomization into individual platelets. New findings on clay self-assembly from both types of units, organically intercalated and exfoliated silicates, for the hierarchical formation of various microstructures are reviewed. The mechanism involving the geometric shape, ionic charge attraction, and platelet pilling direction is also discussed.

2. Recent developments in clay utilization

2.1. Generic multilayered structures and conventional uses

Among many different clay species, smectic clays are naturally abundant with a well-characterized lamellar structure of multiple inorganic plates, high surface area, and ionic charges on the surface [73]. The phyllosilicate clays of the 2:1 type, such as montmorillonite (MMT), bentonite, saponite, and hectorite, have conventionally been employed as catalysts [74–78], adsorbents [79,80], metal chelating agents [81], and polymer nanocomposites [82–92]. The generic multilayered structure is constituted of silicate/aluminum oxide in multilayer stacks, for example a sandwich structure comprising two tetrahedron sheets with an edge-bridged octahedral sheet as the 2:1 type [82,84,89]. The existence of counter ions is due to the variation in composition caused by isomorphic substitution of aluminosilicate elements with other metal ions such as Mg^{2+}, Ca^{2+}, or Fe^{2+}. These counter ions in the galleries can be exchanged with alkali metal ions such as Na^{+} or Li^{+}. By following the ionic exchange capacity and ionic species potential, the clay structure may be altered by organic ion exchange reactions and intercalation with organic components. Multilayered silicates are natively hydrophilic, water-swelling, and exist in nature as large aggregates. For example, MMT clay is found in the form of irregular aggregates of primary stacks consisting of multiple layers of aluminosilicate sheets with individual platelets at

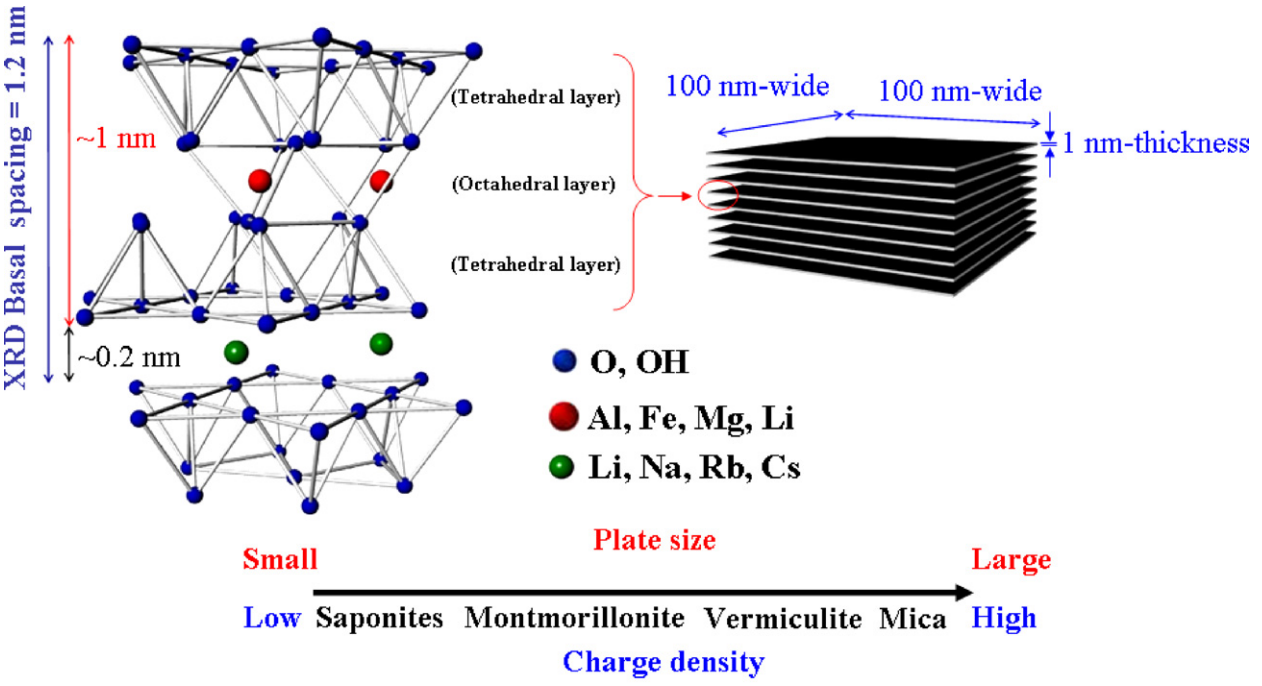

General Formula:

Cationic clays

Na^+-MMT

$M^+_x(Al_{4-x}Mg_x)Si_8O_{20}(OH)_4$

M^+: Li^+, Na^+, Rb^+, Cs^+, et al.

Synthetic fluorine mica

$Na_{0.66}Mg_{2.68}(Si_{3.98}Al_{0.02})O_{10.02}F_{1.96}$

Anionic clays

LDH

$M^{2+}_{1-x}M^{3+}_x(OH)_2(A^{n-})_{x/n}\cdot mH_2O$

M^{2+}: Mg^{2+}, Ni^{2+}, Cu^{2+}, Mn^{2+}, et al.

M^{3+}: Al^{3+}, Fe^{3+}, Cr^{3+}, et al.

A^{n-}: CO_3^{2-}, SO_4^{2-}, NO_3^-, OH^-, et al.

Fig. 2. Chemical structure of smectite clay [94].

© 2009 Elsevier Ltd.

polydispersed dimensions of ca. 100 nm × 100 nm × 1 nm [93,94] (Fig. 2). Another clay, synthetic fluorinated mica (Mica), which is synthesized by Na_2SiF_6 treatment of talc at high temperature [95,96], has unit plate dimensions of 300–1000 nm in width and 1 nm in thickness on average [97]. In addition to clays with cationic counter ions, anionic clays of layered double hydroxides (LDHs) such as $[Mg_6Al_2(OH)_{16}]CO_3{\cdot}4H_2O$ and other inorganic compositions are synthesized by the well-known inorganic salt precipitation method [98–100]. Their structures are similar to the natural clays, consisting of plate-like particles with the dimensions ca. 200 nm × 200 nm × 1 nm. For example, anionic LDHs can possess carbonate counter ions and a charge density of 1.5 e/nm^2. Although these synthetic anionic clays are structurally well defined, little is known of their platelet unit piling properties.

Both of the natural and synthetic clays have been actively studied for their potential as nanofillers for improving the mechanical and physical properties of organic polymers [101,102]. Through organic modification, organically modified clays (organoclays) are obtained than can be homogeneously dispersed and blended in hydrophobic polymer matrices, including polypropylene [103], polystyrene [104], polyurethane [105], polyester [106], epoxy [107,108], and polyimide [82]. A number of review articles have been dedicated to this subject of polymer–clay nanocomposites [82,84–90,109–112]. A common drawback when using polymer–silicate clay nanocomposites is the requirement of overcoming the inherent self-aggregating tendency of the layered structure and the organic affinity for the target hydrophobic polymers. Besides mechanical mixing methods, organic modification [73,91,113–115] to introduce an organic moiety and compatibility is a common approach. In general, intercalative incorporation of organic surfactants into the silicate interlayer galleries affords organoclays suitable for homogeneous mixing with polymers. Despite the significant progress made in clay nanocomposites, the limitations of generating a homogeneous dispersion of clay platelets in polymer matrices have been well documented [89,92,116,117].

2.2. Biomaterial encapsulation

Recent research has focused on the interaction of layered silicate clays with biomaterials. In particular, anionic clays such as synthetic LDHs with charges opposite to natural clays were found to be suitable for embedding DNA

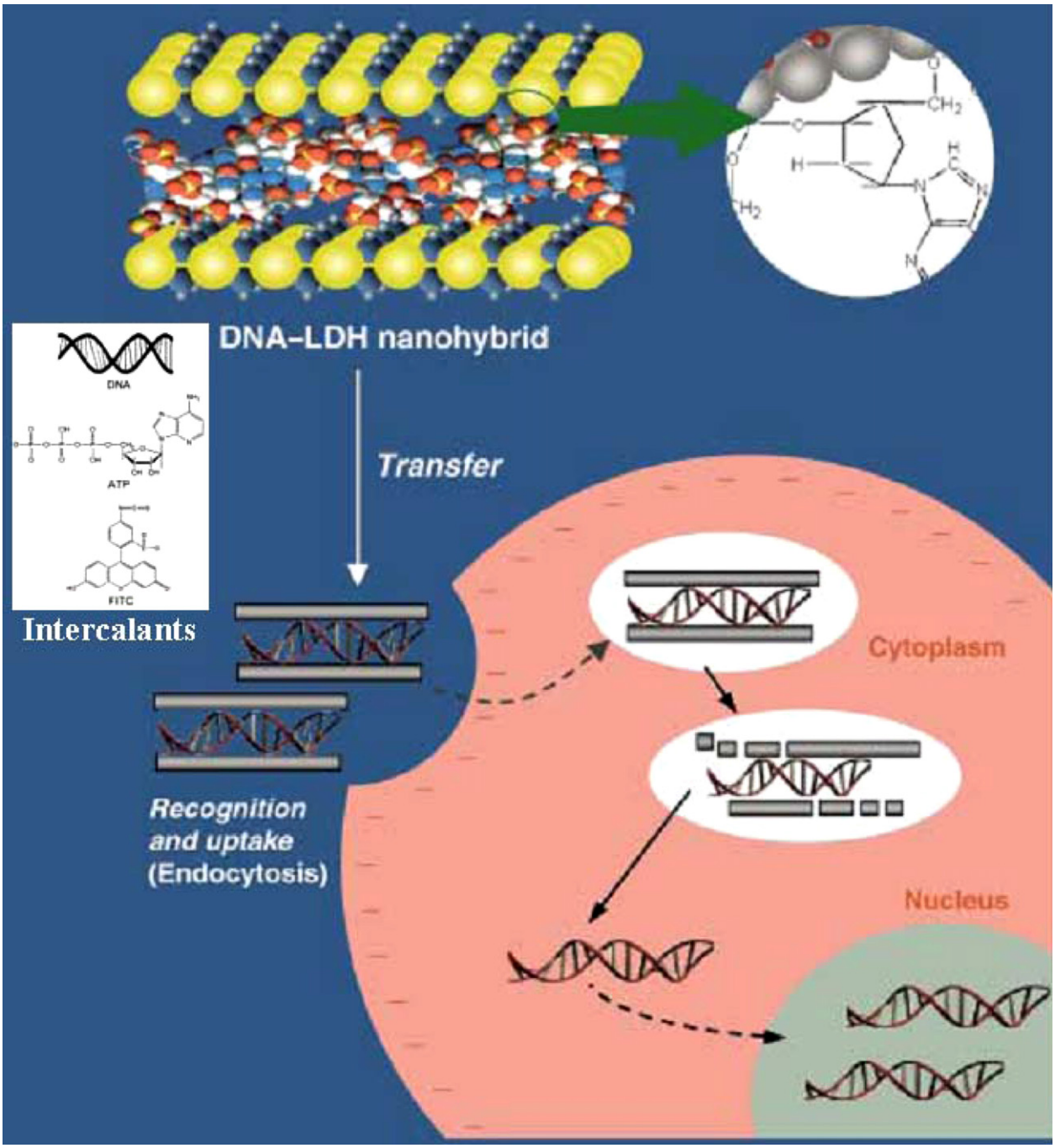

Fig. 3. Schematic illustration of the hybridization and expected transfer mechanism of the bio-LDH hybrid into a cell [118].
© 2000 Wiley-VCH Verlag GmbH & Co. KGaA.

and other biomaterials. The encapsulation was proposed for gene therapy and drug control release (Fig. 3) [118]. LDH with anionic character were compatible for interacting with DNA and spatially allowed for incorporation of bulkier biomaterials in the interlayer galleries. Furthermore, the presence of inorganic composites may protect the guest compounds from degeneration during the necessary penetration into cells through endocytosis. The concept of utilizing the layered inorganic clays may have potential applications for drug delivery and controlled release.

Large protein molecules were possibly embedded in the interlayer galleries in the cases of montmorillonite [58] and synthetic fluorinated mica [59] as represented in Fig. 4. In these disclosures, the hybrid structure of bovine serum albumin (BSA) protein encapsulated in the layered silicate clay with X-ray diffraction (XRD) *d* spacing of

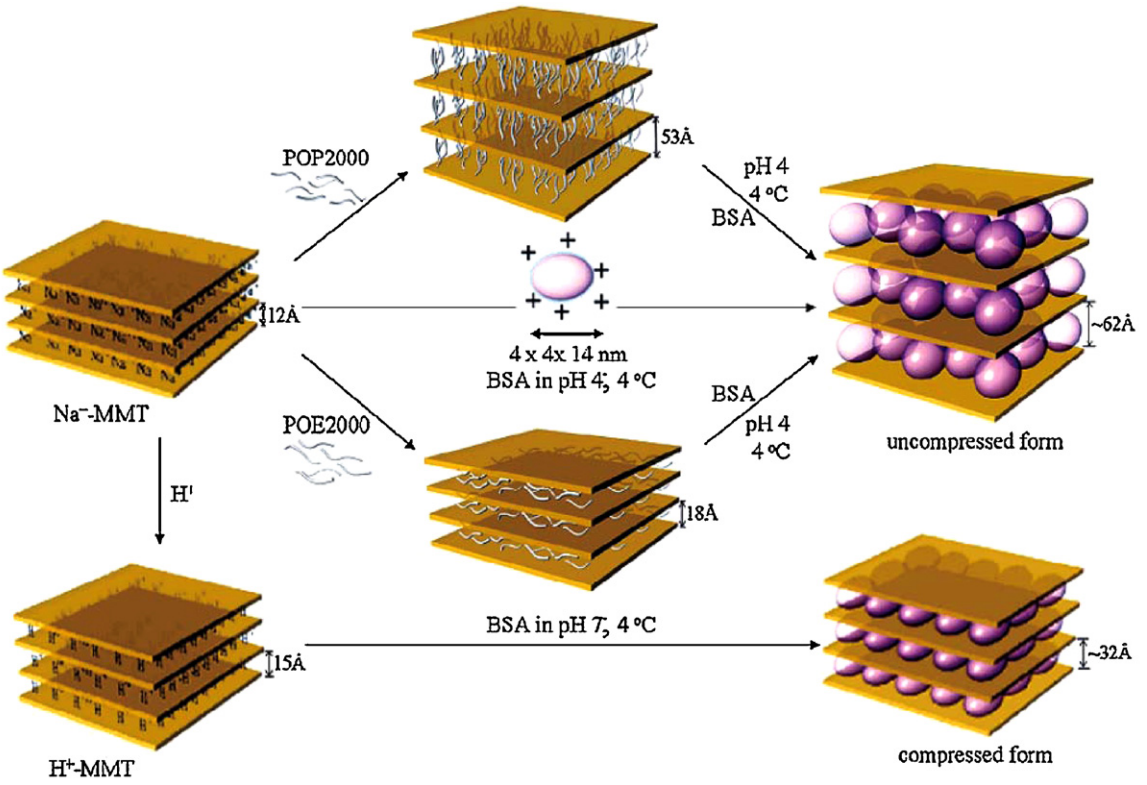

Fig. 4. Conceptual illustration of BSA intercalation into Na^+-MMT (via the direct method and POP2000- or POE2000-enlarged *d* spacing methods), and the acidified MMT but at different pH conditions [58].
© 2007 American Chemical Society.

62 Å was prepared. The first step of the process required clay interlayer space enlargement by intercalation with hydrophobic poly(oxypropylene)-amine (POP-amine) or hydrophilic poly(oxyethylene)-amine (POE). The existence of POP further assisted the accessibility of large BSA protein through a spacing effect and simultaneously increased the organic affinity for the stable embedment. Subsequent replacement of POP by BSA allowed the encapsulation of the large BSA without significant compression in size or conformation. Two different routes of direct BSA intercalation and step-wise organic replacement are illustrated in Fig. 4. Due to spatial constraints, the original layered clay as sodium form of MMT or Mica may be intercalated directly but this required an excess amount of protein. The difficulty of direct intercalation can be seen by comparing the large dimensions required, 4 nm × 4 nm × 14 nm for BSA. Process feasibility is another issue for the preferred POP organic substitution method. The POP/MMT complex was actually shown to have a lower critical solution temperature (LCST) property owing to the hydrogen bonding of the oxypropylene segment with water molecules. The protein exchange reaction with POP was performed at a lower temperature than LCST (<14 °C) with the appropriate pH adjustment. For example, the use of acidified H^+-MMT facilitated the BSA intercalation at a low *d* spacing (33 Å) or a compressed form. The two-step process of first modifying the clay with organic moieties is more suitable for the gallery adjustment and the rendering of large biomaterial embedment.

2.3. Clay–polymer nanocomposite hydrogels

The clay swelling nature in rendering high gelling properties by hybridizing with hydrophilic polymers has been reported [119–130] and compared to conventional organic hydrogels. Clay–polymer nanocomposite (NC) hydrogels have demonstrated the combined properties of mechanically high strengths and elongations at break, high transparency, as well as high rates of swelling/de-swelling. As illustrated in Fig. 5, the NC gel with the compositions of silicate clays and water-soluble poly(*N*-isopropylacrylamide) (PNIPA) is exemplified for a high elongation over ten folds of stretching, high flexibility, and transparent properties in comparison with a conventional organic hydrogel [119]. The inorganic silicate platelets provide high surface area for multiple sites of pseudo-cross-linking in a 3D polymer matrix. A uniform dispersion of exfoliated clay platelets in aqueous media is essential for the advanced performance of the NC gels. In particular, high de-swelling rates and high structural homogeneity (transparencies) were obtained. The selection of hydrophilic polymers such as PNIPA and PEG offered the homogeneous dispersion of clay platelets for chain cross-linking with the clay surface. Because of the long distances between the clay sheets, the water-soluble polymer chains are flexible and can adopt random conformations. In contrast, the PNIPA organic gels (OR) with short cross-liking points generally exhibited a weak and brittle nature. The combined

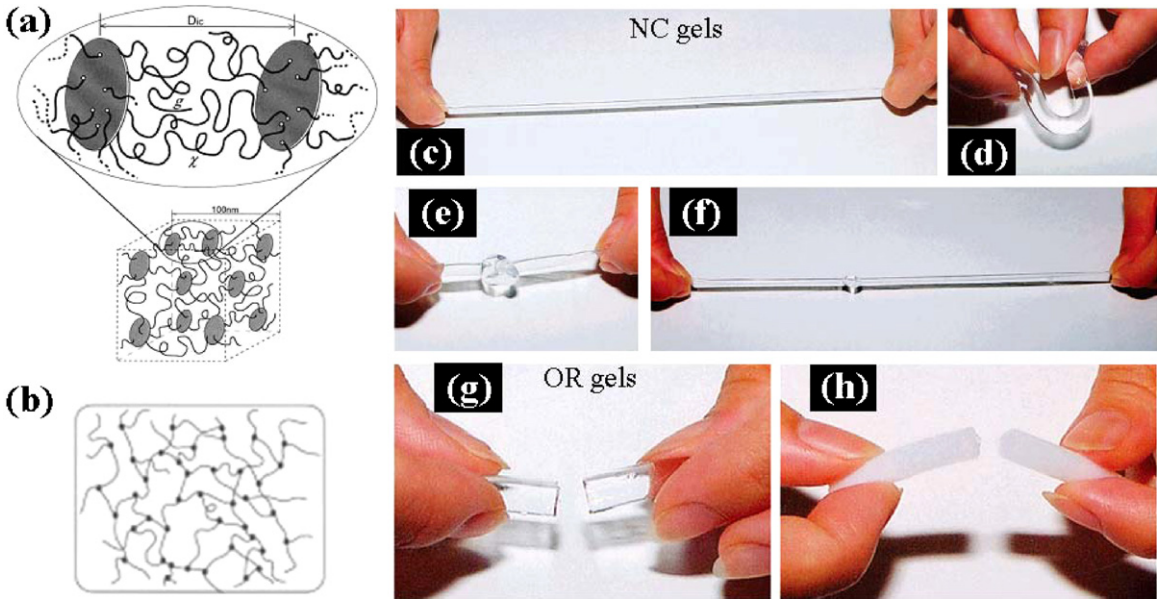

Fig. 5. Comparison of clay/poly(*N*-isopropylacrylamide) NC gels and an organic hydrogel (OR gel): (a) schematic representation of platelet surface interconnected organic/inorganic network in the NC gel, with uniformly dispersed clay sheets and two primary types of flexible polymer chains, *x* and *g*, grafted and pseudo-cross-linked to clay sheets, respectively. (b) Conventional OR gel network structure model. (c–f) NC gels: transparent and flexible and (g and h) OR gels: weak and brittle [119].
© 2002 American Chemical Society.

performance of NC gels largely depended on the clay content (up to ca. 60 wt%) in polymers. Another aspect of the differences for the NC gels is their temperature-dependent transparency change at the LCSTs. In the presence of inorganic clays, it was possible to control the coil-to-globule transition of PNIPA and hence the material transparency and swelling/de-swelling properties could be regulated [123]. The platelet surface interaction allowed the polymer materials to benefit form the combined performances of gelling, adhesion, lubricity, absorption, transparency, and mechanical properties. This development has broadened the use of clay for drug delivery systems, biomedical tissue engineering, sensors, and mechanical devices.

2.4. Clay–polymer nanocomposite films

An aqueous solution of polyvinyl alcohol (PVA)-coated MMT was evaporated into large-area, lightweight, and thick nacre-mimetic films [131]. The combination of soft PVA and rigid silicate clay was homogeneously dispersed and it then self-arranged into orderly aligned clay formation in PVA matrix. A typical 0.5 wt% aqueous dispersion of MMT (Na^+-Cloisite, thickness ca. 1 nm, diameter ca. 50–1000 nm) was evenly distributed and interacted with PVA affording biomimetic materials. Fig. 6 displays SEM images and the conceptual drawings of an orderly alignment of clay platelets with polymers or the assembly grown in layer-by-layer alignment. PVA interacted well with the MMT platelets via weak non-covalent bonds and cross-linking into more rigid structure using glutaraldehyde and alcohol acetal formation. The cross-sectional SEM images show a highly ordered alignment of clay platelets. The strong interaction between clay and polymer allowed facile synthesis of the films on a large scale by the following methods: paper-making, doctor-blading, or simple painting. A similar strategy had been employed by dispersing clays in another hydrophilic polymer, poly(diallyldimethyl-ammonium chloride) (PDADMAC) [132]. The polycation-coated clay stacks generated the supramolecular interactions and reduced the irregular aggregates between the stacks. The generated films were shown to be porous and effective for thermal and flame shielding similar to ceramics. The advantage of strong clay interactions allowed simple film preparation compared to the conventional method, which employs tedious layer-by-layer (LbL) and multilayer deposition approaches.

Several reports deal with the preparation of transparent and mechanically robust thin films by the LbL technique [133–138]. Building blocks of nanometer scale such as clay units are generally difficult to disperse homogeneously in large volume fractions. Micrometer-scaled composites with a high density of non-covalent interactions were prepared by the ordered alignment of nanosheets. The LbL assembling technique was designed to overcome the inherent aggregation tendency of nanosize inorganic unit distribution in a polymer matrix. It was demonstrated from the cross-section SEM images that a well-aligned multilayer structural film could be prepared for 200–300 bilayers of 1.0–1.5 μm thickness, or ca. 5 nm for each bilayer of the clays in the polymer. The transparent and flexible film shown in Fig. 7 was prepared from multiple layer alignment of PVA–clay.

For the advanced function of gas barrier property, transparent and flexible clay films with high thermal resistance were prepared [139–141]. The clay films were fabricated by a casting method involving synthetic

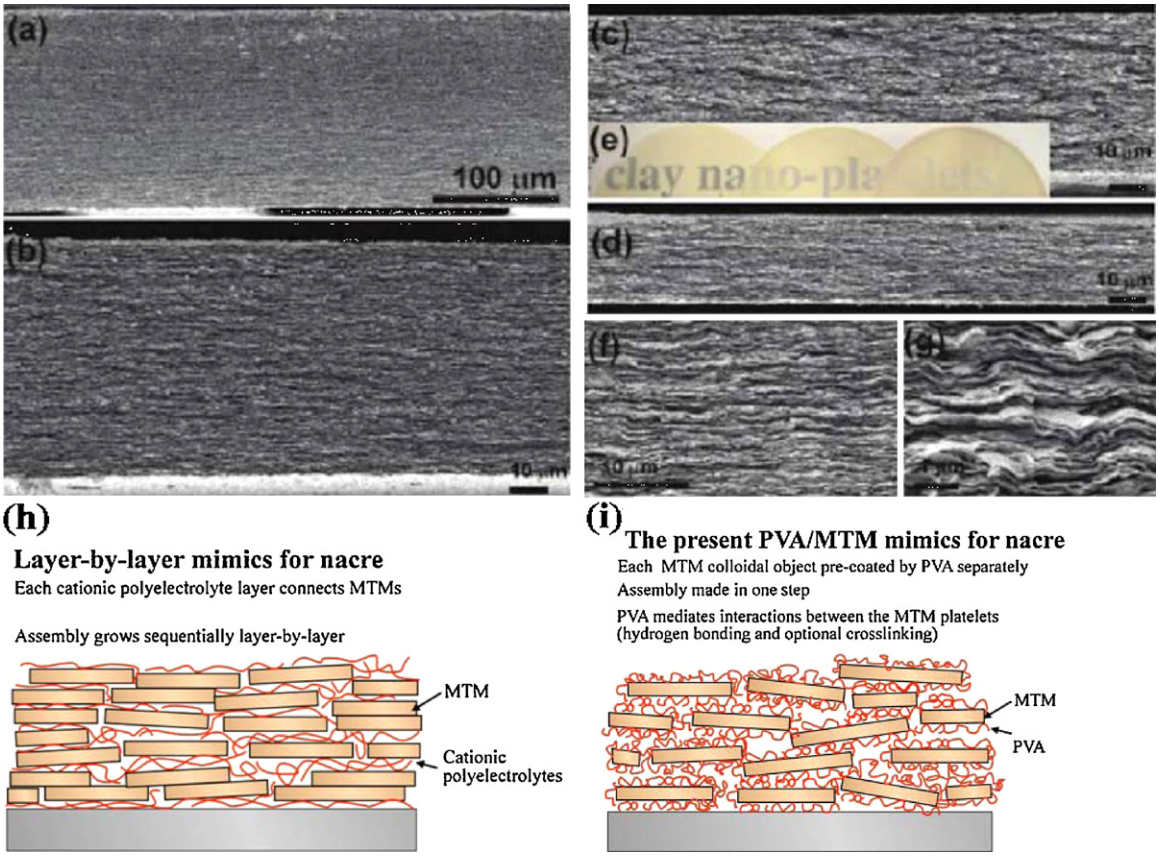

Fig. 6. (a–g) SEM of layered formation of PVA/clay nacre-mimetic paper composites obtained via paper-making process. (h and i) Conceptual illustrations: LbL for nacre mimics using cationic polyelectrolytes and the present one-step concept [131].
© 2010, American Chemical Society.

Na^+-saponite and water-soluble polymers such as sodium salts of polyacrylate (SPA) and carboxymethyl cellulose (SCE). A uniform nanostructure comprising a dense stratified array of clay platelets with flexible polymer chains between clay platelet edges was revealed (Fig. 8d). The polymers possessing sodium anions act as soft binders in connecting the neighboring clay particle edges through ionic interaction. The fine dispersion of polymers prevented clay edge–face contact and clay aggregation. Presumably, the polymer chains bind clay particle edges tightly by fixing the upper and lower layers of the clay platelets. As a result, thermal stability with a high melting point up to 440 °C of the polymer in the clay layers was observed. It was reported that a uniform distribution of polymer in the film interior can be achieved with clay loading in the range of 20–80 wt%. For extremely high clay loading at 80 wt%, the films exhibited excellent optical and physical properties and were proposed for applications such as optoelectronic displays (Fig. 8). In another example, the LbL assembled thin films from MMT and branched polyethylenimine (PEI) were disclosed [142]. The alternating exposure of PEI/MMT for 40 layers afforded transparent films with a high weight composition of clay up to 84 wt%. It is particularly mentioned that very low levels of oxygen permeability were achieved. With the ordered formation of clay platelets in polymer matrices, the gas penetration pathway distance was significantly increased, hence the low permeation rate. The films with highly oriented clay platelets simultaneously may have potential uses for food, biomedical, and electronics packaging applications due to their favorable hardness and elastic modulus.

The colloidal and dispersion properties of natural clays have been studied in order to gauge the influence of interlayer counter ions in cationic clays (Fig. 9) [143]. Various species of MMT clay with Na^+, Li^+, Mg^{2+}, Ca^{2+}, Al^{3+}, and $Fe^{2+,3+}$ counter species were prepared by an ionic exchange reaction. The aqueous solution of colloidal clays without organic additives was coated and evaporated into self-standing films and difference in microstructures investigated. The films prepared from the clay with monovalent interlayer cations exhibited a self-aligned microstructure that was significantly different from those of polyvalent counter-ion clays. In general, the films of polyvalent cations appeared to be a rough and poorly laminated structure. The difference in film formability was attributed to their swellability. MMT with monovalent cations swelled thoroughly in water and became less aggregated. In contrast, the polyvalent cations swell poorly and generated significant amount of clay aggregates in water. It appeared that the ionic species affected the solvation by water and consequently

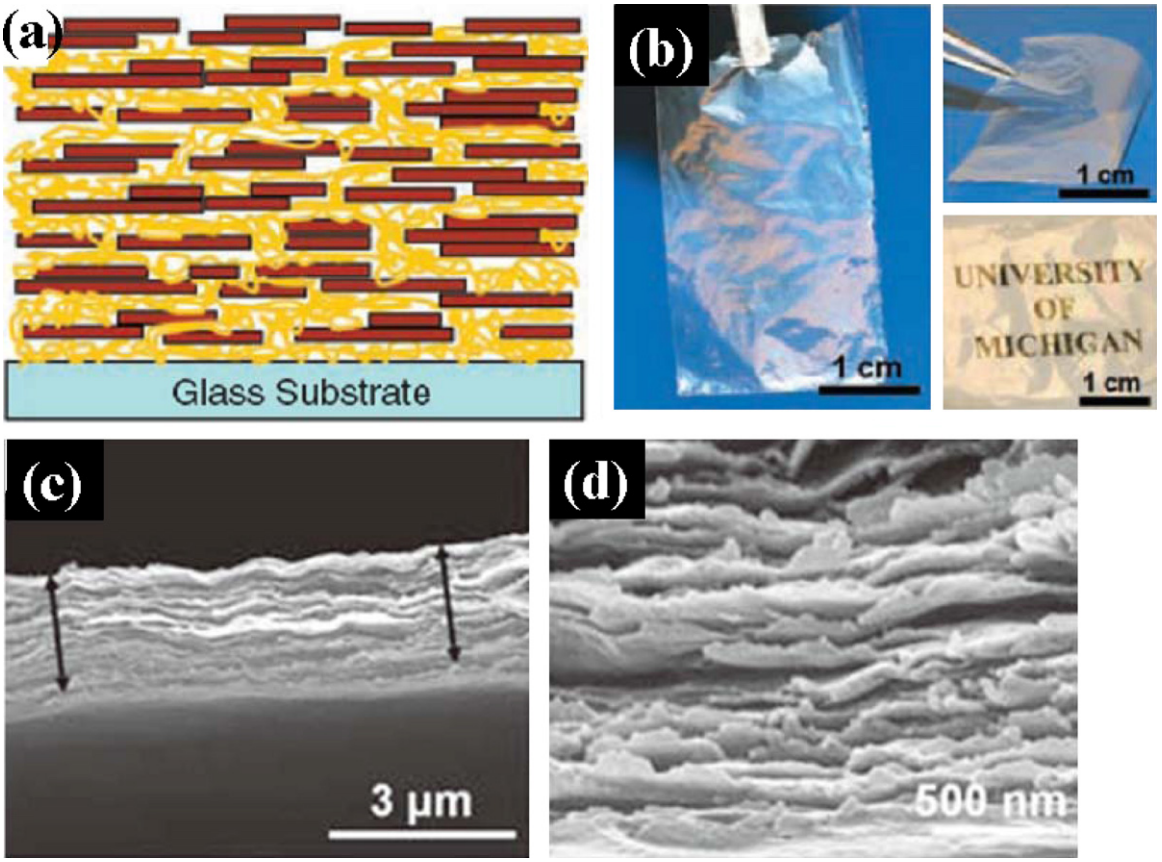

Fig. 7. Flexible and transparent thin film from layer-by-layer process. (a) Schematic illustration for clay unit piling, (b) composite film of PVA/MMT showing high flexibility and transparency and (c and d) cross-section SEM images [133].
© 2007 The American Association for the Advancement of Science.

the unit dispersion before the formation of ordered aligned film structures. Fig. 9d illustrates the different swelling homogeneity of clay units with monovalent and polyvalent cations. The cross-section images of SEM illustrated the uniformity and regularity of the clay alignment (Fig. 9a–c). Three representative films of Li-, Ca-, and Al-MMT showed different alignments in view of the fractured cross-section images. The upper part of the film is laminated with thin sheets, and the lower part is structured with thick large sheets. This difference is particularly prominent in the Al-MMT film with smaller particle units on the top and larger units at the bottom layers. The difference in homogeneity throughout the film thickness implicated the counter ion swelling property in water, which consequently affected the self-aligned morphology. As a result, the interlayer cation affected the self-standing clay film formability and properties attributable to their differing swellability. Montmorillonite samples with monovalent interlayer cations swelled sufficiently and became delaminated. Their flexibility and gas barrier property were correlated to their microstructures.

Flexible and transparent films with clay content of 57 wt% were prepared from Laponite clay and water-soluble poly(ethyleneglycol) (PEG) [144]. The solution casting method with the assistance of triethoxysilane as a sol–gel cross-linking agent generated the hybrid films. The Laponite clay was shown to be intercalated by PEG and further sol–gel cross-linked within the matrix of clay platelets and organic chains as illustrated in Fig. 10. The PEG became amorphous in the clay aligned matrices due to the clay interaction. It was further shown by SEM that the ordered alignment of platelets is parallel to the surface of the film (i.e., in x–z plane). From the small-angle X-ray scattering (SAXS) analysis, the scattering patterns are isotropic in the x–z plane and anisotropic in the x–y plane. In other words, the film had a disco-nematic liquid-crystalline-like structure. These analyses indicated the existence of ordered structure in PEG-modified clay film, and the use of the clay in biomaterials such as tissue adhesive material and artificial skin was proposed.

Polymer NC films with highly aligned clay platelets in epoxy matrix possessed good gas-barrier properties [145]. Films of MMT clay and organic salts of polyethylenimine (PEI)/poly(acrylic acid) (PAA) complex were prepared by the LbL assembly technique and showed a low oxygen permeability rate $<0.002 \times 10^{-6}$ cc/(m day atm). The value is lower than that typically reported for SiOx or multiple EVOH films. The low permeability was believed to be achieved by the ordered nanostructure of the highly oriented clay platelets. It was commented that the film

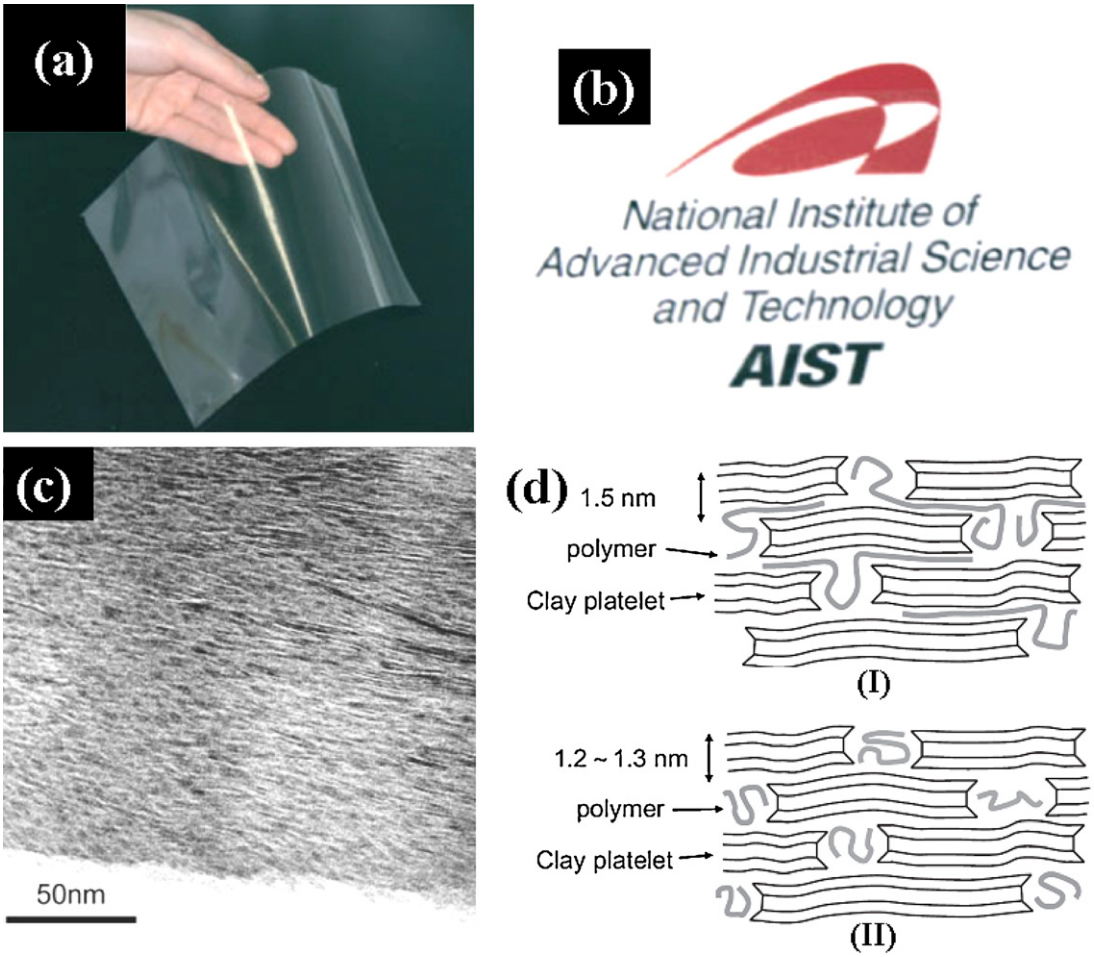

Fig. 8. (a and b) Clay films with flexible, transparent, gas-barrier and thermal stability for optoelectronic devices application. Microstructure of the films: (c) TEM image of a cross-section of the clay film with 20 wt% of carboxymethyl cellulose sodium salt. (d) Schematic representatives of the film microstructures: saponite/carboxymethyl cellulose preventing edge-to-edge and face-to-face clay interactions (I), and saponite/polyacrylic acid preventing edge-to-edge interaction (II) [139].
© 2007 Wiley-VCH Verlag GmbH & Co. KGaA.

transparency of 97.5% was achieved for visible light absorbance with extremely high clay loadings up to ca. 84 wt%. TEM and AFM confirmed the clay platelet orientation parallel to the substrate surface in the same direction of the multiple layers to original polystyrene support surface (Fig. 11). Films with multiple layers of clay–polymer interconnections, which retained flexibility and transparency, have been proposed for packaging applications.

2.5. Clay self-aligned film functions

The regularity of clay sheet stacking in polyethylene oxide (PEO) blended in clay–polyvinyl in clay–polyvinyl pyrrolidone (PVP) nanocomposite films led to lowering of the thermal expansion coefficient (CTE) to ca. 10 ppm/°C, which is similar to that of metals [146]. The heat distortion temperature of the film was much higher than the melting point of PEO. The film also exhibited a much improved gas barrier property, high stiffness, and high strength. The significant improvement in these properties relies on the structure of the clay orientation in the polymer composite. In Fig. 12a, the changes in CTE and heat distortion temperature are plotted against the amount of added clay. It was observed that a critical concentration for the clay loading gave rise to an abrupt change in the property measured. The improvement in the property studied was followed by the percolation of clay loading weight. The cross-section TEM micrograph of the film demonstrated the ordered layer structure (Fig. 12b) and the orientation of the clays parallel to the film plane. The interlayer spacing is 25 Å, which is consistent with that for PVP–clay measured by XRD (Fig. 12c). With a clay addition ca. 20 wt% composition, the significant property improvement was related to the structure of the formed composite. The clay crystal is first intercalated by PVP and this is followed by the stacking of the clay sheets to form a well-ordered intercalated clay crystal. This intercalated clay crystal acts as a nanofiller and directs the crystallization and crystal orientation of the PEO in the composite.

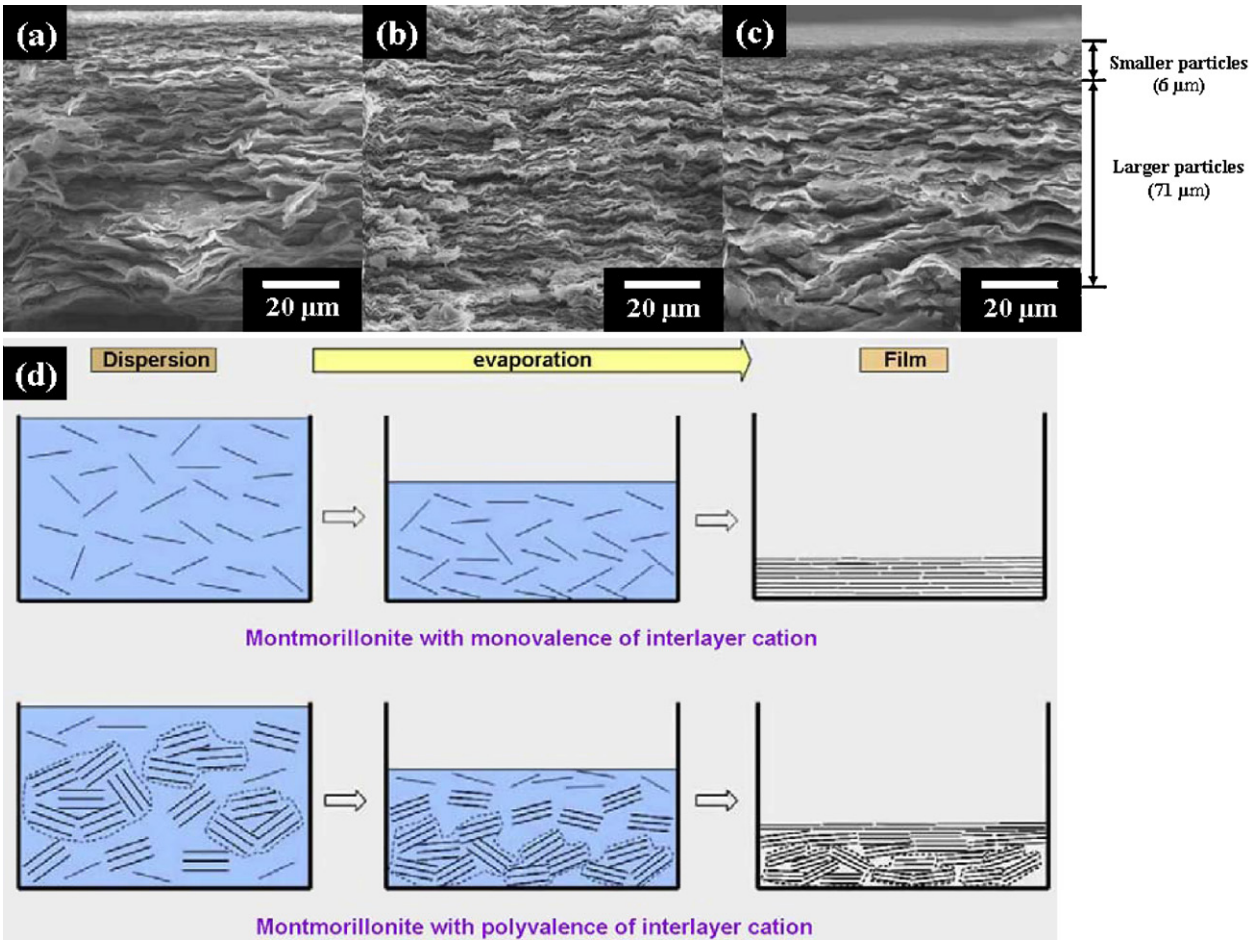

Fig. 9. Fractured cross-section SEM images of the MMT films with different interlayer cations: (a) Li-MMT, (b) Ca-MMT, and (c) Al-MMT. (d) Film formation process from clay swelled aqueous solution by different MMT of low and high valence of interlayer cations [143].
© 2009 Elsevier Ltd.

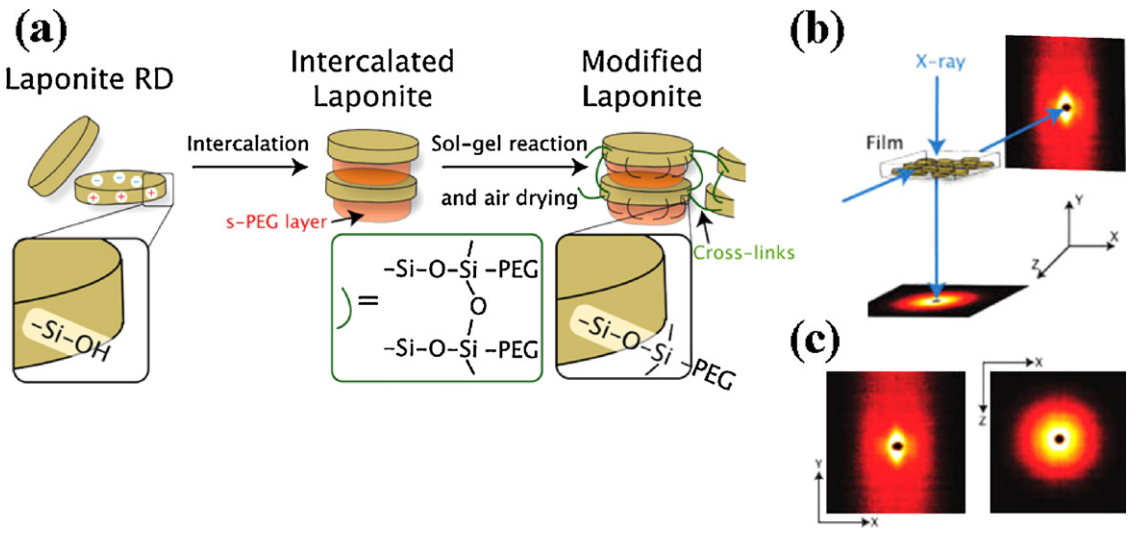

Fig. 10. (a) Schematic illustration of PEG modified Laponite: sol–gel reaction of PEG binding to the silanol of the clay edge and the clay binding into layered structure. (b) SAXS: (c, left) 2D pattern from the *x*–*y* plane or perpendicular to film surface and (right) *x*–*z* plane (i.e., parallel to film surface) [144].
© 2010 American Chemical Society.

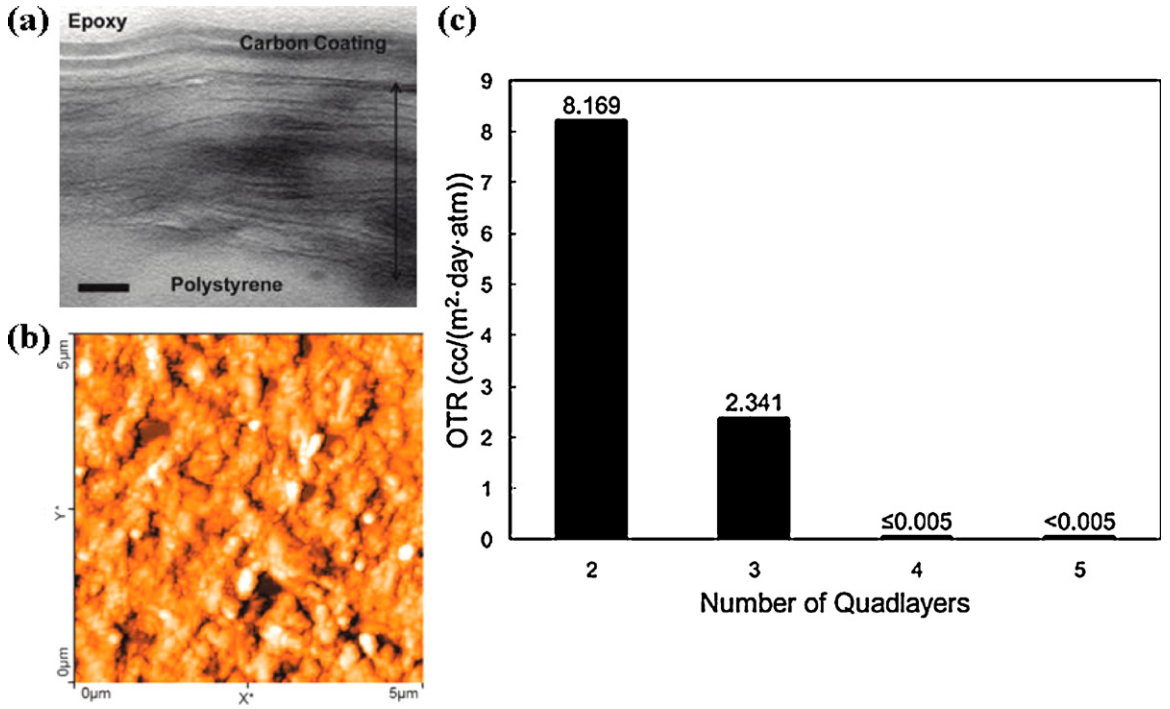

Fig. 11. (a) TEM cross-sectional image of a five quadlayers (QL) thin film deposited on 250 μm polystyrene. Scale bar is 20 nm, and the double arrow spans the film's 80 nm thickness. (b) AFM phase image of a five QL thin film deposited on a polished silicon wafer. (c) Oxygen transmission rate (OTR) as a function of the number of quadlayers deposited on 179 μm thick PET film. "Less than or equal to" and "less than" symbols denote OTR values at or below the low end detection limit for an Ox Tran 2/21 L module, which is 0.005 cc/(m^2 day atm) [145].
© 2010 American Chemical Society.

Clay films can be generally prepared from aqueous solutions of ionic clay and a control amount of water-soluble polymer by simple casting methods and LbL techniques. Taking advantage of the unique platelet structure, ordered arrays can be generated from the interaction of the polymer and clay particle edges. A suspension of Na^+-saponite clay interacted well with sodium polyacrylate. Further treatment with negatively charged semiconductor nanocrystals (NCs) afforded a well-organized structure [147]. The charged NCs were confined in the clay interlayer spaces through strong charge attraction. A highly ordered clay platelet array was uncovered by the XRD analysis. The synthetic strategy employed for the preparation of mercaptopropionic acid capped CdSe/ZnS is illustrated in Fig. 13a. Cross-section HR-TEM characterized the dense coverage of the clay platelets, planar orientation, and NCs location (Fig. 13b). In Fig. 13c, the photoluminescence (PL) emission spectra of the films demonstrated color-emitting NCs as a function of the annealing temperature. It was shown that the PL intensity of the NCs in the clay host was possibly enhanced after thermal annealing at 120 °C. The reason for the enhancement and the role of the clay host are discussed in the article. Fig. 13d shows the emission of three different color-emitting films under a UV-lamp (365 nm). Flexible clay films confining NCs were suggested for future optoelectronic light-emitting devices.

The clay self-assemblages appear to control surface roughness, giving rise to the notion of a super hydrophobic effect [65]. Film surfaces with high water-droplet contact angle of 157° and micrometer roughness (Fig. 14) were fabricated from the clay platelets that were exfoliated from Na^+-MMT in complexation with hydrophobic alkyl amine-salt. The film surfaces resembling lotus leaves were possibly fabricated from the self-aggregation of the silicate clay units associated with the hydrophobic organics. The surface roughness in micrometer scale was attributed to the self-assembly of the clay platelets with strong piling forces and balanced with the interference of organic hydrophobes. Two different non-covalent bonding interactions involving ionic attractions and hydrophobic effects co-existed during this hierarchical aggregation from nanoscale units to micrometer-scale roughness.

It was reported the exfoliated nanoscale silicate platelets (NSP) could be covalently tethered with a thermo-responsive PNIPA by organic linking initiators and copper ion-catalyzed atomic transfer radical polymerization (ATRP) [148]. A novel class of organic–inorganic hybrids under a controlled environment exhibited a self-assembly and phase separation to form a 3D nanodomain as shown in Fig. 15. The high molecular weight of PNIPA grafted on NSP surface exhibited two distinctive second-order transitions in differential scanning calorimetery analysis, indicating the existence of dual-segment density zones. It was explained that polymer fixation on clay surface greatly inhibited chain relaxation movements and hindered reversible coil–globule transitions. Furthermore, a thermally induced self-assembly on the silicon wafer surface was observed. The coated thin film showed a regularity

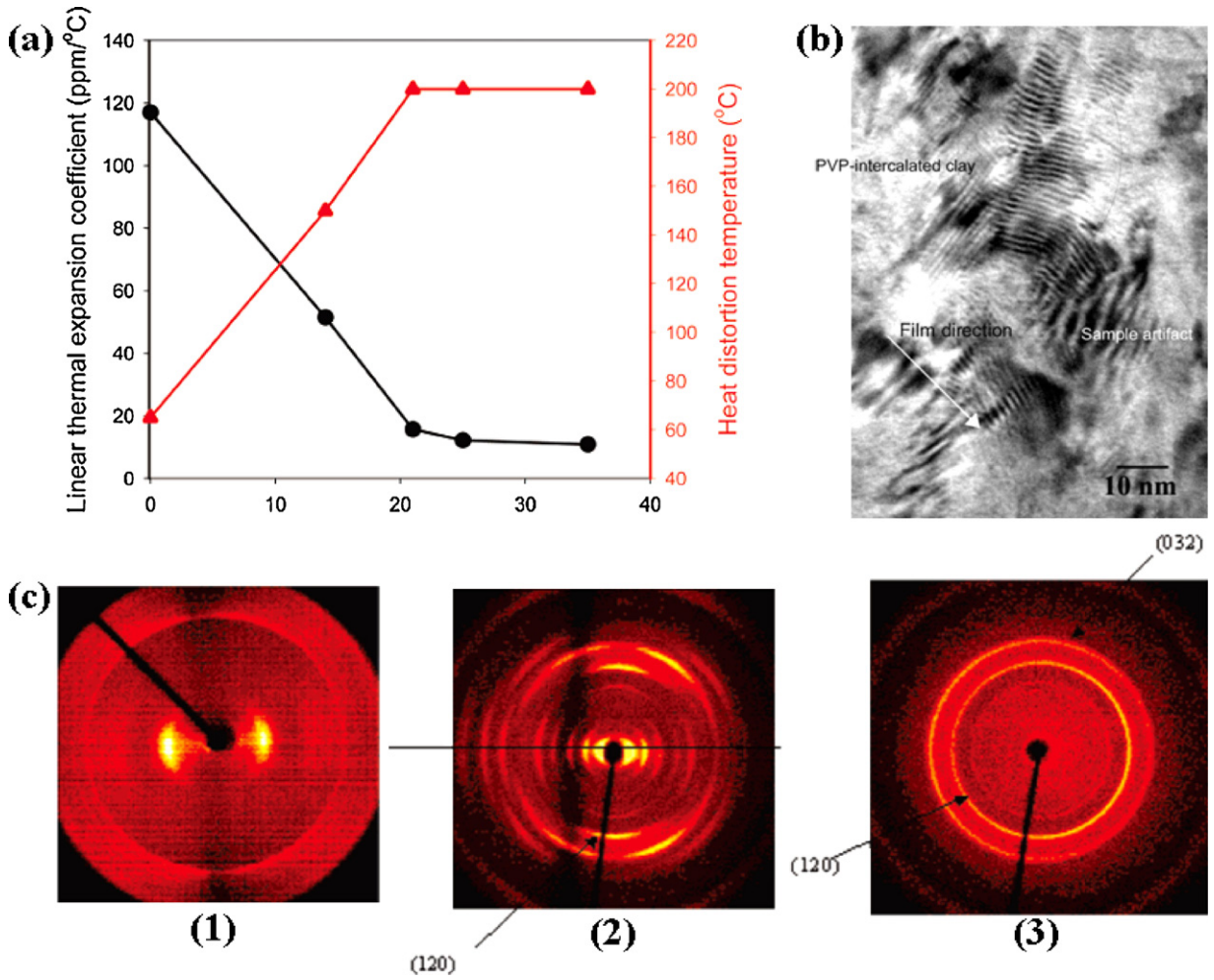

Fig. 12. (a) Thermal properties of PEO and clay in PVP nanocomposite films: a critical composition fraction at ca. 20 wt% for the rapid improvement for both CTE and heat distortion temperature. (b) TEM of the film cross-section. (c) Two-dimensional X-ray diffraction patterns for (1) Cloisite Na^+ clay, edge alignment, (2) PEO–clay (PVP) nanocomposite, 76/12(11) volume ratio, edge alignment, (3) PEO–clay (PVP) nanocomposite, 76/12(11) volume ratio, surface alignment [146].
© 2008 American Chemical Society.

of 3D network nanostructures. An ordered domain network of 100–500 nm was the result of temperature-controlled phase separation as shown in Fig. 15. It was noted that the formation was directed by the platelet shape and also the PNIPA chains had an influence at temperatures higher than the LCST.

2.6. Clay utilization in association with various polymers

Clay chemistry involving non-covalent interactions with various polymers has been documented in the recent literature. A large number of hydrophilic polymers for interacting with the clays have been described, and it is possible to classify these according to their polymeric structure and performances as summarized in Table 1. The clay platelets strongly contribute to the interactions with the polymers forming self-organized nanocomposites such as hydrogels and films.

3. Intercalation and exfoliation of layered clays

3.1. Intercalation with alkyl quaternary and polymeric amine-salts

Intercalation of the layered silicate clay can be performed by the ionic exchange reaction of the counter ions in the interlayer with low organic quaternary ammonium salts. As a result, the hydrophilic and water-swelling clays are converted into hydrophobic organoclays. When intercalating organics are employed, the clay layer basal spacing is expanded and can be easily accessed by hydrophobic monomers or polymers. Thus, the organoclays become compatible with the subsequent steps of exfoliation into silicate platelets and homogeneous dispersion in polymer matrices. Organic surfactants such as alkyl quaternary ammonium [149–154] and phosphonium [155–160] salts are commonly used for the exchange reaction with the counter ions and modification of the clay interlayer

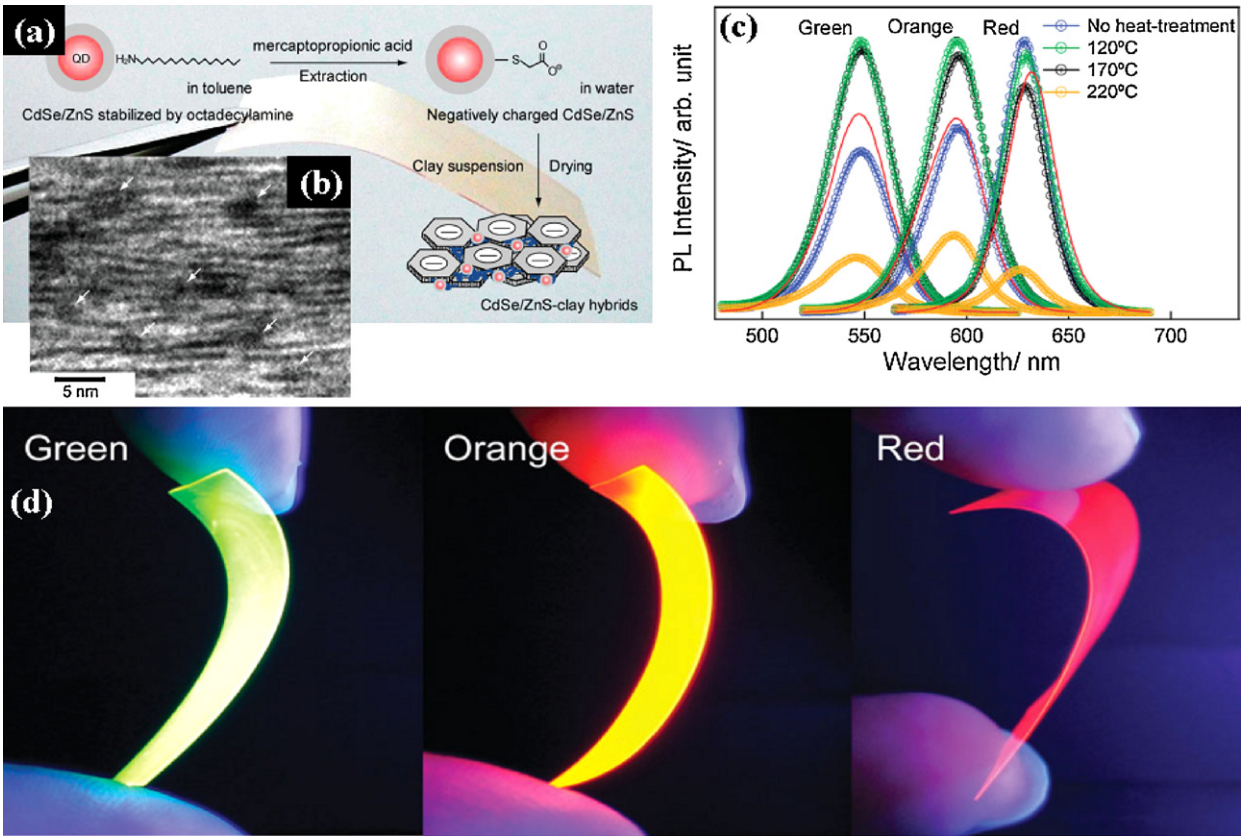

Fig. 13. (a) Schematic illustration of the flexible CdSe/ZnS–clay film preparation process. (b) Cross-sectional high-resolution TEM image of green-emitting CdSe/ZnS–clay film. The image shows some of the CdSe/ZnS NCs appeared in dark spot (indicated by arrows) within the clay layers. The mean diameter of the NCs is 2.4 nm, and the interplanar distance of the clay layers is ca. 1.26 nm. (c) Photoluminescence emission spectra of CdSe/ZnS–clay films with three different color-emitting nanocrystals as function of annealing temperature. The red lines are those of the initial nanocrystals in toluene. (d) Emission images of the flexible CdSe/ZnS–clay films with different-size nanocrystals excited using an ultraviolet lamp (365 nm) [147]. (For interpretation of the references to color in this figure legend, the reader is referred to the web version of the article.)
© 2008 Wiley-VCH Verlag GmbH & Co. KGaA.

spacing. Low-molecular-weight organic salts widen the gallery spacing from the original 12 Å to 20–50 Å. Other organic ions including the imidazolium ionic liquid salts with C_{12}, C_{16}, and C_{18} alkyl chains were reported as effective modifiers in preparing polymer nanocomposites [161–164].

Poly(oxyalkylene)-polyamine hydrochloride salts used to widen the silicate basal spacing have also been reported in addition to intercalation by common alkyl surfactants [165]. The commercially available poly(oxyalkylene)-amines include hydrophobic poly(oxypropylene)-backboned (POP-) and poly(oxyethylene)-backboned (POE-) mono-, di-, and tri-amines (Fig. 16). The POP-diamines in the range of 230–4000 g/mol M_w were converted into the corresponding hydrochloride salts and further incorporated into the MMT layered silicates. The widening of clay basal spacing usually depended on the end-to-end polymer chain length or the corresponding molecular weight of the POP backbones. With the POP-diamines of 2000 and 4000 g/mol molecular weight, the layered structure can be largely expanded up to 58.0 and 92.0 Å basal spacing, accordingly. The interlayer expansion was proportionally dependent on the stretched POP end-to-end length and gave an indication of the POP hydrophobic phase separation in the interlayer confinement. The generation of POP hydrophobic phase in the clay interlayer structure is the driving force for stretching basal spacing that was originally constricted by the existence of counter ion charge attractions in the neighboring platelets. It was reported that the hydrophobic phase segregation occurred in a critical manner similar to the critical micelle concentration (CMC) in surfactant chemistry [166]. In contrast, the use of hydrophilic POE-diamines resulted in only a low spacing expansion (ca. 20 Å) and none of hydrophobic phase formation in the interlayer spacing was observed, regardless of the polymer length. The cause for this was that the POE molecules are hydrophobic and compatible with the silicate platelet surface. The intercalation of POE involved the flat arrangement of POE backbone parallel to the platelet surface rather than generating a new hydrophobic phase. This indicated that the clay interlayer space widening can be controlled by the type of organic intercalating agents and a hydrophobic aggregation of organics in silicate lamellar structure is an essential factor for enlarging interlayer spacing. On a molecular level, the hydrophilic POE backbones were

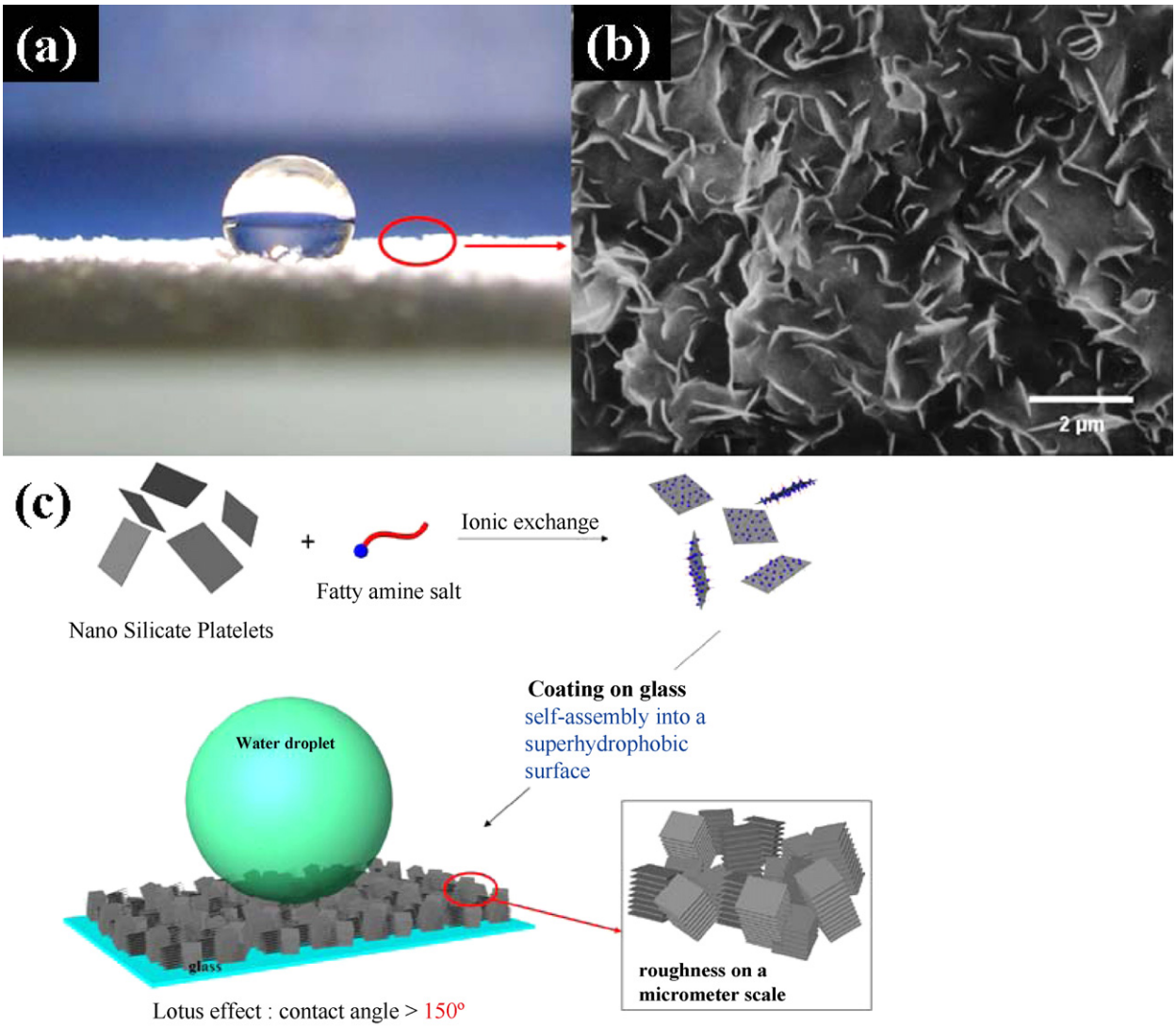

Fig. 14. (a and b) The correlation of water droplet contact angles and surface morphologies according to SEM images and (c) conceptual representation of lotus surface from silicate platelets [65].
© 2006 Wiley-VCH Verlag GmbH & Co. KGaA.

intercalated in the layered confinement aligning in parallel to the silicate surface. The understanding of the essential hydrophobic effect on clay intercalation offered an opportunity of tailoring the hydrophilic/hydrophobic properties of organoclays.

By grafting the POP-amine onto anhydride-functionalized polyolefins, the resultant amphiphilic copolymers were found to be suitable intercalating agents. A wide range of intercalated organoclays with hydrophilic/hydrophobic balanced properties could be prepared accordingly. The intercalating copolymers perform an ionic exchange reaction with the counter ions and hence become incorporated into the clay spacing. The structural varieties are summarized in Fig. 16 for three different copolymer backbones with multiple grafting of POP-amines. The comb-like shape of copolymers include POP-amine grafting poly(propylene-maleic anhydride) (PP-g-MA) [166,167], poly(styrene-ethylene/butadiene-styrene) (SEBS) [168], and poly(styrene-maleic anhydride) (SMA) [169]. These structures are common for functionalities with cationic amine-salts and hydrophobic POP blocks of different molecular weights. These polyvalent and amphiphilic copolymers were found to be effective intercalating agents. The multiple amine pendants in the structures were treated with hydrochloride and a fine emulsion was obtained in water. Subsequent intercalation with sodium montmorillonite [167] afforded clay–copolymer hybrids with high basal spacing and emulsion properties. The intercalated silicate hybrids can be considered as rigid micelle structures comprising inorganic silicates and hydrophobic copolymers in the ionic complexes, In the case of copolymers containing SEBS and SMA backbones, XRD analysis revealed the *d* spacing from 17 Å to 52 Å and 78.0 Å could be obtained depending

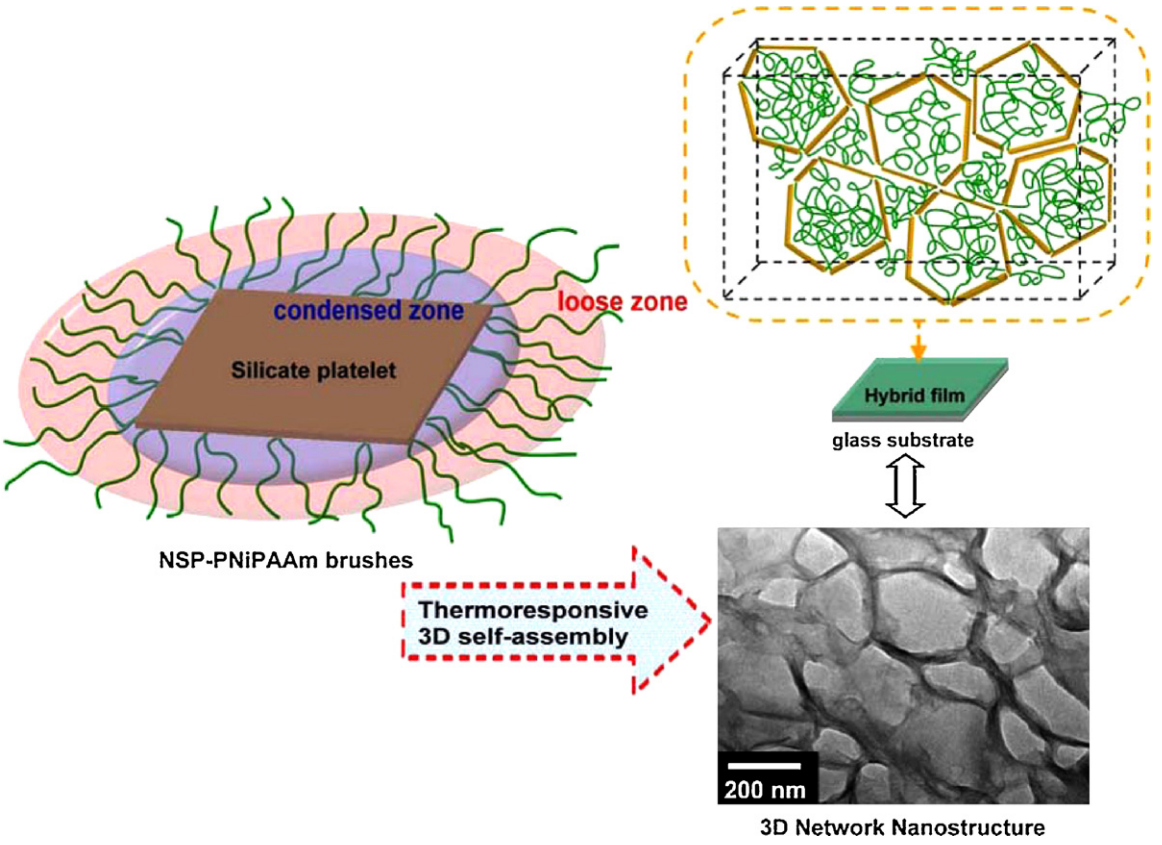

Fig. 15. Covalently bonded NSP–PNIPAAm hybrids exhibited dual phase of thermo-responsiveness and enabled to self-assemble into 3D nanodomain network with high regularity [148].
© 2009 American Chemical Society.

on the intercalating agent. The hydrophilic/hydrophobic properties of layered silicate–polymer hybrids could be attenuated and allowed for lowering of the toluene–water interfacial tension to as low as 5 mN/m [166,168,170].

3.2. Layered structure of organoclays

The layered silicate structure of the natural clays can be modified by embedding hydrophobic organics or polymers via an ionic exchange intercalation. The intercalated organoclays can be expanded into different degrees of interlayer spacing and incorporated using controlled amounts of hydrophobic organics. The organoclays possess the property of hydrophilic/hydrophobic amphiphilic balance and disperse in organic media in contrast to the original water-swelling character of pristine clay. Moreover, the amphiphilic character of the clay units can be tailored for both interlayer basal spacing and amounts of organics present depending on the hydrophobic nature of the organics incorporated. In Table 2, the equivalent ratios of POP organics intercalated into MMT mainly affected the spacing enlargement of clay galleries and dispersion ability in aqueous or organic media [171]. The POP/MMT complexes, derived from the POP amine of 2000 M_w, exhibit an X-ray diffraction basal spacing of 19–20 Å for 0.2–0.8 CEC equivalent exchange and 58 Å for 1.0 CEC equivalent with organic contents (by TGA) ranging from 22 to 63 wt%. The amphiphilic nature was further enhanced by their ability of lowering the surface tension at the water–air interface, for example, from 70 to 41 mN/m at 1 wt% of organoclay. The interfacial activity was mainly controlled by the POP hydrophobic effect. From the viewpoint of surface active agent (surfactant), the inorganic clay–organic hybrids with multilayered silicate rigidity and alternative hydrophobic POPs can be considered as similar to soft micelles of organic surfactants or phase segregation of a block copolymer.

The fundamental geometric structure of the organoclays has been well characterized by XRD and tapping-mode atomic force microscope (AFM) for individual units. The samples were first homogeneously dispersed in water and spin-coated on a glass substrate. The individual clay units can be clearly visualized in detailed 3D structure in terms of platelet shape and alternating organic-silicate lamella in the representative AFM phase images [58]. The average clay units were polydispersed in a manner consistent for their polygonal shape with dimensions in the range of 70–90 nm from a top-view microgram (Fig. 17a and b) for two representative POE-2000 and POP-2000 intercalations. The phase image from the magnified picture is shown to be more or less a square shape with a multilayered shadow. From the topographical view the measurement for the

Table 1
Recent developments of clay utilizations in association with various polymers.

Polymers	Clays	Performance	Clay contribution	References
Poly(*N*-isopropylacrylamide) (PNIPA)	Laponite XLG	(NC hydrogel) Transparent, elongation of 1000%, mechanical properties	Pseudo-cross-linking	[119–130]
Poly(vinyl alcohol) (PVA)	Na^+-MMT	(Clay–polymer film) Large-area, lightweight, thick nacre-mimetic films, tensile strength	Ordered multilayer structures	[131,133–138]
Poly(diallyldimethyl-ammonium chloride) (PDADMAC)	Na^+-MMT	(Clay–polymer film) Lightweight, nacre-mimetic paper, fire-shielding properties	Ordered multilayer structures	[132]
Sodium polyacrylate (SPA)/sodium carboxymethyl cellulose (SCE)	Na^+-saponite	(Clay–polymer film) Flexible, transparent, heat-resistant, gas-barrier, luminescent	Ordered multilayer structures	[139–141]
Polyethylenimine (PEI)	Na^+-MMT	(Clay–polymer film) Clay composition up to 84 wt%, low oxygen permeability	Ordered multilayer structures	[142]
Poly(ethyleneglycol) (PEG)	Laponite RD	(Clay–polymer film) Flexible, transparent	Ordered multilayer structures	[144]
Polyethylenimine (PEI)/poly(acrylic acid) (PAA)	Na^+-MMT	(Clay–polymer film) Flexible, transparent, gas-barrier	Ordered multilayer structures	[145]
Polyethylene oxide (PEO)	Na^+-MMT	(Clay–polymer film) Low thermal expansion coefficient	Ordered layer structure	[146]
Poly(styrene-co-maleic anhydride) (SMA)	Nano silicate platelets	(Clay–polymer film) Superhydrophobic effect, lotus effect	Ribbon like morphology	[65]
Poly(*N*-isopropylacrylamide) (PNIPA)	Nano silicate platelets	(Clay–polymer film) Lower critical solution temperature	3D nanostructures	[148]
2-Carboxyethylphosphonic acid	MgAl-LDH	(Clay–polymer film) Multilayered nanostructural films	Ordered multilayer structures	[183]
None	Na^+, Li^+, Mg^{2+}, Ca^{2+}, Al^{3+}, and $Fe^{2+,3}$-MMT	(Clay film) Flexible, gas-barrier	Ordered multilayer structures	[143]
DNA	MgAl-LDH	(Clay–DNA hybrid) Drug delivery, drug controlled release	Biomaterial encapsulation	[118]
Bovine serum albumin (BSA)	Na^+-MMT/Mica	(Clay–protein hybrid) Drug delivery, drug controlled release	Biomaterial encapsulation	[58,59]

unit heights was found to be 22.3 nm for POE and 38.8 nm or 52.9 nm (for a more accurate measurement under magnification) for POP. Since both samples were derived from the same pristine MMT sample, the observed height was related to the number of layers in a primary unit. In reference to the XRD measurement, the layer multiplicity was calculated to be around 8–10 platelets for both samples on average. The POE and POP intercalation exhibited different backbone alignment conformation in the galleries. The hydrophobic aggregation occurred for POP organics, and the amount incorporated directly affected the interlayer expansion. For the POE intercalation, neither hydrophobic aggregation nor large expansion for interlayer spacing was observed. The fundamental clay dimension of POP/MMT (5.8 nm *d* spacing by XRD analysis) illustrated an average height of 38–52 nm from the AFM topographical image. It

Table 2
Adjustable XRD basal spacing, organic content in interlayer spacing and dispersing properties of the POP2000-amine-salt intercalated MMT at various POP equivalents to clay cationic exchange capacity (CEC) [171]. Copyright 2004, Wiley-VCH Verlag GmbH & Co. KGaA.

POP-amine equivalent to CEC of MMT	*d* spacing (Å)[a]	Weight fraction or O/I ratio (w/w)[b]	Dispersion[c]	
			H_2O	Toluene
0.2	19	22/78	+	–
0.5	20	34/66	+	–
0.8	20	46/54	+	–
1.0	58	63/37	–	+

[a] *d* spacing by X-ray diffraction.
[b] Weight fraction of intercalated organics/silicates (measured by TGA).
[c] +: dispersible; –: aggregate (0.1 g sample in 1.0 g solvent).

amounted to 58 nm, equivalent to 5.8 nm *d* spacing times the platelet number of 8–10 in a stack. The estimated number of 8–10 platelets in one stack corresponded well to the observation of the pristine MMT unit by TEM analysis [172]. As shown in Fig. 17c, the heights were measured to be ca. 40–42 nm for POP2000/MMT organoclay, which is also consistent with the average number of 8–10 platelets. By comparison, the primary units of Mica had been observed to be 500 nm × 500 nm × 1 nm.

3.3. Exfoliation of the layered structure into individual platelets

Since the counter ions can be exchanged by organic ions, the clay layered structure can be modified through ionic exchange reaction. Besides organic intercalation, exfoliation or randomization of the clay crystalline into individual platelet units can be achieved by another design of amphiphilic copolymers with polyvalent amine-salt exchanging sites [167]. Several different mechanisms have been reported (Fig. 18) [97,167,173–175]. The structurally designed amphiphilic copolymers with a proper balance of hydrophobic backbone and ionic charge force were effective in rendering the randomization of the layered structure. In one of these copolymer intercalations, the intermediate of organic-intercalated hybrid underwent a phase inversion from a layer-stacked structure to random platelets. In this case, the clay exfoliation to individual platelet is a thermodynamically controlled process since water is the continuous phase in contacting the exposed ionic platelets. The mechanism was similar to the surfactant water-in-oil to oil-in-water conversion. Another mechanism was reported for the Mannich type reaction of POP-phenol and polyether amines for exfoliation [173,174]. In the structure, the linear shape of multiple amine-salt in the backbone is flexible enough to form a twisted zigzag conformation within the clay galleries. Depending on the segmental length of amine-salt in the backbone and the interacting sites to the silicate surface, the copolymers can accumulate in the galleries and generate hydrophobic phase to stretch the platelet distance into randomization. It was also reported that the exfoliated silicate platelets could be subsequently isolated by a toluene extraction by recycling the polymeric amines with sodium hydroxide. The general process for the exfoliation of several clays including MMT and Mica is conceptually described in Fig. 19. The involvement of the polyamine-salt required the polymeric agents to be water-soluble or fine emulsions in order to enter the clay confinement. The ionic character of the copolymers allows an exchange reaction with the clay counter ions for enlarging the layered structure (intercalation).

The exfoliation of silicate clays was affected by the designed polyvalent amine-salts through the ionic exchange reaction and subsequent randomization of the layered structure into individual platelets. The exfoliated clay platelets can be isolated in water by extractive separation of the polyamine using a biphasic toluene/water process. After a pH adjustment for the amine solubility,

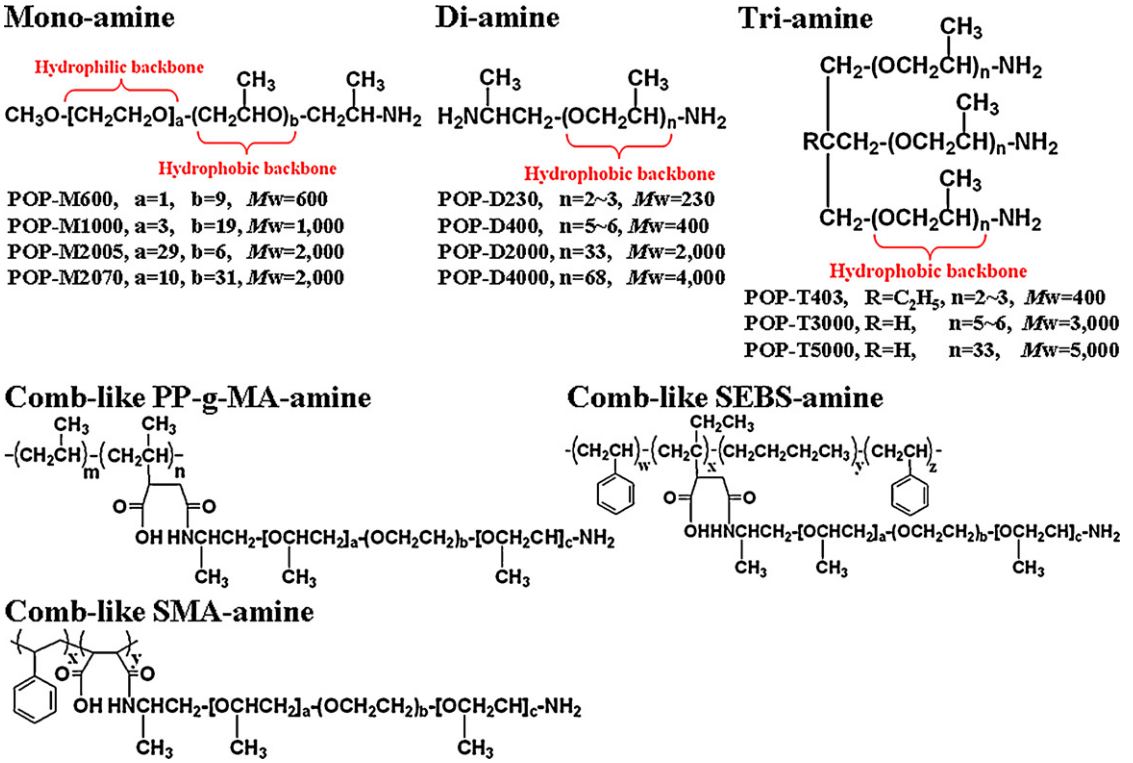

Fig. 16. The structural variations of poly(oxyalkylene)-amines and their grafted polyolefin amphiphilic copolymers.

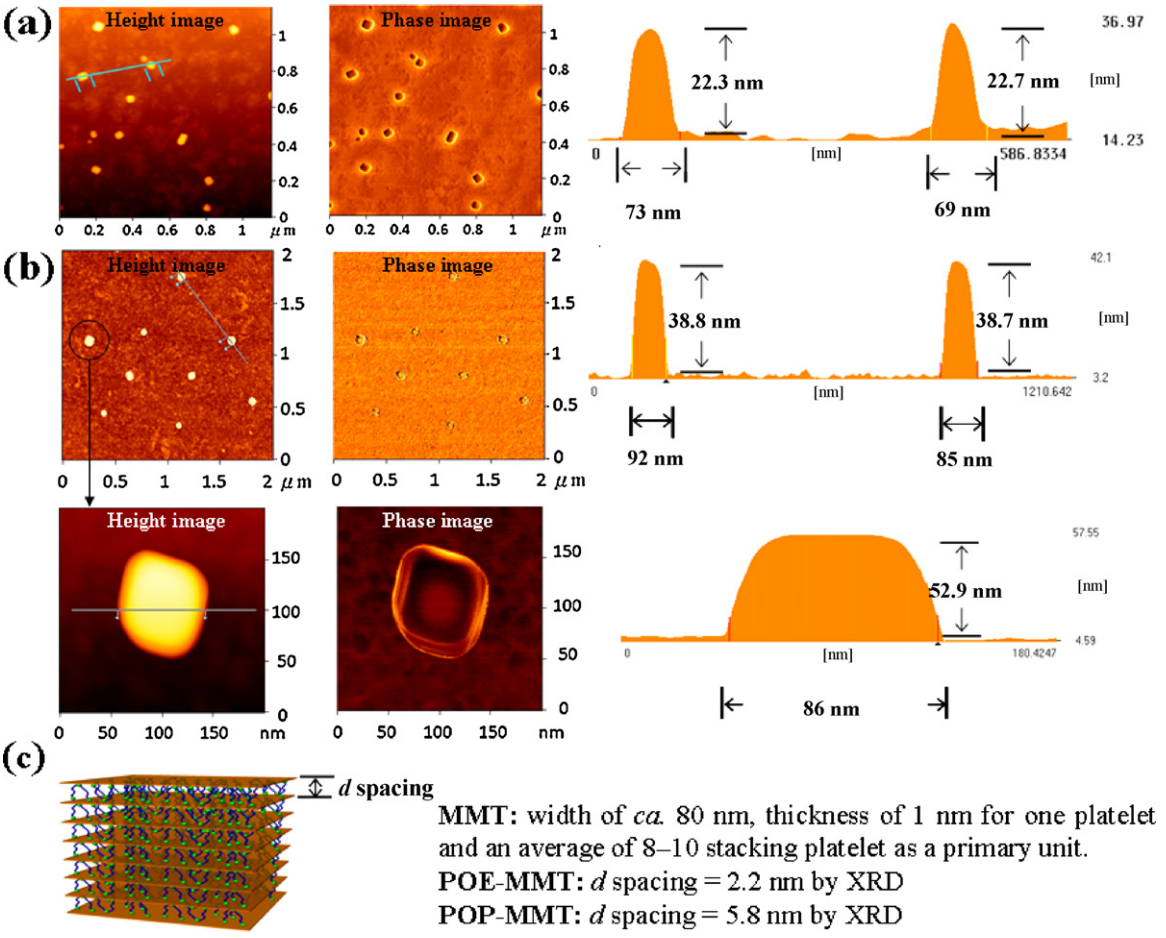

Fig. 17. AFM direct observation of the primary organoclay units for the topographical height and phase image: (a) primary structure of POE2000-MMT, (b) primary structure of POP2000/MMT, and their magnified images, (c) conceptual drawings for the model of multiple-layer structure with reference to XRD analyses for two organoclays [58].
© 2007 American Chemical Society.

repetitive toluene/water extraction removed the organic contamination and afforded the silicate platelets in water. The isolated platelet possessed the same chemical composition as the pristine clay but in a random manner. As a result, the exfoliation generated the same silicate platelets with total exposure of surface charges. The exfoliated platelets have been characterized by zeta potential for ionic character [174], TEM for top-view morphology, and AFM for thickness. While the pH-dependent ionic character was different from the pristine MMT stacks, direct observation elucidated their individual physical appearance and dimension. As shown in Fig. 20, the platelets from MMT were polygonal and circular shapes of 80–100 nm for their lateral dimensions and 1–2 nm in thickness. The platelets from the fluorinated mica clay were also polydispersed polygons 300–1000 nm in diameter and 1–2 nm in thickness (Fig. 21). It was estimated that there were 18,000 ions on an average platelet and 4×10^{16} platelets/g of the weight. The platelets are of thin-platelet geometric shape ca. 1–2 nm in thickness and their surface charged as indicated in Fig. 22. The platelets with high surface charges tended to interact well with polar organic compounds such as polyethylene glycol and also formed hydrogels in water at concentrations ~5%. To illustrate the surface properties, the average surface charge density was estimated on the basis of the pristine MMT with the cationic exchange capacity (CEC) of 120 meq./100 g and surface area of 720 m^2/g:

$$\text{ionic surface charge density} = \frac{\text{surface area}}{\text{CEC} \times \text{Avogadro's number}}$$

$$= \frac{72 \times 10^{20}\ \text{nm}^2/\text{g}}{1.2 \times 10^{-3}\ \text{eq./g} \times 6.02 \times 10^{23}} \cong 1\ \text{nm/cation}$$

The anionic clays, LDH, can be expressed by the general formula $[M_{1-x}^{2+}M_x^{3+}(OH)_2]A_{x/n}^{n-} \cdot mH_2O$ where the metal ions are Mg^{2+}, Ni^{2+}, Cu^{2+}, or Mn^{2+} for divalent and Al^{3+}, Fe^{3+}, or Cr^{3+} for trivalent cations, while A^- is an anion such as OH^-, F^-, Cl^-, Br^-, NO_3^-, CO_3^{2-}, and SO_4^{2-}. Partial M^{2+} to M^{3+} substitution induces positive charge for the layers and counter anion in the interlayer galleries [98]. Exfoliation of LDHs can be performed in polar organic solvents such as formamide to produce colloidal slurries, which allow the coating into transparent and unit-oriented films [176]. The platelets have proven to have a strong

Amine-terminating Mannich oligomers

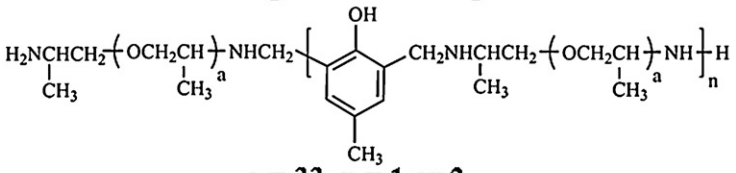

a = 33, n = 1 or 2

Amine-terminating Epoxy oligomers

Linear structure

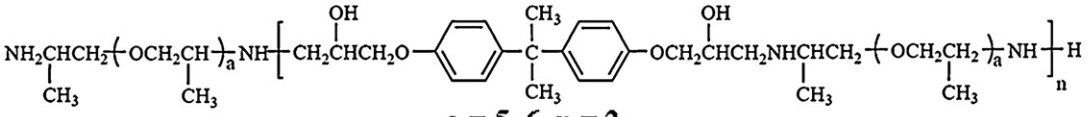

a = 5~6, n = 2

Branched structure

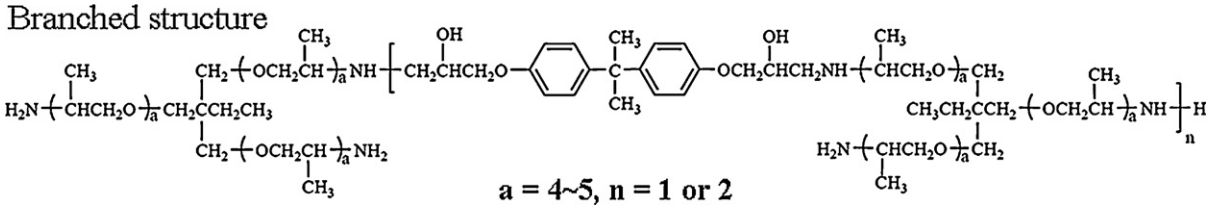

a = 4~5, n = 1 or 2

Fig. 18. The structural design of the polyvalent exfoliating agents including Mannich oligomers, linear and branched bisphenol-A condensates.

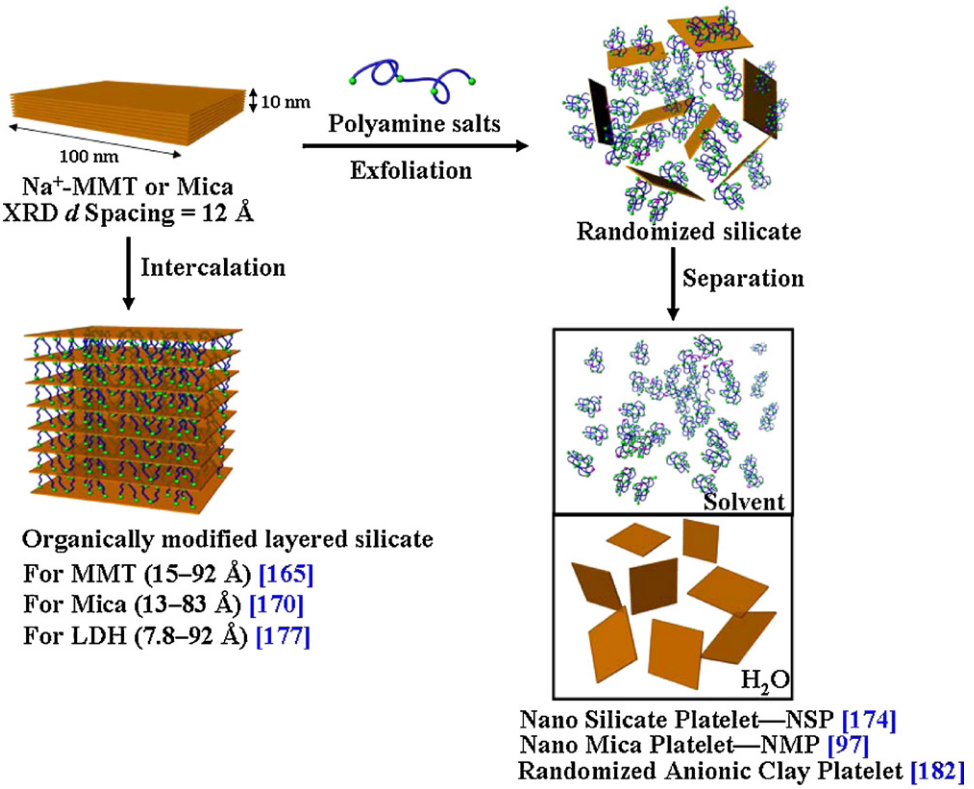

Fig. 19. Conceptual description for intercalation and exfoliation by polyvalent amine-salts as ionic exchange agents.

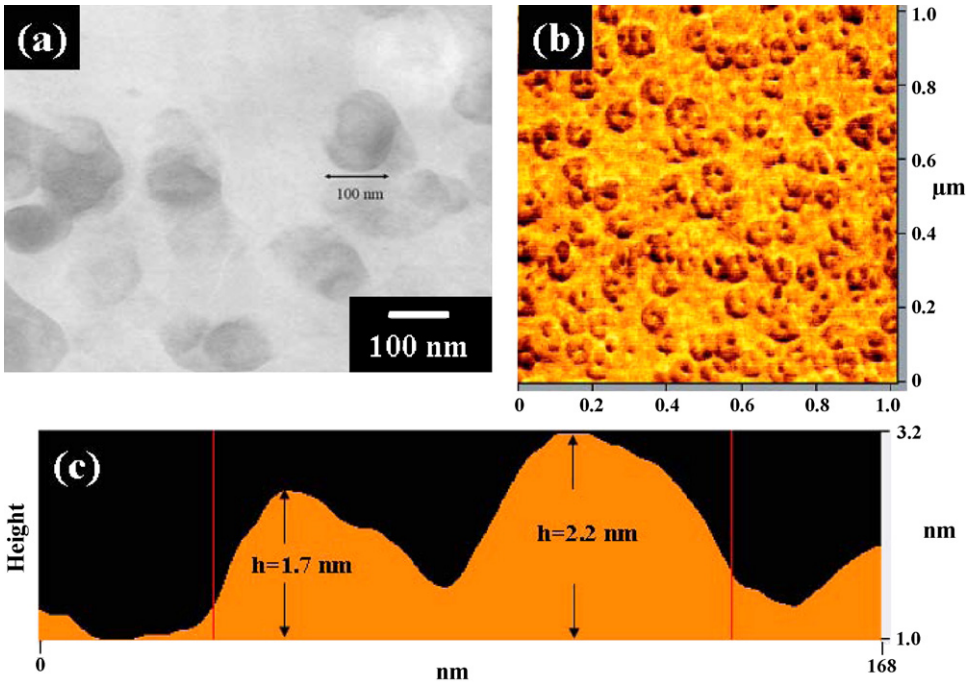

Fig. 20. (a) TEM and (b and c) AFM micrographs of exfoliated silicate platelets suspended in water (0.1 wt%) [174].
© 2006 American Chemical Society.

tendency to rest on their largest faces rather than settling under gravity. C-oriented films on the vertical sides of glass substrates were observed. The sharing of surface anions between platelets or specifically face-to-face platelet aggregation was reported. Along with the edge-to-edge type interaction, a uniform densely packed c-oriented LDH film was generated. For larger polydispersed particles, edge-to-face interactions became more significant and

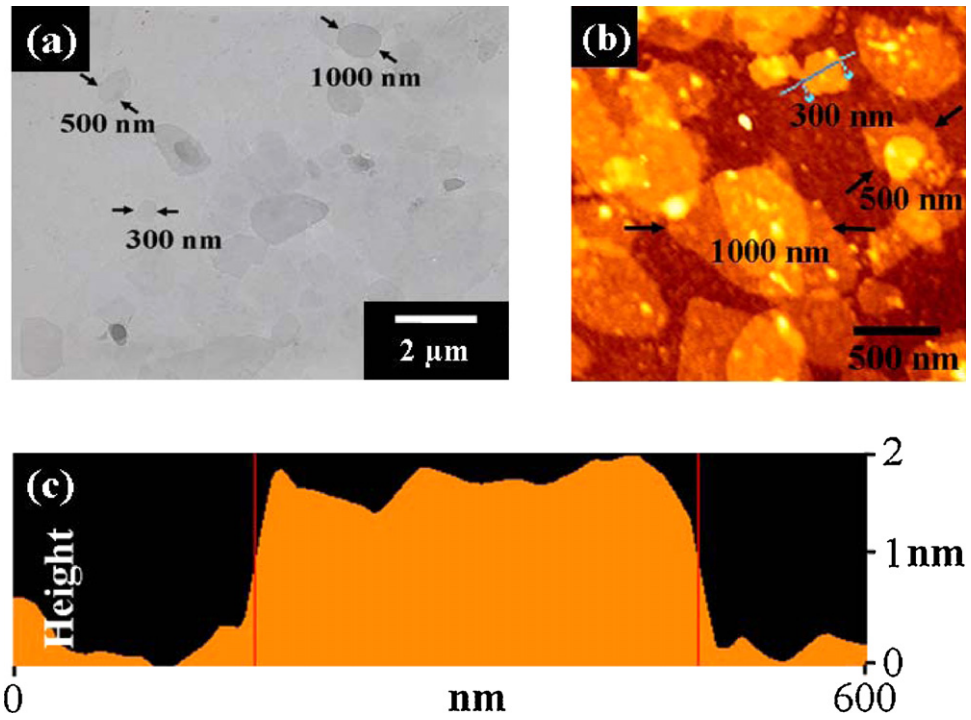

Fig. 21. (a) TEM and (b and c) AFM micrographs of individual Mica platelets suspension [97].
© 2008 American Chemical Society.

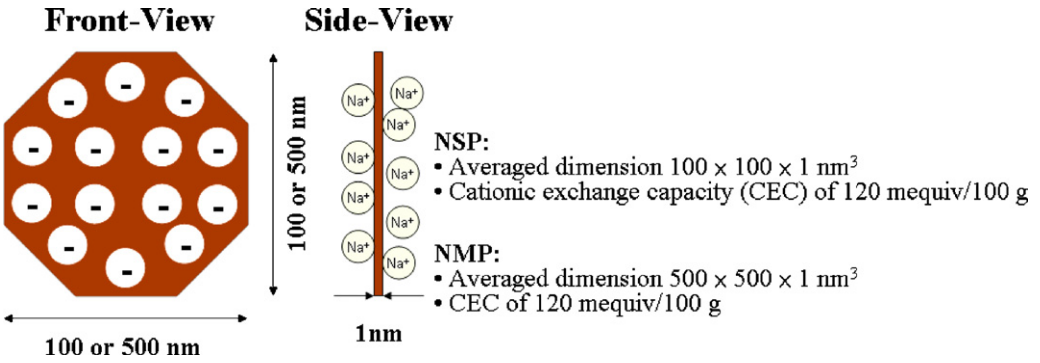

Fig. 22. Conceptual representation of the exfoliated silicate platelets of NSP from MMT and NMP from Mica.

led to inter-particle porosity. The expansion of interlayer spacing was reported by replacing the counter anions with organic ions such as fatty acid salts and anionic surfactants [177–181]. The organic incorporation substantially weakened the clay crystalline structure. The randomization was simply achieved by refluxing the Zn–Al LDH intercalated with dodecyl sulfate solution in alcohol at 120 °C [178]. Similar procedures were reported using amino acids as the intercalating agents and further treating with formamide solvent [179,180]. The example of intercalation and exfoliation procedures for anionic LDH is summarized in Fig. 23 [182]. The oxidative intercalation process involved the addition of iodine in chloroform and the Co^{2+}–Fe^{3+} LDH with perchlorate anions was further delaminated into unilamellar nanosheets in formamide. The intercalated LDH and its exfoliated nanosheet were observed by SEM and TEM on the top view. The synthesis of metal-oxide nanosheets allows the uses of these LDH as potential building blocks for two-dimensional thin layer devices.

The preparation of multilayered nanostructural films from anionic LDH rigid tactoids using LbL technique has been described [183]. Through the alternative interaction with 2-carboxyethylphosphonic acid or other acids, the ionic exchange reaction with the positively charged surface of MgAl-LDH allowed the formation of organic–inorganic clay assembled film in ordered multilayer structures. The LDH complexes are plate-like or disc-like structures with an average diameter of several hundred nanometers and thickness of about 100 nm. Increasing thickness of continuous coverage and ordered orientation on Si surface can be fabricated from multiple layers of LDH unit self-alignment, as shown in the SEM images in Fig. 24. The self-assembly of the additional layers proceeded by unit face-to-face stacking, and the resulting structure was uniform throughout the entire substrate. The measurement of basal spacing

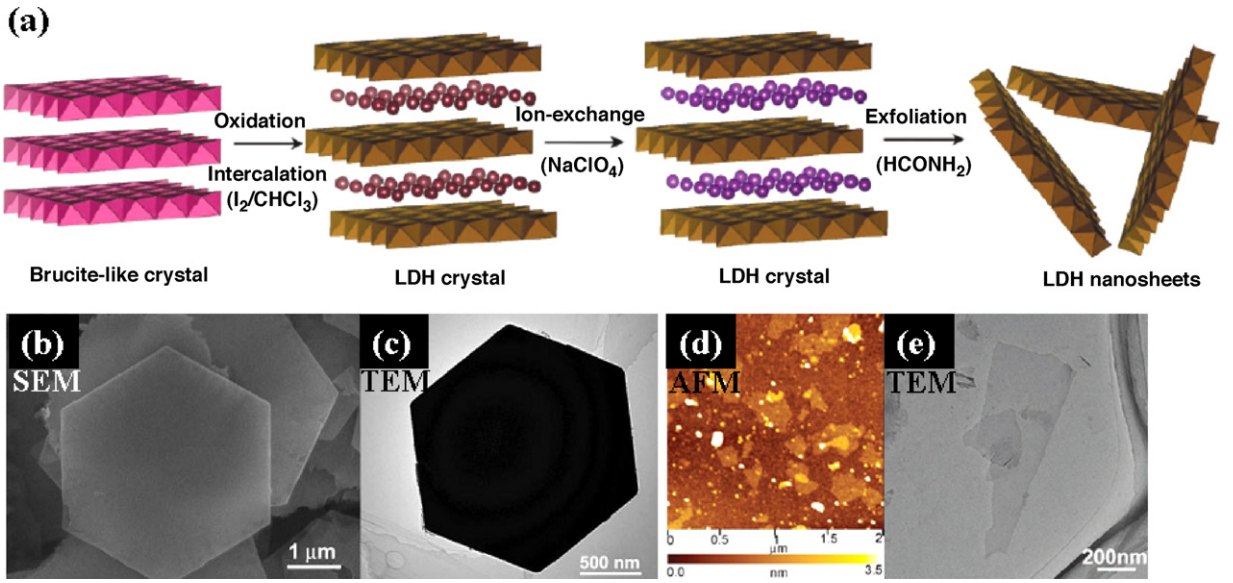

Fig. 23. (a) Schematic illustration of intercalation and exfoliation of Co^{2+}–Fe^{3+} LDHs (b and c) micrographs of ClO_4^- intercalated LDHs and (d and e) individual LDHs nanosheet [182].
© 2007 American Chemical Society.

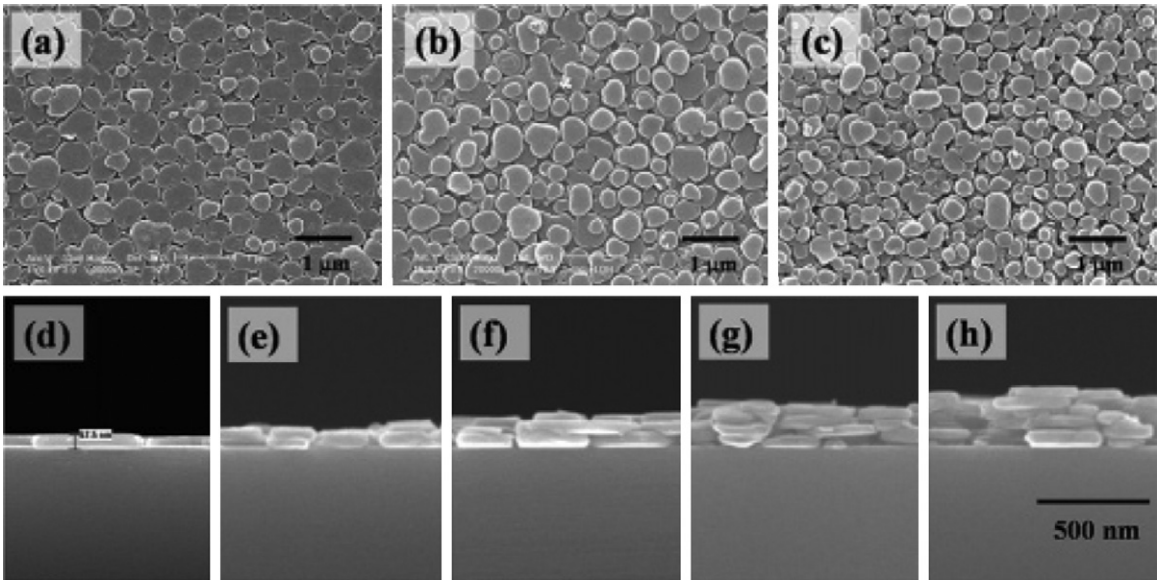

Fig. 24. SEM micrographs of the monolayer (a) 1 L, (b) 3 L, and (c) 5 L MgAl-LDH on Si. Cross-sectional views of (d) 1 L, (e) 2 L, (f) 3 L, (g) 4 L, and (h) 5 L samples [183].
© 2007 American Chemical Society.

at 21 Å implies that the interlayer acid organics are well aligned vertically in parallel layers.

4. Self-organization of intercalated organoclays

4.1. Microsphere and rod-like self-assemblies

Organoclays from the incorporation of organic ions into MMT layered structure were shown to be capable of forming self-organized microstructures (Fig. 25) [184]. Hollow microstructures 3–9 μm in diameter were prepared from self-organization of MMT organoclay units. The direct fabrication of opened hollow microspheres was first reported in 2008. Under the common spray-drying conditions, the formation of hollow spheres from sodium alkylsulfonate intercalated MMT was observed. The mechanism for the formation of unique morphology from organoclay units was explained by comparing two different intercalated organoclays. When the organoclays have a high organic expansion for basal spacing, the aggregates (Fig. 25b) can cross-intercalate each other to form a solid around droplets during the air-drying as the opened spheres. In contrast, the low intercalating clay produced porous and less ordered microstructure from the unit piling (Fig. 25c). The process was further extended to Co^{2+}-intercalated MMT, which allowed the growth of CNT on the hollow spheres. In Fig. 25d and e, the morphologies of CNTs uniformly dispersed on the surface of the clay microspheres are shown. The overall process can be tailored by ionic exchange intercalation for Na^{+}-MMT, H^{+}-MMT, and Co^{2+}-MMT with sodium 1-pentanesulfonate or 1-dodecanesulfonate at specific equivalent ratios. Under the conditions of spray-drying water evaporation at 180 °C, the stacks of organoclays self-organized into regular microstructures of hollow spheres. The formation of ordered microstructures under such dynamic conditions implied that the organoclays have a strong tendency for self-organization.

The layered structure of the silicate clays may be intercalated by organic ions through an ionic exchange reaction. For the cationic clays such as MMT and Mica, the ionic exchange intercalation can be performed in aqueous solvent and the organoclays isolated. By using the POP-amine-salts for POP intercalation, a wide range of hydrophobic organic amounts may be incorporated into the clay interlayer structure. Polyoxypropylene (POP) organics afforded clay units with an expanded spacing and hydrophobic properties. By adjusting the levels of hydrophobic incorporation, the organoclays could be still dispersible in water at low temperatures and they were able to self-assemble into ordered arrays. Under a simple process of heating evaporation, the organoclay units demonstrated the ability of self-assembling without any assistance from foreign surfactants [171]. It was reported that the POP-intercalated MMT organoclay could undergo a self-assembly of lengthy rod-like morphologies, as shown in Fig. 26a and b. Experimentally, the specific organoclay was first dispersed homogeneously in water at low concentrations below 1 wt% and subjected to the process of controlled evaporation at 80 °C. Under SEM analysis, rod- or fiber-like ordered microstructures in high uniformity were observed. The morphologies with average dimensions of 0.1–0.8 μm in width and 2–100 μm in length for these fibers were recorded. The formation of ordered microstructures from hydrophobic POP-intercalated MMT revealed the delicate non-covalent bonding interactions within the clay basal spacing as well as the unit-to-unit interactions.

For other silicate clays, POP-intercalated Mica also self-assembled to form rigid rod morphology of 0.3–2.0 μm in width and 5–30 μm in length, as shown in Fig. 26d

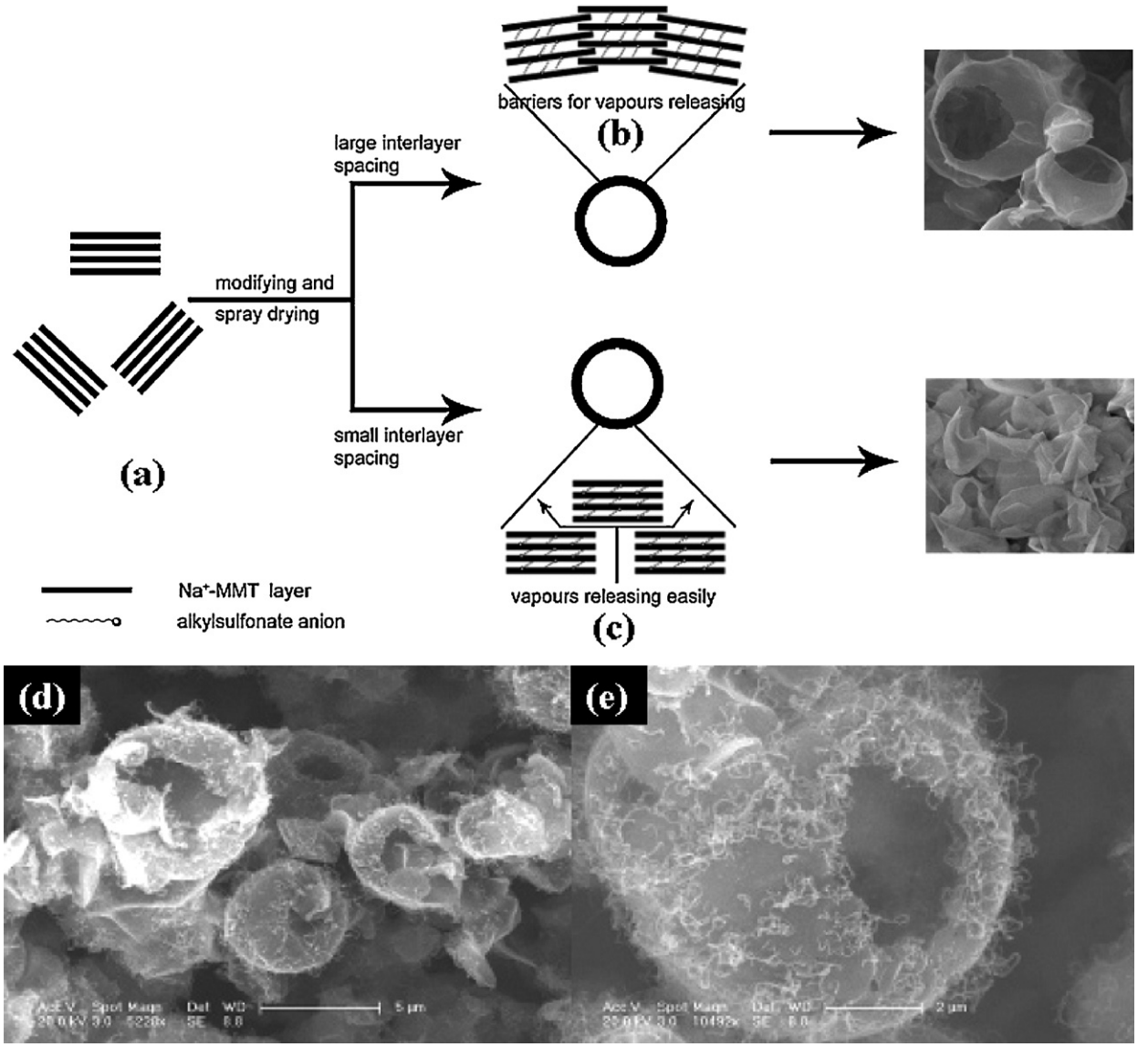

Fig. 25. Schematic diagram of the formation for opened hollow spheres. (a) Na^+-MMT; (b) a solid shell formed through MMT aggregates intercalating across each other during spray drying; (c) a porous shell formed by MMT aggregates overlapping during spray drying. (d and e) FE-SEM micrographs of clay/CNTs composite at low and high magnifications [184].
© 2008 American Chemical Society.

and e [185]. The self-assembling ability was correlated to the amount of POP incorporation in the clay spacing. In the range of 0.2–0.5 eq. ratio of clay CEC (cation exchange capacity), the organomica units possessed appropriate hydrophobic property for self-assembly. However, by increasing the POP ionic exchange amount up to 1.0 CEC, the clay units became too hydrophobic to be dispersed in water. The hydrophobic organoclay was alternatively dispersed in toluene but failed to self-assemble into an ordered structure. The suitability of hydrophobic composition in the clay interlayer spacing appeared to be an important parameter for self-assembly. Fine dispersion in water was necessary for generating the arrays; the aggregated form of organoclay failed to pile up any regularity of ordered structure. The XRD analyses showed that the rod-like crystals had a similar X-ray diffraction pattern to the clay units before the self-assembly, i.e., *d* spacing of 5.8 nm for MMT and 4.1 nm for Mica. This indicates that the self-assemblages were piled from the primary units of organoclays retaining the same XRD pattern. The primary units were revealed to be on average 8–10 plate layers in one stack for MMT and 4–6 plate layers for Mica, as illustrated in Fig. 26c and f [170,172]. Accordingly, it was estimated that each micrometer length of the fibrous arrays could accumulate up to 19 MMT and 39 Mica organoclay units.

The self-assembling mechanism for forming these lengthy rods was rationalized by assuming the unit

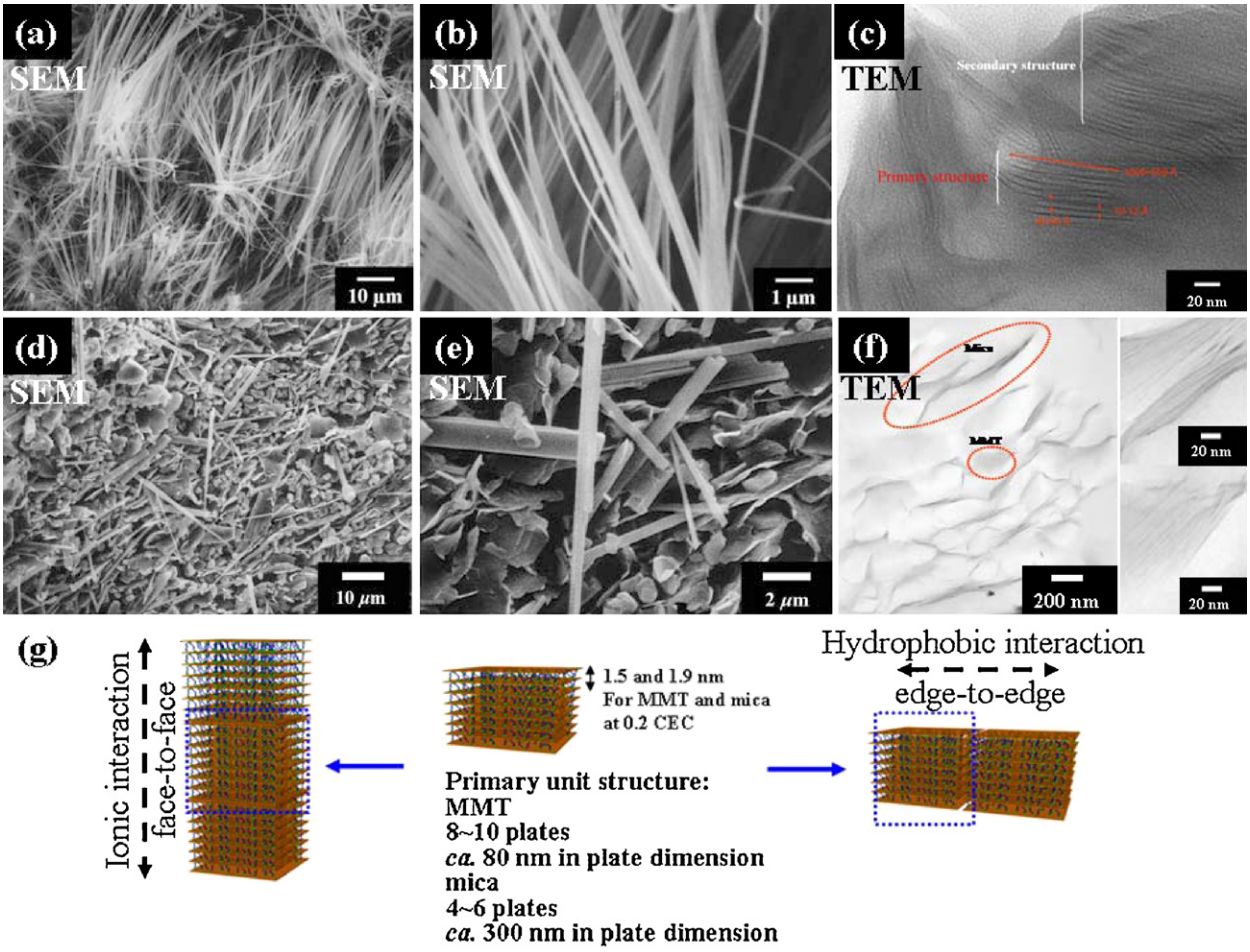

Fig. 26. (a and b) SEM micrographs of fiber-like microstructures from the self-assembling of POP2000/MMT organoclay (at 0.2 eq. of POP intercalation to clay CEC) [171]. Copyright 2004, Wiley-VCH Verlag GmbH & Co. KGaA. (c) TEM micrographs of POP2000/MMT microstructure of a thin film prepared from self-assembling at the toluene/water interface [172]. Copyright 2003, American Chemical Society. (d and e) SEM micrographs of rod-like microstructures from the self-assembling of the POP2000/Mica organoclays (at 0.2 eq. of POP intercalation to clay CEC) [185]. Copyright 2008, American Chemical Society. (f) TEM micrographs of POP2000-intercalated synthetic mica and MMT, prepared from co-intercalation, magnified synthetic mica with an averaged 4–6 layered structure, and MMT with an averaged 8–10 layered structure [170]. © 2004, American Chemical Society. (g) Conceptual explanation for the formation of these rod-like arrays via two possible directions of piling the primary clay units (represented by a four-plate-stack in the center drawing).

alignment through two different directions, POP edge-to-edge and clay platelet face-to-face piling of the units. The mechanism is illustrated in Fig. 26g. The hydrophobic/hydrophilic balanced units of 0.2 CEC MMT or Mica after the appropriate POP intercalation may undergo the unit-to-unit alignments. While the hydrophobic POP organics in galleries favor the edge-to-edge directional growth for the width, the ionic clay platelet surface tends to pile vertically into lengthy rod morphology. Two different directional forces including POP hydrophobic effect and platelet surface charge attraction dictate the growth of rod-shape morphology.

4.2. Self-assembling at toluene–water interface

The water-evaporation method for organoclay self-assembly was suitable for low levels of POP clay interaction. With high POP intercalation or hydrophobic organoclays, a toluene dispersed bi-phasic self-assembling was reported [185]. A similar piling mechanism occurred in a water/toluene bi-phasic system via a two-directional unit orientation. The previously mentioned 0.2 CEC POP organoclays were comprised of hydrophobic POP organics at low composition in the silicate galleries, which was dispersed in water rather than in toluene. The increase of POP organic levels up to 50–60 wt% in silicates or at 1.0 clay CEC made the organoclays hydrophobic and dispersible in toluene. The particular 1.0 CEC sample was hydrophobic and dispersible in toluene rather than in water. When the primary units of the POP-intercalated clays were subjected to a two-phase standing, self-assemblages into ordered structures occurred. Thin film of unit self-piling at the toluene–water interface was generated by a long-term standing of the toluene dispersion with static water phase (Fig. 27). On SEM micrograms, the rod-like microstructures were compared between the POP/MMT and the POP/Mica both at 1.0 CEC. The morphologies of short rods or dendrite structures were observed as shown in Fig. 27a. The difference

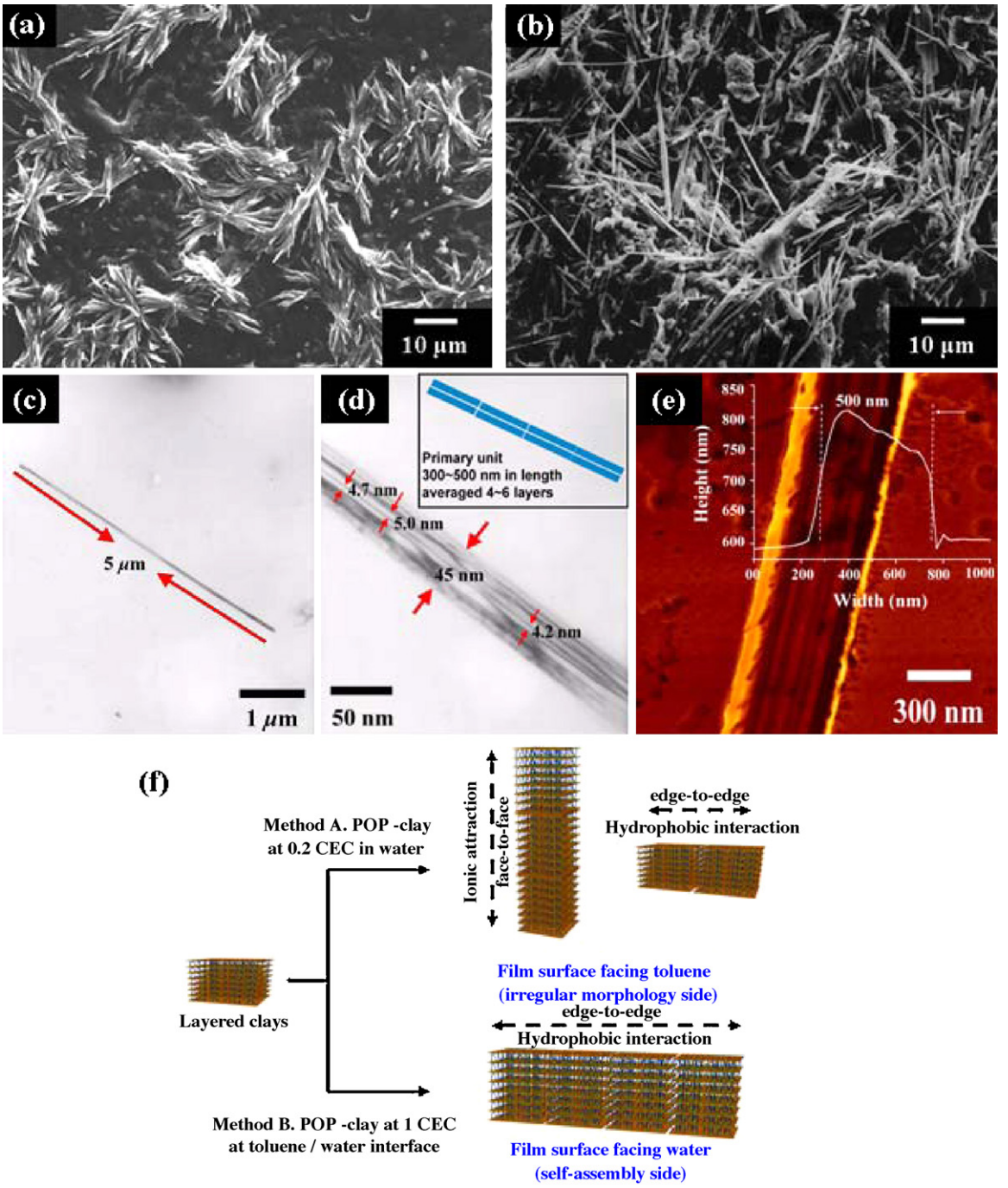

Fig. 27. SEM micrographs of a film surface, self-assembled from POP/clay (1.0 CEC) at the toluene/water surface. (a) Dendrites from POP/MMT; (b) rods at the dimension of 10–40 μm in length and 0.2–0.5 μm in diameter from POP/Mica. Morphologies of two representative POP–Mica (1.0 CEC) rods, isolated from the film surface on water side by using an ultrasonic vibrator to break up from the film surface and placed on the copper grid holder: (c and d) TEM of the rod at 5 μm in length and 45 nm in diameter; the inset represents the piling of eight primary clay units with the analysis of X-ray *d* spacing at 4.1 nm. (e) AFM topographical image of another rod at 200 nm in height and 500 nm in width, and showing the texture of rod formation similar to (d). (f) Conceptual diagram of POP/clay self-assembling procedures. (A) Direct water-evaporation method: POP/clay (0.2 CEC intercalation) dispersed in water and then evaporated to dryness; (B) toluene/water interfacial film method: POP/clay (1.0 CEC) dispersed in toluene, adding water phase and standing for a film formation [185].

© 2008 American Chemical Society.

in morphological change was rationalized by the presence of hydrophobic POP organics, which tended to favor the unit edge-to-edge piling as the main driving force over the platelet face-to-face charge interaction. With a large platelet of Mica, it appeared to be more straight and lengthy in shape than those of POP/MMT in a dendrite shape. Rod-like morphologies of 10–40 μm in length and 0.2–0.5 μm in width were observed (Fig. 27b). The platelet size influenced the hydrophobic interaction and surface ionic charges. The dimension of platelet size significant contributed to the piling force. A thin-platelet geometric shape is a significant factor for controlling the self-assembling process. In the case of organoclay, it led to the formation of lengthy rod structures. Geometric shape, hydrophobic effect, and surface ionic charge are the controlling factors for directing the unit piling and self-assembly.

The degree of hydrophobic nature of the organoclays is summarized in Table 3, and three representative POP-intercalated clays of MMT and Mica are selected for comparing their self-assembling ability and morphology in water and toluene. Different hydrophobic amounts of POP intercalating organics at 0.2, 0.5, and 1.0 CEC equivalent ratios affect their dispersing ability in water or toluene. The organoclays at the 0.2 CEC equivalent ratio were dispersible in water rather than in toluene and self-assembled under the direct water-evaporation method. Rod structures were observed at average dimensions of 0.1–0.8 μm in width, 10 μm in length for MMT and even longer dimensions for Mica. Similar results were observed for the 0.5 CEC organoclay. For the pristine clays and highly hydrophobic organoclays such as the POP at 1.0 CEC intercalation, the hydrophobic/hydrophobic balance fails to afford an orderly morphology of self-assembling under the same self-assembling conditions.

4.3. Self-assembling in epoxy matrices during curing

POP-intercalated clays with layered structure have been shown to self-assemble in a third way. During in situ epoxy ring-opening polymerization of glycidyl-ether BPA, the POP-amine-salt intercalated clays may serve as initiators and further self-organize into unpredictable silicate skeleton morphologies [186,187]. In particular, the POP–Mica of 5.2 nm basal spacing organoclay was hydrophobic and dispersible in the epoxy monomer at room temperature. The silicate layered structure was readily accessible by the epoxy monomer. While heating to 180 °C, the POP-intercalated silicates started a rapid initiation and epoxy polymerization. The reaction occurred at a fast rate to convert the liquid monomers to a powder material within a few minutes. The final product, as a powder material instead of a common solid cured lump, was analyzed to have silicates of interlayer expanded spacing beyond the XRD detection limit (>10 nm) from the pristine 5.2 nm. The process and mechanism are described in Fig. 28a. The epoxy self-polymerization was initiated by the intercalated species of ≡Si–O$^-$NH$_3^+$–R that resulted from the exchange of the POP salts with sodium counter ions. The epoxy monomer started the initiation with the amine-salts associated with the silicate platelet surface ion site. The reaction profile proceeded from monomer–organoclay cloudy mixtures to

Table 3
Self-assemblies of POP-intercalated clays with different XRD *d* spacing and hydrophobic organics [185]. Copyright 2008, American Chemical Society.

Equivalent ratio of POP–salt to clay CEC	*d* spacing (nm) and organic fraction (wt% in parenthesis)		Dispersion (MMT and Mica)		Observation of self-assemblies from MMT or Mica	
	MMT	Mica	Water	Toluene	Method A: direct water-evaporation method	Method B: toluene–water interfacial film method
Pristine	1.2	1.2	Dispersible	Aggregated	None	None
0.2	1.9 (22)	1.5 (24)	Dispersible	Aggregated	Rods (from MMT: 0.1–0.8 μm in width and ~10 μm in length; from Mica: 0.3–2.0 μm in width and ~30 μm in length)	None
0.5	2.0 (34)	4.0 (48)	Partially aggregated	Partially aggregated	Rods	None
1.0	5.8 (63)	4.1 (53)	Aggregated	Dispersible	None	Rod-bundles (from Mica: ca. 3 μm in width and ~40 μm in length) dendrites (from MMT)

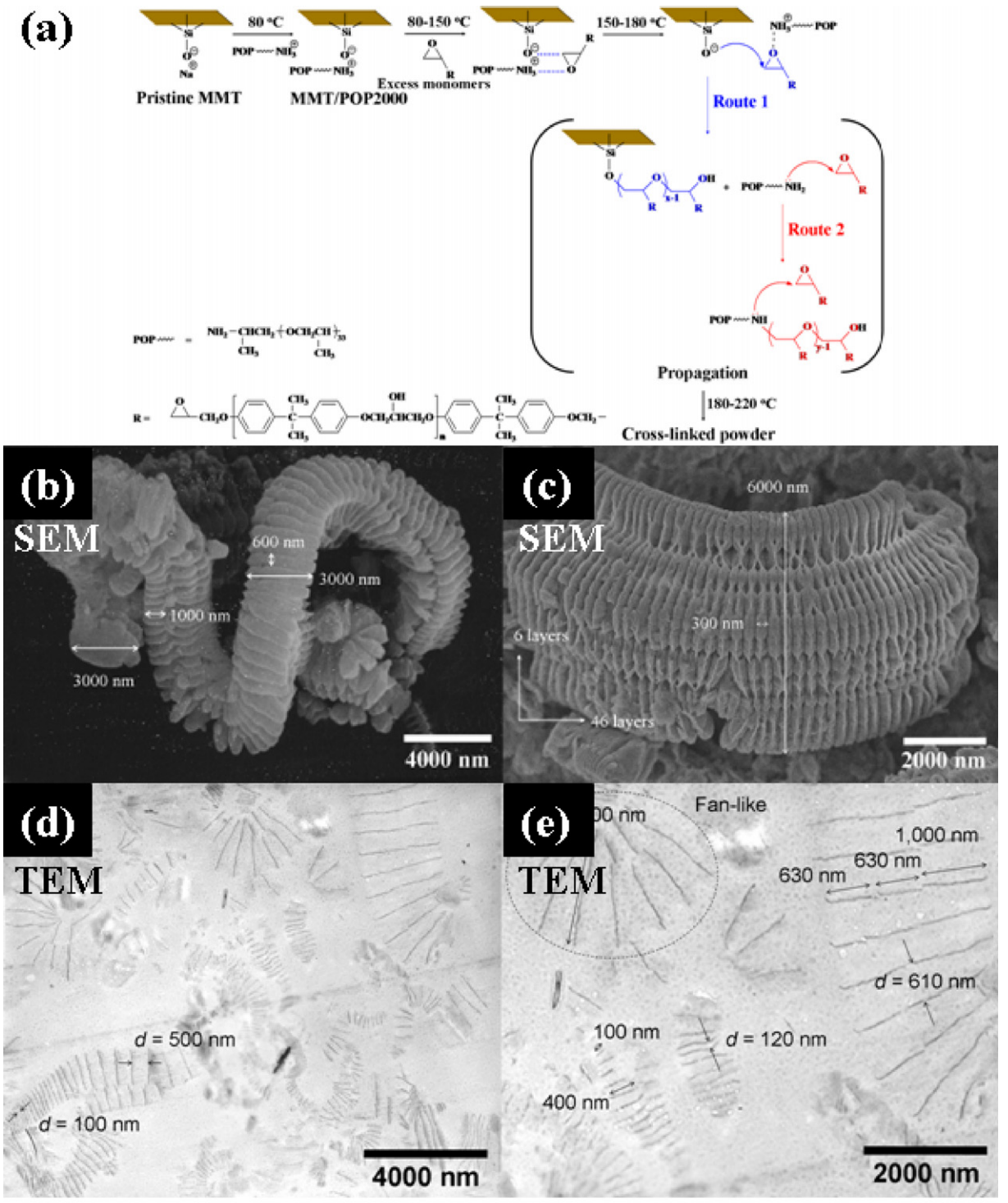

Fig. 28. (a) Proposed mechanism for epoxy self-polymerization with the intercalated ≡Si–O⁻ NH_3^+ species and the second stage of cross-linking. (b and c) SEM micrographs of 3 wt% Mica/POP2000 cured epoxy powder material. (d and e) TEM micrographs of 3 wt% Mica/POP2000 cured epoxy powder material [186,187].

© 2009 American Chemical Society.

a transparent liquid (at 150–180 °C) and finally to a loose powder (at 180–220 °C). This was correlated to the DSC exothermic peaks for the occurrence of at least two different reactions including the epoxy monomer ring-opening polymerization by siloxanol and amine initiation, following an inter-chain cross-linking reaction. The multiple sites of silicate platelets were transformed into unique microstructure morphologies.

In Fig. 28b and c, the SEM micrograms demonstrate three-dimensional multilayered morphologies such as foreign worms and semi-coliseum. The microstructures appeared to have local dimensions of 8–10 μm in length (estimated ca. 46 layers of platelets) and 5–6 μm in height. The formation was estimated as consisting of fundamental units at 1000 nm width consistent with the average dimensions of the pristine Mica. The stacking of the primary organomica units through the polymer interconnection twisted into curvatures. Under TEM (Fig. 28d and e), the side view of silicate platelets as lines appeared to consist ca. 8–60 layers in individual clusters. Exceptionally large interlayer spacing between the neighboring platelets at 100 nm, 120 nm, 610 nm, or mostly 500 nm was observed. The existence of radial or fan-like arrangements further implied the twisted formation of microstructures observed in SEM. The interlayer spacing in the range of 120–610 nm appeared in an ordered alignment much larger than that of the XRD analyses for POP2000/Mica. It was envisioned that the formation of parallel or fan-like shapes was caused by the epoxy chain propagation in kinetic manner. During the process, the epoxy monomers may access the interlayer spacing and initiate the epoxy ring-opening chain propagation. The expansion of interlayer spacing and uneven interconnection among the organoclay units may well have occurred simultaneously and self-organized the clay units into microstructures by the bending of epoxy polymer chains of the organoclay as indicated in Fig. 29.

5. Self-organization of exfoliated platelets

5.1. Dendritic microstructures from platelet self-piling

The clay layered structure was possibly exfoliated by polyamine-salts via several different mechanisms. After aqueous exfoliation, the randomized silicate platelets could be isolated by toluene extraction out of the organics leaving the silicates dispersible in water without any organic contamination. The isolated thin-platelets with high-aspect-ratio geometric shape and ionic character tended to self-pile and aggregate into ordered stacks due to their high surface charge attraction [168]. When subjected to water evaporation, the platelets in polydispersed dimensions self-aggregated to form lengthy rod-like morphologies. For example, when the 6 wt% of silicate suspension was evaporated at 80 °C until dryness, a solid lump was generated. The cross-section of the internal surface was analyzed by SEM. The dissected surface appeared to be uniform in patterns of foreign flower-like clusters over a large area (Fig. 30a and b). At high magnification, the branches were fibrous arrays with an average length up to several micrometers. The texture of fibers could be further observed to contain several individual fibers in bundles, consisting of 4–6 single fibers of ca. 100 nm in width in one average bundle (Fig. 30c and d). On the basis of these analyses, the mechanism was believed to be platelet self-piling through the face-to-face ionic charge attraction from the fundamental units of high-aspect-ratio platelets. The platelet self-piling mechanism is conceptually illustrated in Fig. 30e. It is assumed that the charge interaction is the predominant factor for the formation. Previously, the platelet ionic charges were analyzed by zeta potential measurement showing a pH-dependent charge species existed on the surface of the random platelets. A large charge intensity and a transition in charge identity at the pH of 6.4 have been reported [174]. Accordingly, the platelet face-to-face alignment into lengthy fibers under the condition of pH 9 is favored over other types of edge-to-face or edge-to-edge irregular aggregation.

5.2. Hierarchical transformation of self-assemblies

The self-assembling behavior of exfoliated platelets from fluorinated mica was also examined. The average mica platelets have larger dimensions than the corresponding MMT platelets and hence theoretically a higher tendency for self-assembly [97]. The dispersion of mica platelets in 5–10 wt% was subjected to water evaporation at 80 °C to form powdered materials and examined by SEM (Fig. 31a). Depending on the concentration, the powder from 5 wt% dispersion showed a rod-like microstructure 20 μm in length and 300–1000 nm in width. At high concentrations such as 10 wt%, the morphologies appeared to be short arrays averaging 3 μm but having a similar width of 300–1000 nm (Fig. 31b). For comparison purposes, pristine mica clay without exfoliation failed to generate any form of ordered structure but instead formed irregular aggregates after water evaporation.

The self-assembled lengthy rod structures could undergo a further hierarchical rearrangement into shortened morphologies under conditions of ultrasonic force. In the process of re-dispersing the self-assembled powder in water (1 wt%) and then agitating by ultrasonic vibration for 1–2 h, the original lengthy rods were transformed into fern-leaf dendrites, observed by TEM (Fig. 31c and d). The mechanism involved the fracturing of lengthy rods and restacking into dendrites of short rods. The ultrasonic treatment provided energy for the hierarchical transformation. During the prolonged energy treatment for 2 h, the appearance of dendrites became more regular in branching. The phenomenon of hierarchical fracturing and restacking of the self-assemblages under ultrasonic energy is described in Fig. 31e.

5.3. Transformation under electron beam bombardment

The formation of rod-like ordered arrays from the exfoliated platelets is the result of the intense ionic attracting forces on the platelet surface. The nature of high-aspect-ratio geometric shape further affects the self-piling. The experimental conditions were typically performed by a controlled evaporation drying at 80 °C in an oven for 4 h and the resultant powder solid was subsequently examined by SEM. Different substrates such as glass and metal

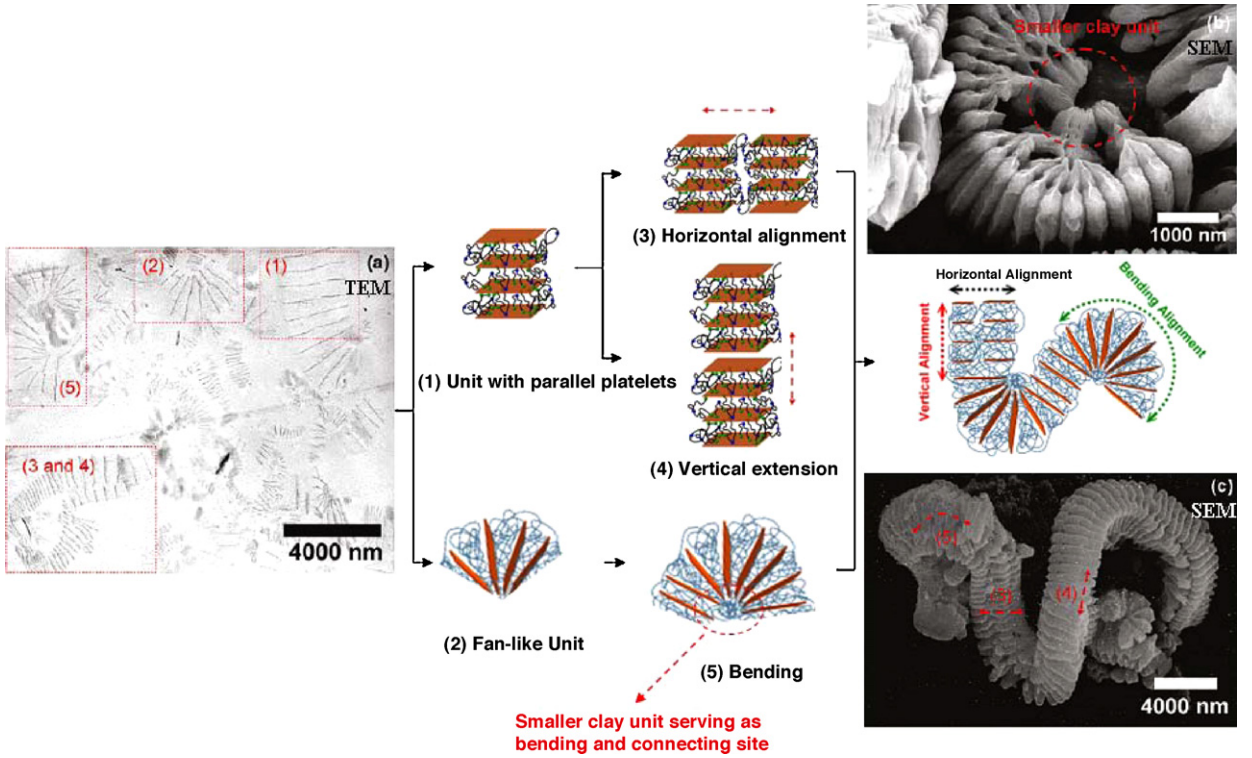

Fig. 29. Schematic illustration of the self-assembling mechanism through two types of clay units (1) parallel platelets and (2) fan-like; and units alignment via (3) horizontal, (4) vertical, and (5) bending direction, corresponding to TEM micrograph (a) and SEM morphologies (b and c) [186].
© 2009 American Chemical Society.

surface could affect the formation of the self-assemblages due to the nucleation effect. Other conditions such as concentration, dispersion, and standing time after evaporation drying may affect the formation of the thermodynamic equilibrium morphology. An example of fiber- or rod-like arrays up to 10 μm lengths is illustrated in Fig. 32a and b [188]. Different widths of the fibers were generated from the ordered aggregation of platelets. The fiber width can be mechanistically explained by the edge-to-edge alignment of the individual platelets, ranging from 100 nm to 300 nm in dimension. The platelet vertical piling was the dominant direction for the lengthy growth, thus implying the high affinity of the surface charge attraction. The individual fibers could be isolated by physical manipulation and placed on copper grids for TEM analysis. Under electron bombardment and at the early stages of TEM examination, the images of fiber size and dimensions recorded were similar to those observed by SEM. For example, two representative samples of 0.1 μm × 3.0 μm and 0.3 μm × 6.2 μm are displayed in Fig. 32c. However, under the continuous exposure of high-energy fields or continuous electron bombardment, the silicate arrays were observed to shatter and evaporate under TEM electron current. The kinetic disappearance or platelet diffusion was possibly intercepted by a low-energy and rapid image recording taking during TEM examination. The micrograph shot shows an image representing a tube-like array (Fig. 32d). It represents one of the intermediate images under transformation before the complete shattering that occurs under electron beam energy (Fig. 32e). The structure shattering resulted in the platelet arrays undergoing a fast transformation into other morphologies with dimensions of 5.6 μm in length, 120 nm in diameter and 30 nm in wall thickness. The array is presumably formed through silicate platelets scattering under the electron beam bombardment. The shattering process can be observed during the TEM electron beam bombardment and also deduced from the shadow surrounding the tube picture. The diameter of the tube-like array structure is approximately 100 nm; the space originally occupied by the layered platelets. The occurrence of this unique transformation under TEM was attributed to the properties of platelets with a high aspect ratio of geometric shape and surface electrostatic charges.

6. Self-organizing mechanism and thin-platelet directing factor

6.1. From intercalated clay stacks

In the past decade, the intercalation of layered silicate clays by organic salts affording a number of organoclays has been reported. Their ability for self-assembly was subsequently disclosed. Through the ionic charge exchange intercalation with hydrophobic polymer amine-salts, the clay layered structures can be incorporated with hydrophobic organics and assume an amphiphilic

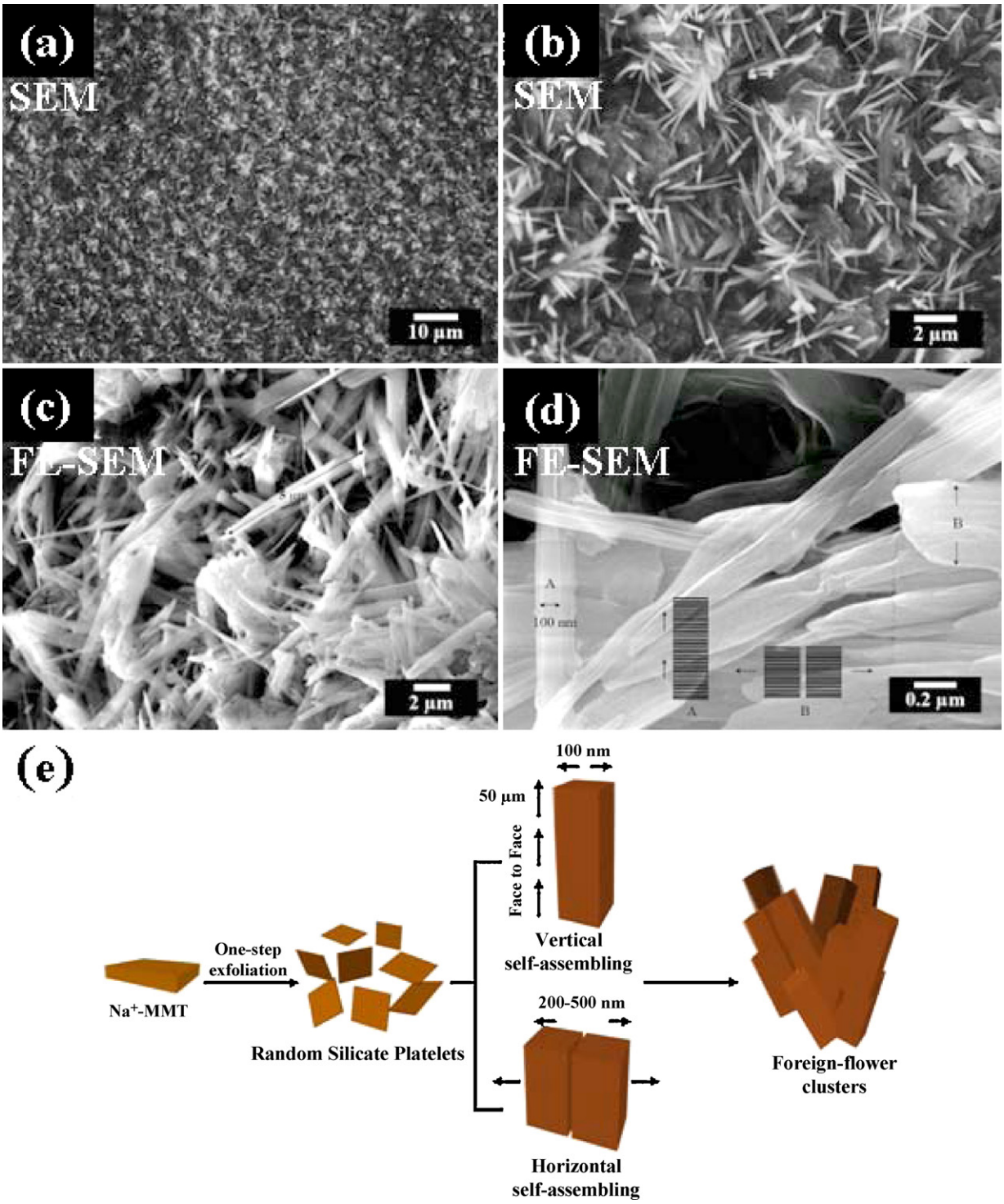

Fig. 30. Self-assembly of platelets and 80 °C evaporation: (a and b) foreign-flower clusters from 6 wt% suspension by SEM and (c and d) fibrous bundles by FE-SEM at different magnifications. (e) Conceptual diagrams of vertical and horizontal self-assembling of individual platelets into fibrous arrays [174].
© 2006 American Chemical Society.

character because of the existence of both surface ionic charges and hydrophobic organics. Under the methods of controlled water evaporation or toluene–water interfacial equilibrium, the amphiphilic clays are able to self-organize into ordered arrays. A variety of microstructure morphologies such as rods, fibers, worm-like curvatures, and hollow spherical shapes were observed. All of these unique morphologies are derived from similar clay units under

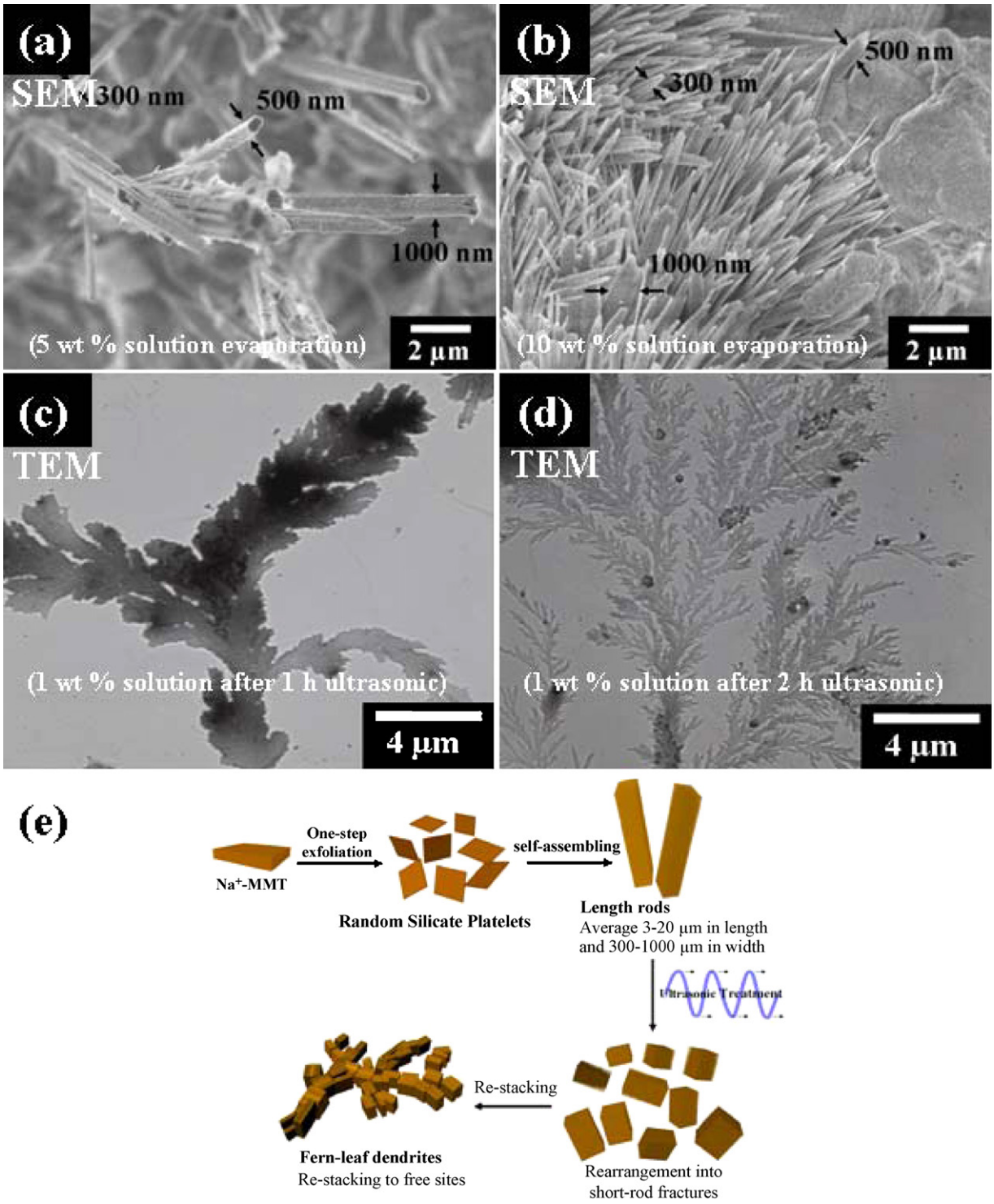

Fig. 31. FE-SEM micrographs of self-assembly (a) from 5 wt% and (b) 10 wt% of random mica platelets in water under the conditions of water removal at 80 °C. TEM micrographs of the fern-leaf dendrites after (c) 1 h and (d) 2 h ultrasonic treatment and dried on copper grid. (e) Conceptual diagrams of polydisperse platelets under self-assembling into rods of different diameters but with a high uniformity in individuals [97].
© 2008 American Chemical Society.

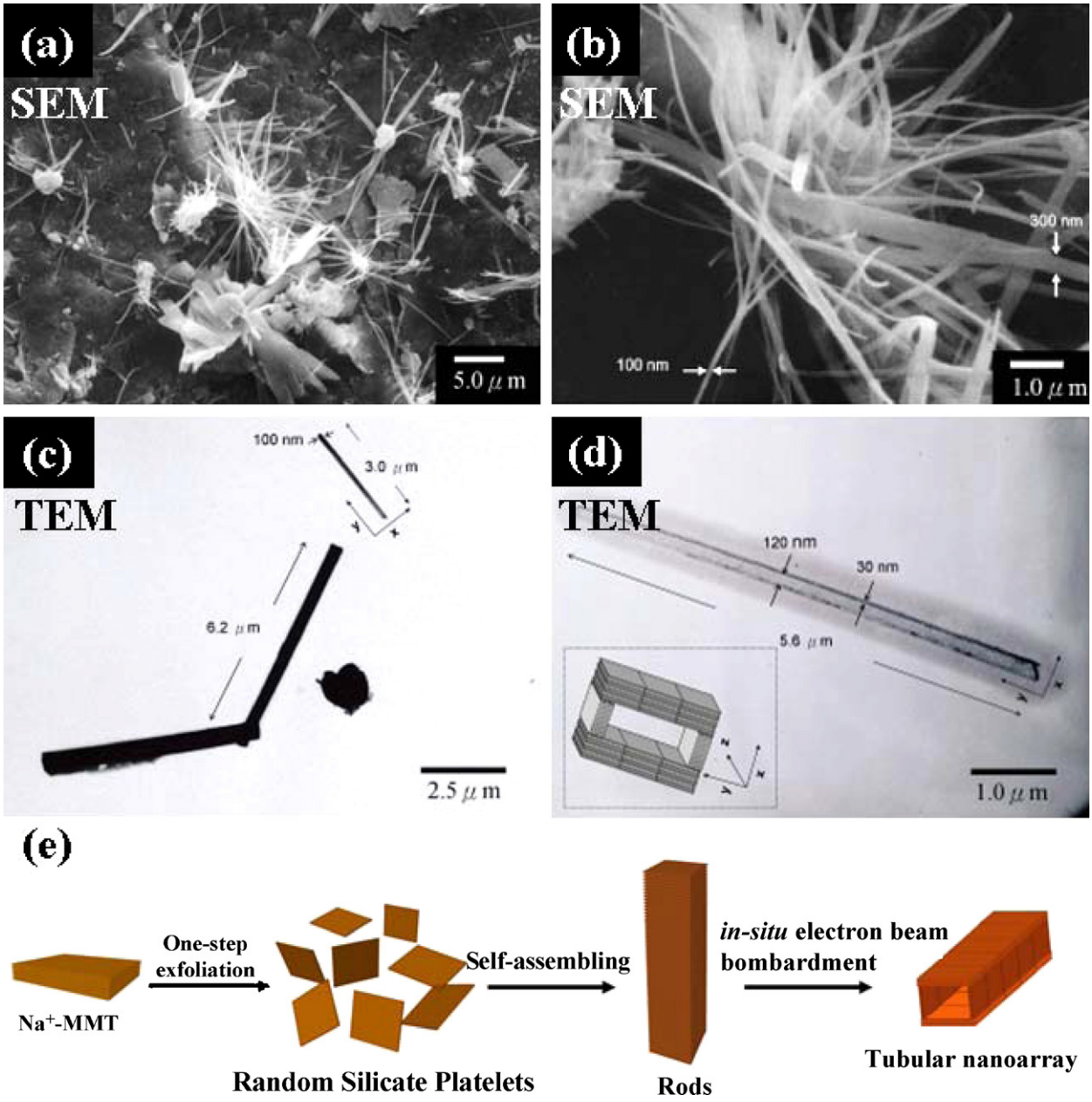

Fig. 32. (a and b) SEM of lengthy fiber arrays from self-assembling of random silicate platelets on glass surface. (c) TEM micrographs of silicate platelet arrays under initial observation and (d) transformation into after further electron beam bombardment (conceptually proposed picture in the inserted). (e) Conceptual representation of transformation of a silicate fiber to a nano-array under electron-beam bombardment during TEM observation [188].
© 2005 Wiley-VCH Verlag GmbH & Co. KGaA.

different environmental conditions. The self-assembly is the result of non-covalent bonding interactions and is enhanced by the platelet surface ionic charge attraction force. The mechanism involves two different clay unit piling directions, platelet face-to-face attraction and hydrophobic edge-to-edge alignment. Various morphological controls are summarized and illustrated in Figs. 33 and 34, showing the diverse routes by which the clay unit can self-assemble. The polymer-modified clay stacks with interlayer spacing of 2–5 nm XRD diffraction can undergo self-alignment to form ordered microstructures. The vertical piling direction is generally believed to be driven by the platelet surface charge attraction. Another direction is the organic hydrophobic aggregation through unit edge-to-edge interactions, contributed mostly by the organics incorporated in the galleries. By using water evaporation method, the platelet face-to-face piling is favored for growing lengthy rod-like morphologies Fig. 34(1). However, by the toluene–water interfacial method, the edge-to-edge orientation along the interface

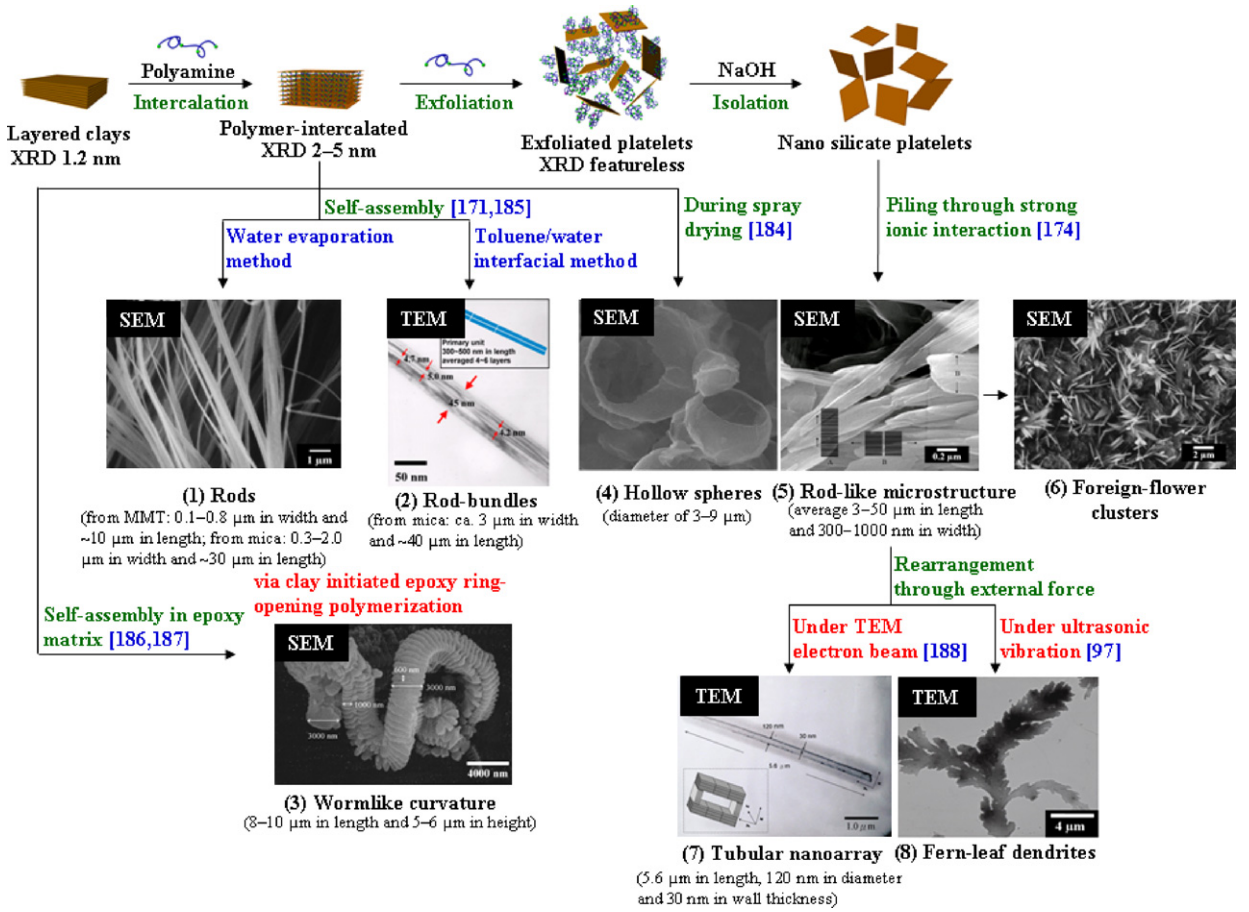

Fig. 33. Conceptual illustration of the mechanism of clay self-assembly from pristine clay, hydrophobic clay and exfoliated clay to form versatile geometric shapes.

is favored for the lengthy rod growing direction Fig. 34(2). Both directions of unit piling into similar morphologies of rods or fibers were further elucidated by TEM, to observe the texture of the self-assemblages. The self-assembling largely relied on the proper balance of amphiphilic propensities involving clay ionic charges on platelet surfaces and hydrophobic organic interactions.

It has also been shown that the unit interconnectivity may occur under a dynamic environment. During in situ epoxy ring-opening polymerization at high temperature, the POP-amine-salt intercalated clays were simultaneously expanded and unit interconnected to form large aggregates of microstructures. A group of worm-like and curve silicate skeletons in the cured epoxy matrices were observed by SEM and TEM Fig. 34(3). The detailed elucidation of the clay three-dimensional (3D) layered structure is useful to explain the self-organization. Firstly, the amine-salts intercalated in the clay galleries were responsible for the initiation of epoxy ring-opening polymerization. The 3–10 wt% of layered silicates accessed by epoxy monomers initiated the epoxy chain growth and were simultaneously pulled apart in 3D directions. During the epoxy chain growth, the clay units were interconnected through multiply connected polymer chains undergoing propagation and cross-linking at the chain ends. The clay units further self-aggregated through the interconnection of different units. The occurrence of curvature microstructure of silicate skeletons was observed in a dynamic manner and fast formation during the clay unit interconnection and simultaneous epoxy chain growth polymerization. In another independent report, hollow spheres were obtained during the spray drying process of the organically intercalated clays Fig. 34(4). The layered silicate units could undergo self-alignment to form micrometer shells with a hollow center under the condition of hot air drying and expansion process. These findings of new morphologies of the intercalated organoclays indicate the intensive clay self-piling forces involving two directions of face-to-face and edge-to-edge interactions.

6.2. From exfoliated platelets

The self-assembling occurrences are even more prominent for the exfoliated platelets than the intercalated organoclays with hydrophobic organics in the primary units. The layered structure can be transformed into individual silicate platelets as compared to the organoclays. After removing the organics, the geometric shape of the silicate platelets is of high aspect ratio of 1.0 nm in thickness. The inorganic silicate platelets possess multiple charges

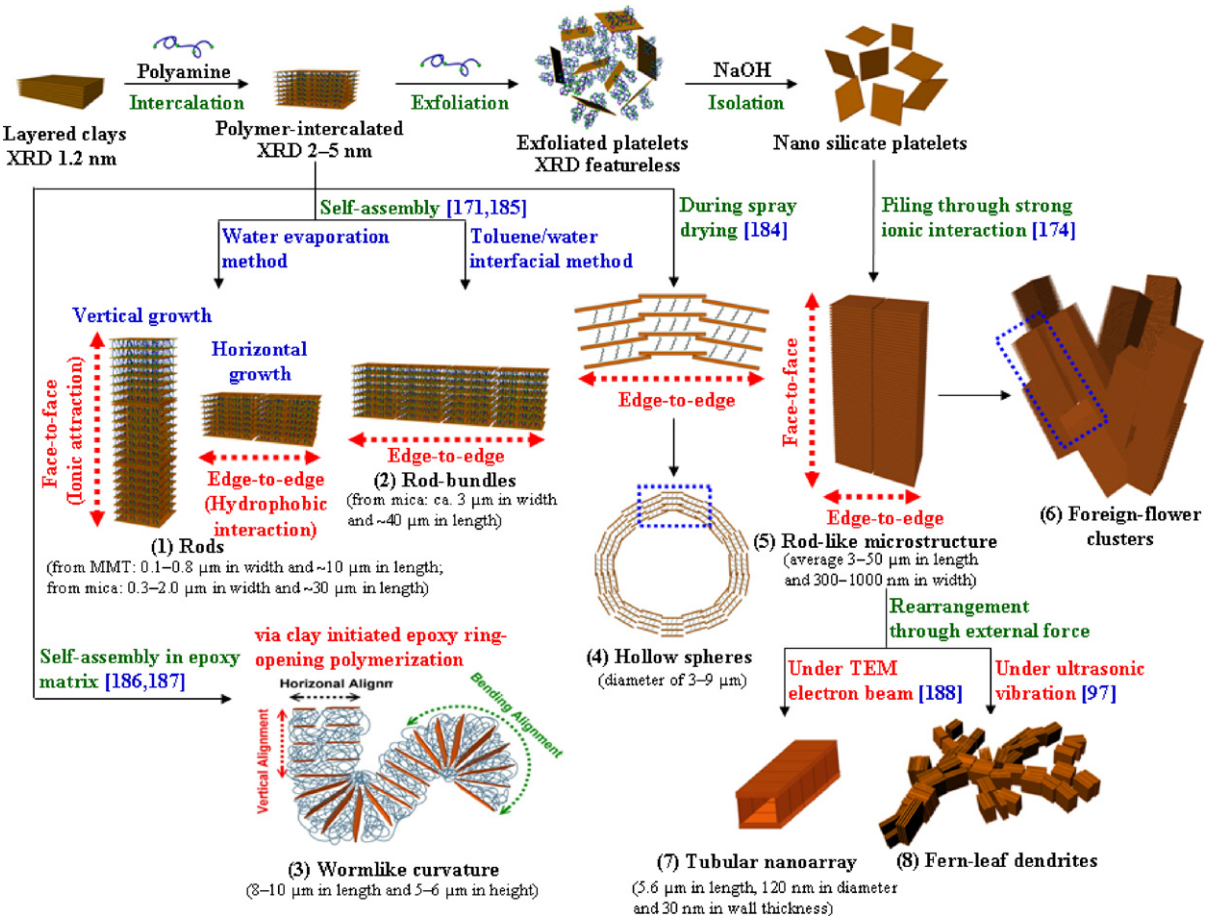

Fig. 34. Overview of clay self-assemblies from polymer-modified organoclay and exfoliated platelets to form versatile microstructures.

of counter ions on the surface of such thin-platelets and tend to attract each other for self-assembling. Fig. 34(5 and 6) summarizes the self-piling of silicate platelets into micrometer-scale rod or fiber bundles. The piling is dominated by the strong force of platelet face-to-face ionic charge attraction.

The nature of the self-piled rods may be affected by external forces such as electron beam and ultrasonic vibration. Under TEM electron beam bombardment, the self-assembled rods were structurally transformed into different formations Fig. 34(7). It appeared that the silicate platelets in self-assemblages were unstable and re-shattered by the electron beam energy. Similarly, the fern-leaf dendrites were formed after rearranging the lengthy rods into shorter stacks under ultrasonic vibration Fig. 34(8). It was shown that the self-assemblages were kinetically stable under certain conditions. Through the non-covalent bonding equilibrium and pathway, other morphologies could be derived. All of theses examples illustrate the possible transformations via fracturing and restacking of the primary platelet unit. The formation of highly ordered self-assemblies is an implication of the geometric shape as a factor in self-assembly, besides the conventional non-covalent bonding forces.

7. Conclusions and outlook

Recent developments in clay chemistry involving organic polymer-assisted intercalation and exfoliation have shown that thin-platelet geometric shapes are an important factor for self-assembly. Literature reports have revealed extensive clay–polymer interactions for fabrication of nanocomposite clay gels, hydrophilic polymer–clay films, layered structure encapsulation for biomaterials, quantum dots, and controlling super hydrophobic surface. Previous efforts at modifying clays by organic intercalation have led to spatial expansion of the clay multilayered structure and conferred the clay units with hydrophobic and self-assembling properties. The use of POP hydrophobic amine-salts and their polymer derivatives allowed systematic control in tailoring the clay XRD basal spacing from 13 to 92 Å and the isolation of completely randomized silicate platelets. The two different clay units, the organically intercalated stacks and the exfoliated platelets without organics, demonstrated their colloidal dispersion nature and self-assembling property under solution evaporation. The basic self-organizing forces arise from the non-covalent bonding interaction of the incorporated hydrophobic organics and the exfoliated silicate platelet

charge attraction. For the clay units, two complementary directions of vertical and horizontal self-stacking occurred simultaneously. In epoxy cuing process, the layered silicate units were self-organized into worm-like microstructures, further demonstrating the strong force of self-piling even under dynamic conditions. Under TEM electron bombardment and ultrasonic vibration, the self-assemblages could be further converted into hierarchical microstructures. All of these occurrences including the ease of self-assembly and hierarchical transformation are predominately affected by the silicate platelet piling tendency. The relatively strong charge attraction forces of the geometrically thin silicate platelets are assisted by the organic hydrophobic effect. The observation of various forms of self-assemblages with high regularity gave rise to the understanding of self-assembling mechanism and suggestions for practical uses of constructing the three-dimensional silicate arrays. The high surface interaction involving the silicate platelets may lead to further developments in clay applications.

Acknowledgments

We acknowledge financial support from the Ministry of Economic Affairs and the National Science Council (NSC) of Taiwan.

References

[1] Whitesides GM, Grzybowski B. Self-assembly at all scales. Science 2002;295:2418–21.
[2] Kim JK, Yang SY, Lee Y, Kim Y. Functional nanomaterials based on block copolymer self-assembly. Prog Polym Sci 2010;35:1325–49.
[3] Piirma I. Polymeric surfactants. Surfactant science series, vol. 42. New York: Marcel Dekker; 1992.
[4] Rosen MJ. Surfactants and interfacial phenomena. New York: Wiley-Interscience; 1989.
[5] Bates FS, Fredrickson GH. Block copolymer thermodynamics: theory and experiment. Annu Rev Phys Chem 1990;41:525–57.
[6] Hayward RC, Pochan DJ. Tailored assemblies of block copolymers in solution: it is all about the process. Macromolecules 2010;43:3577–84.
[7] Cornelissen JJLM, Fischer M, Sommerdijk NAJM, Nolte RJM. Helical superstructures from charged poly(styrene)-poly(isocyanodipeptide) block copolymers. Science 1998;280:1427–30.
[8] Xia YN, Whitesides GM. Soft lithography. Annu Rev Mater Sci 1998;28:153–84.
[9] Darling SB. Directing the self-assembly of block copolymers. Prog Polym Sci 2007;32:1152–204.
[10] Kuo SW. Hydrogen bond-mediated self-assembly and supramolecular structures of diblock copolymer mixtures. Polym Int 2009;58:455–64.
[11] Cheng JY, Ross CA, Smith HI, Thomas EL. Templated self-assembly of block copolymers: top-down helps bottom-up. Adv Mater 2006;18:2505–21.
[12] Muthukumar M, Ober CK, Thomas EL. Competing interactions and levels of ordering in self-organizing polymeric materials. Science 1997;277:1225–32.
[13] Lehmann W, Skupin H, Tolksdorf C, Gebhard E, Zentel R, Kruger P, Losche M, Kremer F. Giant lateral electrostriction in ferroelectric liquid-crystalline elastomers. Nature 2001;410:447–50.
[14] Breiner U, Krappe U, Thomas EL, Stadler R. Structural characterization of the "knitting pattern" in polystyrene-block-poly(ethylene-co-butylene)-block-poly(methyl methacrylate) triblock copolymers. Macromolecules 1998;31:135–41.
[15] Tselikas Y, Hadjichristidis N, Lescanec RL, Honeker CC, Wohlgemuth M, Thomas EL. Architecturally-induced tricontinuous cubic morphology in compositionally symmetric miktoarm starblock copolymers. Macromolecules 1996;29:3390–6.
[16] Bates FS, Fredrickson GH. Block copolymers—designer soft materials. Phys Today 1999;52:32–8.
[17] Dutta J, Hofmann H. Encyclopedia of nanoscience and nanotechnology. New York: American Scientific Publishers; 2003.
[18] Ahmed T, Marcal H, Lawless M, Wanandy NS, Chiu A, Foster LJR. Polyhydroxybutyrate and its copolymer with polyhydroxyvalerate as biomaterials: influence on progression of stem cell cycle. Biomacromolecules 2010;11:2707–15.
[19] Palmer LC, Stupp SI. Molecular self-assembly into one-dimensional nanostructures. Acc Chem Res 2008;41:1674–84.
[20] Parviz BA, Ryan D, Whitesides GM. Using self-assembly for the fabrication of nano-scale electronic and photonic devices. IEEE Trans Adv Pack 2003;26:233–41.
[21] Chowdhury D, Maoz R, Sagiv J. Wetting driven self-assembly as a new approach to template-guided fabrication of metal nanopatterns. Nano Lett 2007;7:1770–8.
[22] Herranz MA, Colonna B, Echegoyen L. Metal ion recognition and molecular templating in self-assembled monolayers of cyclic and acyclic polyethers. Proc Natl Acad Sci USA 2002;99:5040–7.
[23] Kim JH, Rahman MS, Lee JS, Park JW. Liquid crystalline ordering in the self-assembled monolayers of tethered rodlike polymers. J Am Chem Soc 2007;129:7756–7.
[24] Bhargava P, Zheng JX, Li P, Quirk RP, Harris FW, Cheng SZD. Self-assembled polystyrene-block-poly(ethylene oxide) micelle morphologies in solution. Macromolecules 2006;39:4880–8.
[25] Agut W, Brulet A, Taton D, Lecommandoux S. Thermoresponsive micelles from Jeffamine-b-poly(L-glutamic acid) double hydrophilic block copolymers. Langmuir 2007;23:11526–33.
[26] Mountrichas G, Pispas S. Synthesis and pH responsive self-assembly of new double hydrophilic block copolymers. Macromolecules 2006;39:4767–74.
[27] Alexandridis P, Yang L. SANS investigation of polyether block copolymer micelle structure in mixed solvents of water and formamide, ethanol, or glycerol. Macromolecules 2000;33:5574–87.
[28] Schmitt J, Decher G, Dressick WJ, Brandow SL, Geer RE, Shashidhar R, Calvert JM. Metal nanoparticle/polymer superlattice films: fabrication and control of layer structure. Adv Mater 1997;9:61–5.
[29] Medintz IL, Uyeda HT, Goldman ER, Mattoussi H. Quantum dot bioconjugates for imaging, labelling and sensing. Nat Mater 2005;4:435–46.
[30] Forster S, Antonietti M. Amphiphilic block copolymers in structure-controlled nanomaterial hybrids. Adv Mater 1998;10:195–217.
[31] Moffitt M, Eisenberg A. Size control of nanoparticles in semiconductor–polymer composites. 1. Control via multiplet aggregation numbers in styrene-based random ionomers. Chem Mater 1995;7:1178–84.
[32] Favier F, Walter EC, Zach MP, Benter T, Penner RM. Hydrogen sensors and switches from electrodeposited palladium mesowire arrays. Science 2001;293:2227–31.
[33] Cui Y, Wei Q, Park H, Lieber CM. Nanowire nanosensors for highly sensitive and selective detection of biological and chemical species. Science 2001;293:1289–92.
[34] Zayats M, Baron R, Popov I, Willner I. Biocatalytic growth of Au nanoparticles: from mechanistic aspects to biosensors design. Nano Lett 2005;5:21–5.
[35] Cheng FY, Su CH, Yang YS, Yeh CS, Tsai CY, Wu CL, Wu MT, Shieh DB. Characterization of aqueous dispersions of Fe_3O_4 nanoparticles and their biomedical applications. Biomaterials 2005;26:729–38.
[36] Kim TH, Jang EY, Lee NJ, Choi DJ, Lee KJ, Jang J, Choi J, Moon SH, Cheon J. Nanoparticle assemblies as memristors. Nano Lett 2009;9:2229–33.
[37] Springholz G, Holy V, Pinczolits M, Bauer G. Self-organized growth of three-dimensional quantum-dot crystals with fcc-like stacking and a tunable lattice constant. Science 1998;282:734–7.
[38] Sun Y, Xia Y. Shape-controlled synthesis of gold and silver nanoparticles. Science 2002;298:2176–9.
[39] Murphy CJ. Nanocubes and nanoboxes. Science 2002;298:2139–41.
[40] Hu J, Odom TW, Lieber CM. Chemistry and physics in one dimension: synthesis and properties of nanowires and nanotubes. Acc Chem Res 1999;32:435–45.
[41] Kondo Y, Takayangi K. Synthesis and characterization of helical multi-shell gold nanowires. Science 2000;289:606–8.
[42] Sommer AP, Franke RP. Biomimicry patterning with nanosphere suspensions. Nano Lett 2003;3:573–5.
[43] Fleming MS, Mandal TK, Walt DR. Nanosphere–microsphere assembly: methods for core–shell materials preparation. Chem Mater 2001;13:2210–6.

[44] Zhang Y, Suenaga K, Colliex C, Iijima S. Coaxial nanocable: silicon carbide and silicon oxide sheathed with boron nitride and carbon. Science 1998;281:973–5.
[45] Sherry LJ, Chang SH, Schatz GC, Van RP. Localized surface plasmon resonance spectroscopy of single silver nanocubes. Nano Lett 2005;5:2034–8.
[46] Yu D, Yam VWW. Controlled synthesis of monodisperse silver nanocubes in water. J Am Chem Soc 2004;126:13200–1.
[47] Liao H, Hafner JH. Gold nanorod bioconjugates. Chem Mater 2005;17:4636–41.
[48] Atienzar P, Ishwara T, Illy BN, Ryan MP, O'Regan BC, Durrant JR, Nelson J. Control of photocurrent generation in polymer/ZnO nanorod solar cells by using a solution-processed TiO_2 overlayer. J Phys Chem Lett 2010;1:708–13.
[49] Lehn JM. Dynamers: dynamic molecular and supramolecular polymers. Prog Polym Sci 2005;30:814–31.
[50] Lehn JM. Supramolecular chemistry. Weinheim: Wiley-VCH; 1995.
[51] Lehn JM. Toward self-organization and complex matter. Science 2002;295:2400–3.
[52] Ikkala O, Brinke G. Functional materials based on self-assembly of polymeric supramolecules. Science 2002;295:2407–9.
[53] Widesides GM, Mathias JP, Seto CT. Molecular self-assembly and nanochemistry: a chemical strategy for the synthesis of nanostructures. Science 1991;254:1312–9.
[54] Reinhoudt DN, Crego-Calama M. Synthesis beyond the molecule. Science 2002;295:2403–7.
[55] Philp D, Stoddart JF. Self-assembly in natural and unnatural systems. Angew Chem Int Ed Engl 1996;35:1154–96.
[56] Warner MG, Hutchison JE. Linear assemblies of nanoparticles electrostatically organized on DNA scaffolds. Nat Mater 2003;2: 272–7.
[57] Klug A. From macromolecules to biological assemblies. Angew Chem Int Ed Engl 1983;22:565–82.
[58] Lin JJ, Wei JC, Juang TY, Tsai WC. Preparation of protein–silicate hybrids from polyamine intercalation of layered montmorillonite. Langmuir 2007;23:1995–9.
[59] Lin JJ, Wei JC, Tsai WC. Layered confinement of protein in synthetic fluorinated mica via stepwise polyamine exchange. J Phys Chem B 2007;111:10275–80.
[60] Morse DE. Silicon biotechnology: harnessing biological silica production to construct new materials. Trends Biotechnol 1999;17:230–2.
[61] Brinker CJ, Lu Y, Sellinger A, Fan H. Evaporation-induced self-assembly: nanostructures made easy. Adv Mater 1999;11:579–85.
[62] Weiner S, Wagner HD. The material bone: structure–mechanical function relations. Annu Rev Mater Sci 1998;28:271–98.
[63] Hartgerink JD, Beniash E, Stupp SI. Self-assembly and mineralization of peptide-amphiphile nanofibers. Science 2001;294:1684–8.
[64] Oaki Y, Imai H. The hierarchical architecture of nacre and its mimetic material. Angew Chem 2005;117:6729–33.
[65] Lin JJ, Chu CC, Chiang ML, Tsai WC. Manipulating assemblies of high-aspect-ratio clays and fatty amine salts to form surfaces exhibiting a lotus effect. Adv Mater 2006;18:3248–52.
[66] Vukusic P, Sambles JR. Photonic structures in biology. Nature 2003;424:852–5.
[67] Wang CHS, Tsai WC, Wei KL, Lin JJ. Formation of molecular bundles from self-assembly of symmetrical poly(oxyalkylene)-diamido acids. J Phys Chem B 2005;109:13510–4.
[68] Lin JJ, Tsai WC, Wang CH. Formation of hierarchical molecular assemblies from poly(oxypropylene)-segmented amido acids under AFM tapping. Langmuir 2007;23:4108–11.
[69] Tsai WC, Lin JJ. Hierarchical rearrangement of self-assembled molecular bundle strands from poly(oxyethylene)-segmented amido acids. J Phys Chem B 2009;113:6240–5.
[70] Ho RM, Chen CK, Chiang YW. Novel nanostructures from self-assembly of chiral block copolymers. Macromol Rapid Commun 2009;30:1439–56.
[71] Bihannic I, Michot LJ, Lartiges BS, Vantelon D, Labille J, Thomas F, Susini J, Salome M, Fayard B. First direct visualization of oriented mesostructures in clay gels by synchrotron-based X-ray fluorescence microscopy. Langmuir 2001;17:4144–7.
[72] Gabriel JP, Davidson P. New trends in colloidal liquid crystals based on mineral moieties. Adv Mater 2000;12:9–20.
[73] Theng BKG. The chemistry of clay–organic reactions. New York: John Wiley & Sons; 1974.
[74] Pinnavaia TJ. Intercalated clay catalysts. Science 1983;220:365–71.
[75] Cseri T, Bekassy S, Figueras F, Rizner S. Benzylation of aromatics on ion-exchanged clays. J Mol Catal A Chem 1995;98: 101–7.
[76] Ajjou AN, Harouna D, Detellier C, Alper H. Cation-exchanged montmorillonite catalyzed hydration of styrene derivatives. J Mol Catal A Chem 1997;126:55–60.
[77] Laszlo P. Chemical reactions on clays. Science 1987;235: 1473–7.
[78] Corma A, Fornes V, Pergher SB, Maesen LM, Buglass JG. Delaminated zeolite precursors as selective acidic catalysts. Nature 1998;396:353–6.
[79] Celis R, Hermosin MC, Carrizosa MJ, Cornejo J. Inorganic and organic clays as carriers for controlled release of the herbicide hexazinone. J Agric Food Chem 2002;50:2324–30.
[80] Rawajfih Z, Nsour N. Characteristics of phenol and chlorinated phenols sorption onto surfactant-modified bentonite. J Colloid Interface Sci 2006;298:39–49.
[81] Kiraly Z, Veisz B, Mastalir A, Kofarago G. Preparation of ultrafine palladium particles on cationic and anionic clays, mediated by oppositely charged surfactants: catalytic probes in hydrogenations. Langmuir 2001;17:5381–7.
[82] Alexandre M, Dubois P. Polymer-layered silicate nanocomposites: preparation, properties and uses of a new class of materials. Mater Sci Eng 2000;28:1–63.
[83] Giannelis EP. Polymer layered silicate nanocomposites. Adv Mater 1996;8:29–35.
[84] Ray SS, Okamoto M. Polymer/layered silicate nanocomposites: a review from preparation to processing. Prog Polym Sci 2003;28:1539–641.
[85] Pavlidou S, Papaspyrides CD. A review on polymer-layered silicate nanocomposites. Prog Polym Sci 2008;33:1119–98.
[86] Bordes P, Pollet E, Averous L. Nano-biocomposites: biodegradable polyester/nanoclay systems. Prog Polym Sci 2009;34: 125–55.
[87] Kumar AP, Depan D, Tomer NS, Singh RP. Nanoscale particles for polymer degradation and stabilization—trends and future perspectives. Prog Polym Sci 2009;34:479–515.
[88] Kiliaris P, Papaspyrides CD. Polymer/layered silicate (clay) nanocomposites: an overview of flame retardancy. Prog Polym Sci 2010;35:902–58.
[89] Utracki LA, Sepehr M, Boccaleri E. Synthetic, layered nanoparticles for polymeric nanocomposites (PNCs). Polym Adv Technol 2007;18:1–37.
[90] Giannelis EP. Polymer-layered silicate nanocomposites: synthesis, properties and applications. Appl Organomet Chem 1998;12:675–80.
[91] Olphen HV. An introduction to clay colloid chemistry. 2nd ed. New York: John Wiley & Sons; 1977.
[92] Balogh M, Laszlo P. Organic chemistry using clays. Berlin Heidelberg: Springer-Verlag; 1993.
[93] Usuki A, Hasegawa N, Kadoura H, Okamoto T. Three-dimensional observation of structure and morphology in nylon-6/clay nanocomposite. Nano Lett 2001;1:271–2.
[94] Lai YH, Chiu CW, Chen JG, Wang CC, Lin JJ, Lin KF, Ho KC. Enhancing the performance of dye-sensitized solar cells by incorporating nanosilicate platelets in gel electrolyte. Sol Energy Mater Sol Cells 2009;93:1860–4.
[95] Tateyama H, Nishimura S, Tsunematsu K, Jinnai K, Adachi Y, Kimura M. Synthesis of expandable fluorine mica from talc. Clays Clay Miner 1992;40:180–5.
[96] Lehn JM. Synthesis of Na-2-mica from metakaolin and its cation exchange properties. J Mater Chem 2001;11:2072–9.
[97] Chiu CW, Chu CC, Dai SA, Lin JJ. Self-piling silicate rods and dendrites from high aspect-ratio clay platelets. J Phys Chem C 2008;112:17940–4.
[98] Rives V, Ulibarri MA. Layered double hydroxides (LDH) intercalated with metal coordination compounds and oxometalates. Coord Chem Rev 1999;181:61–120.
[99] Rives V. Characterisation of layered double hydroxides and their decomposition products. Mater Chem Phys 2002;75: 19–25.
[100] Khan AI, O'Hare D. Intercalation chemistry of layered double hydroxides: recent developments and applications. J Mater Chem 2002;12:3191–8.
[101] Okada A, Usuki A. The chemistry of polymer–clay hybrids. Mater Sci Eng C 1995;3:109–15.
[102] Okada A, Usuki A. Twenty years of polymer–clay nanocomposites. Macromol Mater Eng 2006;291:1449–76.
[103] Bohning M, Goering H, Fritz A, Brzezinka KW, Turky G, Scholnhals A, Schartel B. Dielectric study of molecular mobility in poly(propylene-graft-maleic anhydride)/clay nanocomposites. Macromolecules 2005;38:2764–74.

[104] Robello DR, Yamaguchi N, Blanton T, Barnes C. Spontaneous formation of an exfoliated polystyrene–clay nanocomposite using a star-shaped polymer. J Am Chem Soc 2004;126:8118–9.
[105] Tien YI, Wei KH. The effect of nano-sized silicate layers from montmorillonite on glass transition, dynamic mechanical, and thermal degradation properties of segmented polyurethane. J Appl Polym Sci 2002;86:1741–8.
[106] Lepoittevin B, Pantoustier N, Alexandre M, Calberg C, Jerome R, Dubois P. Polyester layered silicate nanohybrids by controlled grafting polymerization. J Mater Chem 2002;12:3528–32.
[107] Wang MS, Pinnavaia TJ. Clay–polymer nanocomposites formed from acidic derivatives of montmorillonite and an epoxy resin. Chem Mater 1994;6:468–74.
[108] Lan T, Kaviratna PD, Pinnavaia TJ. Epoxy self-polymerization in smectite clays. J Phys Chem Solids 1996;57:1005–10.
[109] LeBaron PC, Wang Z, Pinnavaia TJ. Polymer-layered silicate nanocomposites: an overview. Appl Clay Sci 1999;15:11–29.
[110] Zanetti M, Lomakin S, Camino G. Polymer layered silicate nanocomposites. Macromol Mater Eng 2000;279:1–9.
[111] Ishida H, Campbell S, Blackwell J. General approach to nanocomposite preparation. Chem Mater 2000;12:1260–7.
[112] Wang Z, Pinnavaia TJ. Hybrid organic–inorganic nanocomposites: exfoliation of magadiite nanolayers in an elastomeric epoxy polymer. Chem Mater 1998;10:1820–6.
[113] Theng BKG. Formation and properties of clay–polymer complexes. New York: Elsevier; 1979.
[114] Triantafillidis CS, LeBaron PC, Pinnavaia TJ. Homostructured mixed inorganic–organic ion clays: a new approach to epoxy polymer-exfoliated clay nanocomposites with a reduced organic modifier content. Chem Mater 2002;14:4088–95.
[115] Muzny CD, Butler BD, Hanley HJM, Tsvetkov F, Peiffer DG. Clay platelet dispersion in a polymer matrix. Mater Lett 1996;28:379–84.
[116] Lin JJ, Chan YN, Chang WH. Amphiphilic poly(oxyalkylene)-amines interacting with layered clays: intercalation, exfoliation, and new applications. In: Geckeler KE, Nishide H, editors. Advanced nanomaterials. New York: John Wiley & Sons Inc.; 2010. p. 459–80.
[117] Lin JJ, Chan YN, Lan YF. Hydrophobic modification of layered clays and compatibility for epoxy nanocomposites. Materials 2010;3:2588–605.
[118] Choy JH, Kwak SY, Jeong YJ, Park JS. Inorganic layered double hydroxides as nonviral vectors. Angew Chem Int Ed 2000;39:4041–5.
[119] Haraguchi K, Takehisa T, Fan S. Effects of clay content on the properties of nanocomposite hydrogels composed of poly(N-isopropylacrylamide) and clay. Macromolecules 2002;35:10162–71.
[120] Haraguchi K, Takehisa T. Nanocomposite hydrogels: a unique organic–inorganic network structure with extraordinary mechanical, optical, and swelling/de-swelling properties. Adv Mater 2002;14:1120–4.
[121] Haraguchi K, Farnworth R, Ohbayashi A, Takehisa T. Compositional effects on mechanical properties of nanocomposite hydrogels composed of poly(N,N-dimethylacrylamide) and clay. Macromolecules 2003;36:5732–41.
[122] Haraguchi K, Li HJ, Matsuda K, Takehisa T, Elliott E. Mechanism of forming organic/inorganic network structures during in-situ free-radical polymerization in PNIPA–clay nanocomposite hydrogels. Macromolecules 2005;38:3482–90.
[123] Haraguchi K, Li HJ. Control of the coil-to-globule transition and ultrahigh mechanical properties of PNIPA in nanocomposite hydrogels. Angew Chem Int Ed 2005;44:6500–4.
[124] Haraguchi K, Li HJ, Song L, Murata K. Tunable optical and swelling/deswelling properties associated with control of the coil-to-globule transition of poly(N-isopropylacrylamide) in polymer–clay nanocomposite gels. Macromolecules 2007;40: 6973–80.
[125] Haraguchi K, Li HJ, Okumura N. Hydrogels with hydrophobic surfaces: abnormally high contact angles for water on PNIPA nanocomposite hydrogels. Macromolecules 2007;40:2299–302.
[126] Shibayama M, Karino T, Miyazaki S, Okabe S, Takehisa T, Haraguchi K. Small-angle neutron scattering study on uniaxially stretched poly(N-isopropylacrylamide)–clay nanocomposite gels. Macromolecules 2005;38:10772–81.
[127] Miyazaki S, Endo H, Karino T, Haraguchi K, Shibayama M. Gelation mechanism of poly(N-isopropylacrylamide)–clay nanocomposite gels. Macromolecules 2007;40:4287–95.
[128] Haraguchi K, Song L. Microstructures formed in co-cross-linked networks and their relationships to the optical and mechanical properties of PNIPA/clay nanocomposite gels. Macromolecules 2007;40:5526–36.
[129] Haraguchi K, Takada T. Synthesis and characteristics of nanocomposite gels prepared by in situ photopolymerization in an aqueous system. Macromolecules 2010;43:4294–9.
[130] Haraguchi K. Synthesis and properties of soft nanocomposite materials with novel organic/inorganic network structures. Polym J 2011;43:223–41.
[131] Walther A, Bjurhager I, Malho JM, Pere J, Ruokolainen J, Berglund LA, Ikkala O. Large-area, lightweight and thick biomimetic composites with superior material properties via fast, economic, and green pathways. Nano Lett 2010;10:2742–8.
[132] Walther A, Bjurhager I, Malho JM, Ruokolainen J, Berglund L, Ikkala O. Supramolecular control of stiffness and strength in lightweight high-performance nacre-mimetic paper with fire-shielding properties. Angew Chem Int Ed 2010;49:6448–53.
[133] Podsiadlo P, Kaushik AK, Arruda EM, Waas AM, Shim BS, Xu JD, Nandivada H, Pumplin BG, Lahann J, Ramamoorthy A, Kotov NA. Ultrastrong and stiff layered polymer nanocomposites. Science 2007;318:80–3.
[134] Tang Z, Kotov NA, Magonov S, Ozturk B. Nanostructured artificial nacre. Nat Mater 2003;2:413–8.
[135] Podsiadlo P, Michel M, Lee J, Verploegen E, Kam NWS, Ball V, Lee J, Qi Y, Hart AJ, Hammond PT, Kotov NA. Exponential growth of LbL films with incorporated inorganic sheets. Nano Lett 2008;8:1762–70.
[136] Podsiadlo P, Tang Z, Shim BS, Kotov NA. Counterintuitive effect of molecular strength and role of molecular rigidity on mechanical properties of layer-by-layer assembled nanocomposites. Nano Lett 2007;7:1224–31.
[137] Kaushik AK, Podsiadlo P, Qin M, Shaw CM, Waas AM, Kotov NA, Arruda EM. The role of nanoparticle layer separation in the finite deformation response of layered polyurethane–clay nanocomposites. Macromolecules 2009;42:6588–95.
[138] Podsiadlo P, Kaushik AK, Shim BS, Agarwal A, Tang Z, Waas AM, Arruda EM, Kotov NA. Can nature's design be improved upon? High strength, transparent nacre-like nanocomposites with double network of sacrificial cross links. J Phys Chem B 2008;112:14359–63.
[139] Ebina T, Mizukami F. Flexible transparent clay films with heat-resistant and high gas-barrier properties. Adv Mater 2007;19:2450–3.
[140] Tetsuka H, Ebina T, Nanjo H, Mizukami F. Highly transparent flexible clay films modified with organic polymer: structural characterization and intercalation properties. J Mater Chem 2007;17:3545–50.
[141] Tetsuka H, Ebina T, Tsunoda T, Nanjo H, Mizukami F. Flexible organic electroluminescent devices based on transparent clay films. Nanotechnology 2007;18, 355701/1–4.
[142] Priolo MA, Gamboa D, Grunlan JC. Transparent clay–polymer nano brick wall assemblies with tailorable oxygen barrier. ACS Appl Mater Interfaces 2010;2:312–20.
[143] Nam HJ, Ebina T, Mizukami F. Formability and properties of self-standing clay film by montmorillonite with different interlayer cations. Colloids Surf A 2009;346:158–63.
[144] Shikinaka K, Aizawa K, Fujii N, Osada Y, Tokita M, Watanabe J, Shigehara K. Flexible, transparent nanocomposite film with a large clay component and ordered structure obtained by a simple solution-casting method. Langmuir 2010;26:12493–5.
[145] Priolo MA, Gamboa D, Holder KM, Grunlan JC. Super gas barrier of transparent polymer–clay multilayer ultrathin films. Nano Lett 2010;10:4970–4.
[146] Rao Y, Blanton TN. Polymer nanocomposites with a low thermal expansion coefficient. Macromolecules 2008;41:935–41.
[147] Tetsuka H, Mizukami F. Highly luminescent flexible quantum dot–clay films. Adv Mater 2008;20:3039–43.
[148] Chen YM, Lin HC, Hsu RS, Hsieh BZ, Su YA, Sheng YJ, Lin JJ. Thermoresponsive dual-phase transition and 3D self-assembly of poly(N-isopropylacrylamide) tethered to silicate platelets. Chem Mater 2009;21:4071–9.
[149] Mahadevaiah N, Venkataramani B, Prakash BSJ. Restrictive entry of aqueous molybdate species into surfactant modified montmorillonites—a breakthrough curve study. Chem Mater 2007;19:4606–12.
[150] Vaia RA, Teukolsky RK, Giannelis EP. Interlayer structure and molecular environment of alkylammonium layered silicates. Chem Mater 1994;6:1017–22.
[151] Hotta S, Paul DR. Nanocomposites formed from linear low density polyethylene and organoclays. Polymer 2004;45:7639–54.
[152] Zeng C, Lee LJ. Poly(methyl methacrylate) and polystyrene/clay nanocomposites prepared by in-situ polymerization. Macromolecules 2001;34:4098–103.

[153] Fu X, Qutubuddin S. Polymer–clay nanocomposites: exfoliation of organophilic montmorillonite nanolayers in polystyrene. Polymer 2001;42:807–13.
[154] Fu X, Qutubuddin S. Synthesis of polystyrene–clay nanocomposites. Mater Lett 2000;42:12–5.
[155] Imai Y, Nishimura S, Abe E, Tateyama H, Abiko A, Yamaguchi A, Aoyama T, Taguchi H. High-modulus poly(ethylene terephthalate)/expandable fluorine mica nanocomposites with a novel reactive compatibilizer. Chem Mater 2002;14:477–9.
[156] Chang JH, Jang TG, Ihn KJ, Lee WK, Sur GS. Poly(vinyl alcohol) nanocomposites with different clays: pristine clays and organoclays. J Appl Polym Sci 2003;90:3208–14.
[157] Kim MH, Park CI, Choi WM, Lee JW, Lim JG, Park OO, Kim JM. Synthesis and material properties of syndiotactic polystyrene/organophilic clay nanocomposites. J Appl Polym Sci 2004;92:2144–50.
[158] Ijdo WL, Pinnavaia TJ. Solid solution formation in amphiphilic organic–inorganic clay heterostructures. Chem Mater 1999;11:3227–31.
[159] Maiti P, Yamada K, Okamoto M, Ueda K, Okamoto K. New polylactide/layered silicate nanocomposites: role of organoclays. Chem Mater 2002;14:4654–61.
[160] Xie W, Xie R, Pan WP, Hunter D, Koene B, Tan LS, Vaia R. Thermal stability of quaternary phosphonium modified montmorillonites. Chem Mater 2002;14:4837–45.
[161] Bottino FA, Fabbri E, Fragala IL, Malandrino G, Orestano A, Pilati F, Pollicino A. Polystyrene–clay nanocomposites prepared with polymerizable imidazolium surfactants. Macromol Rapid Commun 2003;24:1079–84.
[162] Fox DM, Maupin PH, Harris RH, Gilman JW, Eldred DV, Katsoulis D, Trulove PC, DeLong HC. Use of a polyhedral oligomeric silsesquioxane (POSS)-imidazolium cation as an organic modifier for montmorillonite. Langmuir 2007;23:7707–14.
[163] Wang ZM, Chung TC, Gilman JW, Manias E. Melt-processable syndiotactic polystyrene/montmorillonite nanocomposites. J Polym Sci B Polym Phys 2003;41:3173–87.
[164] Gilman JW, Awad WH, Davis RD, Shields J, Harris RH, Davis C, Morgan AB, Sutto TE, Callahan J, Trulove PC, DeLong HC. Polymer/layered silicate nanocomposites from thermally stable trialkylimidazolium-treated montmorillonite. Chem Mater 2002;14:3776–85.
[165] Lin JJ, Cheng IJ, Wang R, Lee RJ. Tailoring basal spacings of montmorillonite by poly(oxyalkylene)diamine intercalation. Macromolecules 2001;34:8832–4.
[166] Lin JJ, Hsu YC, Chou CC. Copolymer-layered silicate hybrid surfactants from the intercalation of montmorillonite with amphiphilic copolymers. Langmuir 2003;19:5184–7.
[167] Chou CC, Lin JJ. One-step exfoliation of montmorillonite via phase inversion of amphiphilic copolymer emulsion. Macromolecules 2005;38:230–3.
[168] Chang YC, Chou CC, Lin JJ. Emulsion intercalation of smectite clays with comb-branched copolymers consisting of multiple quaternary amine salts and a poly(styrene–butadiene–styrene) backbone. Langmuir 2005;21:7023–8.
[169] Lin JJ, Hsu YC, Wei KL. Mechanistic aspects of clay intercalation with amphiphilic poly(styrene-co-maleic anhydride)-grafting polyamine salts. Macromolecules 2007;40:1579–84.
[170] Lin JJ, Chen YM. Amphiphilic properties of poly(oxyalkylene)amine-intercalated smectite aluminosilicates. Langmuir 2004;20:4261–4.
[171] Lin JJ, Chou CC, Lin JL. Lengthy rod formation from a poly(oxyalkylene)amine-intercalated smectite clay by a self-aligning mechanism. Macromol Rapid Commun 2004;25:1109–12.
[172] Chou CC, Shieu FS, Lin JJ. Preparation, organophilicity, and self-assembly of poly(oxypropylene)amine–clay hybrids. Macromolecules 2003;36:2187–9.
[173] Chu CC, Chiang ML, Tsai CM, Lin JJ. Exfoliation of montmorillonite clay by Mannich polyamines with multiple quaternary salts. Macromolecules 2005;38:6240–2.
[174] Lin JJ, Chu CC, Chiang ML, Tsai WC. First isolation of individual silicate platelets from clay exfoliation and their unique self-assembly into fibrous arrays. J Phys Chem B 2006;110:18115–20.
[175] Chiu CW, Chu CC, Cheng WT, Lin JJ. Exfoliation of smectite clays by branched polyamines consisting of multiple ionic sites. Eur Polym J 2008;44:628–36.
[176] Wang L, Li C, Liu M, Evans DG, Duan X. Large continuous, transparent and oriented self-supporting films of layered double hydroxides with tunable chemical composition. Chem Commun 2007:123–5.
[177] Lin JJ, Juang TY. Intercalation of layered double hydroxides by poly(oxyalkylene)-amidocarboxylates: tailoring layered basal spacing. Polymer 2004;45:7887–93.
[178] Leroux F, Pagano MA, Intissar M, Chauviere S, Forano C, Besse JP. Delamination and restacking of layered double hydroxides. J Mater Chem 2001;11:105–12.
[179] Hibino T, Jones W. New approach to the delamination of layered double hydroxides. J Mater Chem 2001;11:1321–3.
[180] Hibino T. Delamination of layered double hydroxides containing amino acids. Chem Mater 2004;16:5482–8.
[181] O'Leary S, O'Hare D, Seeley G. Delamination of layered double hydroxides in polar monomers: new LDH–acrylate nanocomposites. Chem Commun 2002:1506–7.
[182] Ma R, Liu Z, Takada K, Iyi N, Bando Y, Sasaki T. Synthesis and exfoliation of Co^{2+}–Fe^{3+} layered double hydroxides: an innovative topochemical approach. J Am Chem Soc 2007;129:5257–63.
[183] Lee JH, Rhee SW, Jung DY. Selective layer reaction of layer-by-layer assembled layered double-hydroxide nanocrystals. J Am Chem Soc 2007;129:3522–3.
[184] Du X, Jiang Z, Meng X, Wang Z, Yu H, Li M, Tang T. Syntheses of opened hollow clay microspheres through a spray-drying approach and their derivative clay/carbon nanotubes composites. J Phys Chem C 2008;112:6638–42.
[185] Lin JJ, Chen YM, Tsai WC, Chiu CW. Self-assembly of lamellar clays to hierarchical microarrays. J Phys Chem C 2008;112:9637–43.
[186] Chan YN, Dai SA, Lin JJ. Simultaneous occurrence of self-assembling silicate skeletons to wormlike microarrays and epoxy ring-opening polymerization. Macromolecules 2009;42:4362–5.
[187] Chan YN, Hsu RS, Lin JJ. Mechanism of silicate platelet self-organization during clay-initiated epoxy polymerization. J Phys Chem C 2010;114:10373–8.
[188] Lin JJ, Chu CC, Chou CC, Shieu FS. Self-assembly nanofibers from random silicate platelets. Adv Mater 2005;17:301–4.